Tectonics®

RESEARCH ARTICLE
10.1029/2025TC008955

Key Points:

- Katangan basin subsidence and structure proves rift driven crustal extension increased from the basin margin to a central rift zone
- Provenance analysis shows the rift basins filled locally and also from the NE and that the central rift zone acted as a sediment boundary
- Eo-Cambrian orogeny caused closure of the central rift, regional inversion of pre-existing structure and focused fluid migration

Supporting Information:

Supporting Information may be found in the online version of this article.

Correspondence to:

M. C. Daly,
mike.daly@earth.ox.ac.uk

Citation:

Daly, M. C., Zimba, M., Purkiss, M., & Chibesakunda, F. (2025). The inter-cratonic Neoproterozoic Katangan basin of Central Africa: Rift basin formation, orogenic inversion and potential fluid pathways. *Tectonics*, *44*, e2025TC008955. https://doi.org/10.1029/2025TC008955

Received 6 MAY 2025
Accepted 6 JUN 2025

Author Contributions:

Conceptualization: M. C. Daly
Data curation: M. Zimba
Formal analysis: M. C. Daly, M. Purkiss, F. Chibesakunda
Funding acquisition: M. C. Daly, M. Zimba
Investigation: M. C. Daly, M. Zimba, M. Purkiss
Methodology: M. C. Daly, M. Zimba, M. Purkiss, F. Chibesakunda
Project administration: M. C. Daly, F. Chibesakunda
Resources: M. C. Daly, F. Chibesakunda
Supervision: M. C. Daly, F. Chibesakunda
Validation: M. Zimba, M. Purkiss

The Inter-Cratonic Neoproterozoic Katangan Basin of Central Africa: Rift Basin Formation, Orogenic Inversion and Potential Fluid Pathways

M. C. Daly[1], M. Zimba[2], M. Purkiss[1], and F. Chibesakunda[3]

[1]Department of Earth Sciences, Oxford University, Oxford, UK, [2]First Quantum Minerals Ltd., Solwezi, Zambia, [3]Geological Survey Department, Lusaka, Zambia

Abstract The tectono-stratigraphic development of continental basins is critical to an understanding of continental tectonics and the formation of metal deposits. The Neoproterozoic, inter-cratonic Katangan copper basin of Central Africa records a tectono-stratigraphic evolution and the generation of potential metal transporting fluid pathways. Integration of lithospheric structure, quantitative basin analysis, sediment routing systems, and basin structure defines the tectono-stratigraphic model of the basin. The basin lies between the Congo and Kalahari cratons, on lithosphere distinctly thinner than the adjacent craton cores. Crustal scale fault zones parallel the craton margins and suggest lithospheric weaknesses influenced the basin shape. Basin subsidence analysis indicates two phases of rift-driven subsidence and increasing lithospheric extension from the basin boundary to a Central Rift Zone (CRZ). The CRZ also marks a sediment provenance boundary. Drill core and seismic reflection data show extensional, half graben geometries. Subsequent, Late Ediacaran and Cambrian orogenesis and basin closure and inversion occurred regionally and most intensively within the CRZ. The deformation resulted in crustal thickening, preserved as a ~50 km wide zone of garnet-amphibolite facies metamorphism. The CRZ is underlain by relatively thin, continental lithosphere, and is characterized by intense orogenic tectonics and inversion of the earlier formed rifts. The reactivated fault structures imply crustal weakening and define several tectonic domains that occur as fluid pathways for high volume fluid migration of metal bearing brines.

Plain Language Summary The world requires copper to deliver the energy transition. Large sedimentary basins in continents can be prolific sources of copper, however, our understanding of this process is poor. Here we examine the world's most copper rich basin, the Katangan basin of Central Africa, to understand key aspects of copper deposit formation. Existing copper mines were discovered by detecting surface indications of copper. To discover new copper we need to look deeper into unexplored rock formations. By integrating four independent geological perspectives we can define pathways along which copper fluids may have moved. This will enable us to find deep deposits unseen by conventional surface detection. Specifically, we consider the thickness, and therefore strength, of continents, searching for regional weaknesses where a suitable basin may have formed. We then analyze the basin's shape and structure and its rock fill, to understand both how the basin formed and the type of rocks that filled it. Finally, we analyze how the basin has deformed and how the resulting heat and pressure caused mineral rich fluids to move and accumulate. Merging these different perspectives allows us to define potential fluid channels for metal migration and deposition.

1. Introduction

The Neoproterozoic Katangan basin lies on inter-cratonic lithosphere between the Archean and Paleoproterozoic Congo, Kalahari and Bangweulu cratons of Central Africa. The basin context, structure and stratigraphy appears strongly related to the margins of these cratons. The basin is also the world's largest, sediment-hosted copper (Cu) and cobalt (Co) province (Selley et al., 2006) and contributes about 14% and 60% respectively to the world's Cu and Co production. This unique mineral endowment has resulted in the mines and mineral deposits of the basin having been widely studied (Fleischer et al., 1976; Hitzman, 2000; Hitzman et al., 2005; Mendelsohn, 1961; Selley et al., 2006). Although the basin history has been extensively analyzed in the context of the local mining activities (Coward & Daly, 1984; Daly, 1986a, 1986b; Fleischer et al., 1976; Hitzman et al., 2012; Mendelsohn, 1961; Porada & Berhorst, 2000), there remain significant unknowns about the tectonostratigraphic

Writing – original draft: M. C. Daly, M. Purkiss
Writing – review & editing: M. Zimba

development of the basin as a whole, and the crustal controls on the basins tectonic and mineral development (Alessio et al., 2019).

The uncertainties of the tectonic and geodynamic development of the Katangan basin are in part due to the paucity of modern basin analysis and deep crustal data. Chronostratigraphic correlation between the well-known mining locations is difficult due to very few reliable stratigraphic age markers beyond two well recognized but non-diagnostic diamictite units. No quantitative analysis of the subsidence history of the basin has been published. Similarly, there is little geometric analysis of the nature of the basin wide rift tectonics and their relationship with the subsequent Ediacran and Cambrian basin inversion and thrust tectonics. These deficiencies and singular scientific approaches, result in differing perspectives on the basin formation process based on magmatic data (Kampunzu et al., 2000), stratigraphic correlations (Binda, 1994; Cailteaux & De Putter, 2019; Werndorff, 2003), the role of salt tectonics and brecciation (Jackson et al., 2003; Mambwe et al., 2023), and the distribution, heterogeneity and degree of deformation and metamorphism experienced by the basin (Cosi et al., 1992; Coward & Daly, 1984; John et al., 2004).

We build on this earlier work to develop a tectono-stratigraphic model for the northern Katangan basin and the development of its major fluid pathways. We integrate four distinct but complementary geological perspectives of the basin into a single tectonostratigraphic model. The inputs include: lithospheric context of basin location; the basin forming process and its variability; the stratigraphic provenance of basin fill; and the basin's subsequent deformational history and tectonic development. These perspectives are summarized as several tectonic domains that reflect the current heterogeneity and architecture of the basin, and identify a range of potential fluid pathways that may ultimately assist in the deep exploration for copper minerals.

2. Lithospheric Context of the Katangan Basin of Central Africa

The Neoproterozoic Katangan basin extends some 2,500 km from the Katanga province of the Democratic Republic of Congo, southwestwards across Zambia and southeastern Angola to northwestern Namibia (Figure 1). It lies between the Archean Congo Craton to the northwest and the Archean and Proterozoic Kalahari Craton to the south. It is also bordered by the Paleoproterozoic Bangweulu Craton to the northeast. From western Zambia, southwestwards to the Kamanjab inlier of Namibia (Figure 1), the basin is covered by Mesozoic sediments of the Okavango basin and Plio-Pleistocene sands of the paleo-Kalahari Desert (Miller, 2013). Beneath the Quaternary cover Singletary et al. (2003) describe a southward trend to the Katangan basin basement that is reflected in Figure 1. Throughout this poorly exposed basin there is broad consistency in tectono-stratigraphic units indicating a contiguous basin with comparable tectonic and climatic environments (Miller, 2013). However, the extensive evaporitic sections in the DRC and Zambia, and the associated breccias, are not significant in Namibia and nor are the extensive, large Cu deposits.

2.1. The Cratonic Margins of the Katangan Basin

During the past two decades Rayleigh wave tomography has been used to map the thickness of continental lithospheric and, together with earthquake depths, has been used as an indicator of thick, cold and strong lithosphere (Jackson et al., 2021). This technique has resulted in relatively consistent global models of continental lithospheric thickness (Jackson et al., 2021). Augmenting this global scale view, a less constrained, two-dimensional profile of lithospheric thickness across a part of the Katangan basin, has been made using magneto-telluric (MT) inversion (Sarafian et al., 2018). The technique maps lithospheric resistivity variations driven by rock, fluid, or melts, and can give broad indications of the depth of sub-continental lithospheric mantle. Data from both techniques are used to define the cratonic margins of the Katangan basin. These geophysical data sources are supported by regional isotopic age data together with estimated Sm-Nd model ages (De Waele et al., 2006).

Rayleigh wave Lithospheric thickness maps of southern Africa, derived from the model of Schaeffer and Lebedev (2013) (Figure 2a), are superposed with the regional fault structures of the Katangan basin in Figure 2b. The contoured base map (Figure 2a) shows 10 km spaced lithospheric thickness contours from 100 to 300 km. Southern Africa comprises two large areas of thick lithosphere that define the extent of the Congo Craton and the Kalahari Craton. These two cratons reach thicknesses of over 250 km and are separated by an elliptical zone of thinner but still relatively thick lithosphere of about 140 km thick (Figures 2a and 2b). Both cratons include

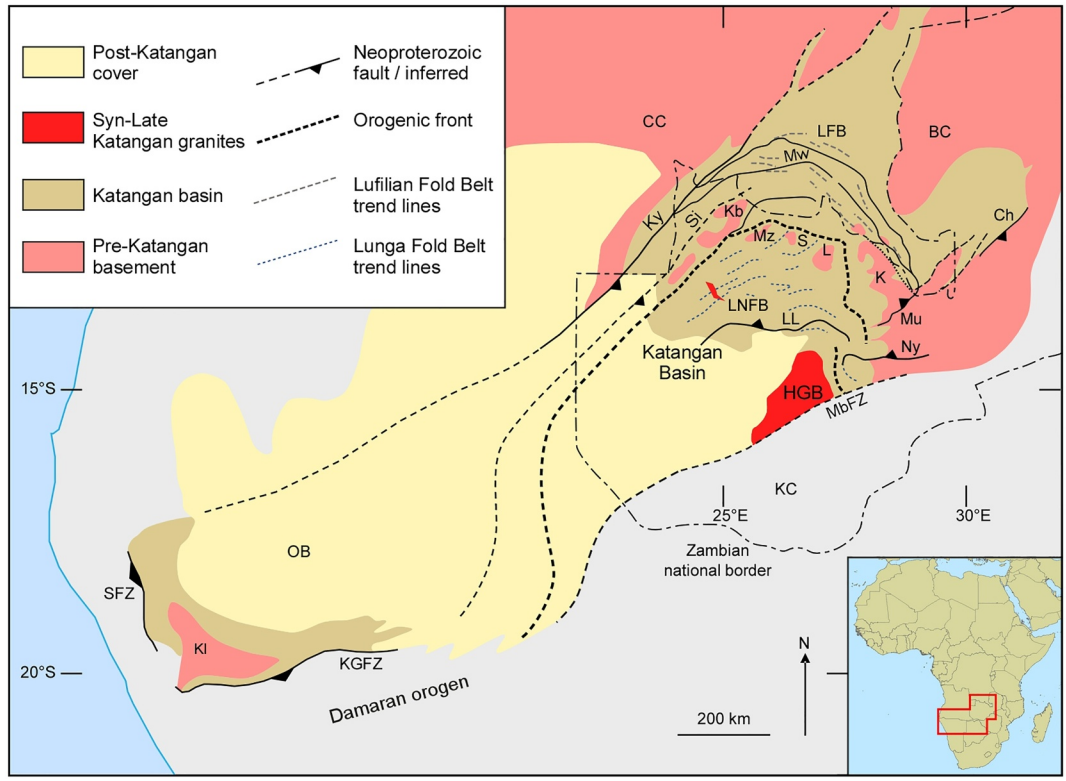

Figure 1. Map showing the Katangan basin, covered and exposed. Geological outline of the greater Katangan basin from the DRC in the NE to Namibia in the SW. The map shows the central part of the basin is overlain by widespread cover of Mesozoic and Cenozoic sediments. The area discussed in this paper is the northeastern area known as the Central African Copper Belt. Abbreviations: CC, Congo Craton; BC, Bangweulu Craton; KC, HGB, Hook Granite Batholith: K, Kafue Anticline; Kb, Kabompo Dome; KC, Kalahari Craton; Kf, Kafue fault; KGFZ, Khorixas-Gaseneirob fault zone: KI, Kamanjab inlier; Ky, Kanyama fault; L, Luswishi Dome; LFB, Lufilian fold belt; LL, Lungu/Lamala thrust fault; LNFB, Lunga fold belt; MbFZ, Mwembeshi fault zone; Mu, Mubalashi fault; Mz, Mwombezhi Dome; NKB, north Katangan basin; NRB, northern rift basin; Ny, Nyama fault; OB, Ovambo basin; P, Pedicle fault; S, Solwezi Dome; SFZ, Sesfontaine fault zone, Si, Sailunga fault; SRB Southern rift basin.

lithosphere comprising Archean and Proterozoic terranes within the thickened lithosphere. We now discuss the relationship of the Katangan basin and these cratonic units.

2.1.1. The Congo Craton Margin

Based on the tomography, surface mapping and the major fault structures (Figures 2b and 3), three features define the southeastern margin of the Congo craton and its relationship with the overlying Katangan basin (Figure 3). Firstly, a parallelism of the northwestern Katangan basin and its major.

Firstly, a parallelism of the northwestern Katangan basin margin with the southeastern lithospheric thickness contour of 160 ± 10 km extends for over 1,000 km along strike (Figures 2a and 3). The outcrops between the Congo craton and the Katangan sedimentary basin have two distinct and overlapping modes: a flat to gently dipping stratigraphic onlapping relationship to the west of the Mwinilunga fault zone (Figure 2b); and a linear, southeast dipping monoclinal relationship along the NE/SW eastern margin of the Kibara mountain range (Francois, 1987) (Figure 3). In addition to the margin parallel faults there is an extensive zone of andesitic and basaltic lava flows, volcanics and gabbroic intrusions that also parallel the craton margin in Zambia (Liyunga et al., 2000; Wingate et al., 2010) and to the north in the DRC (Kampunzu et al., 2000; Key et al., 2001; Twite et al., 2017) (Figures 2b and 3).

Secondly the 140 km, closed lithospheric thickness contour beneath the center of the Katangan basin, broadly follows the trend and shape of the basin and its continuity to the SW. The steady gradient from the NW parallels the mappable fault zones (see Section 3.1) between the Archean outcrop and the center of the basin, implying the

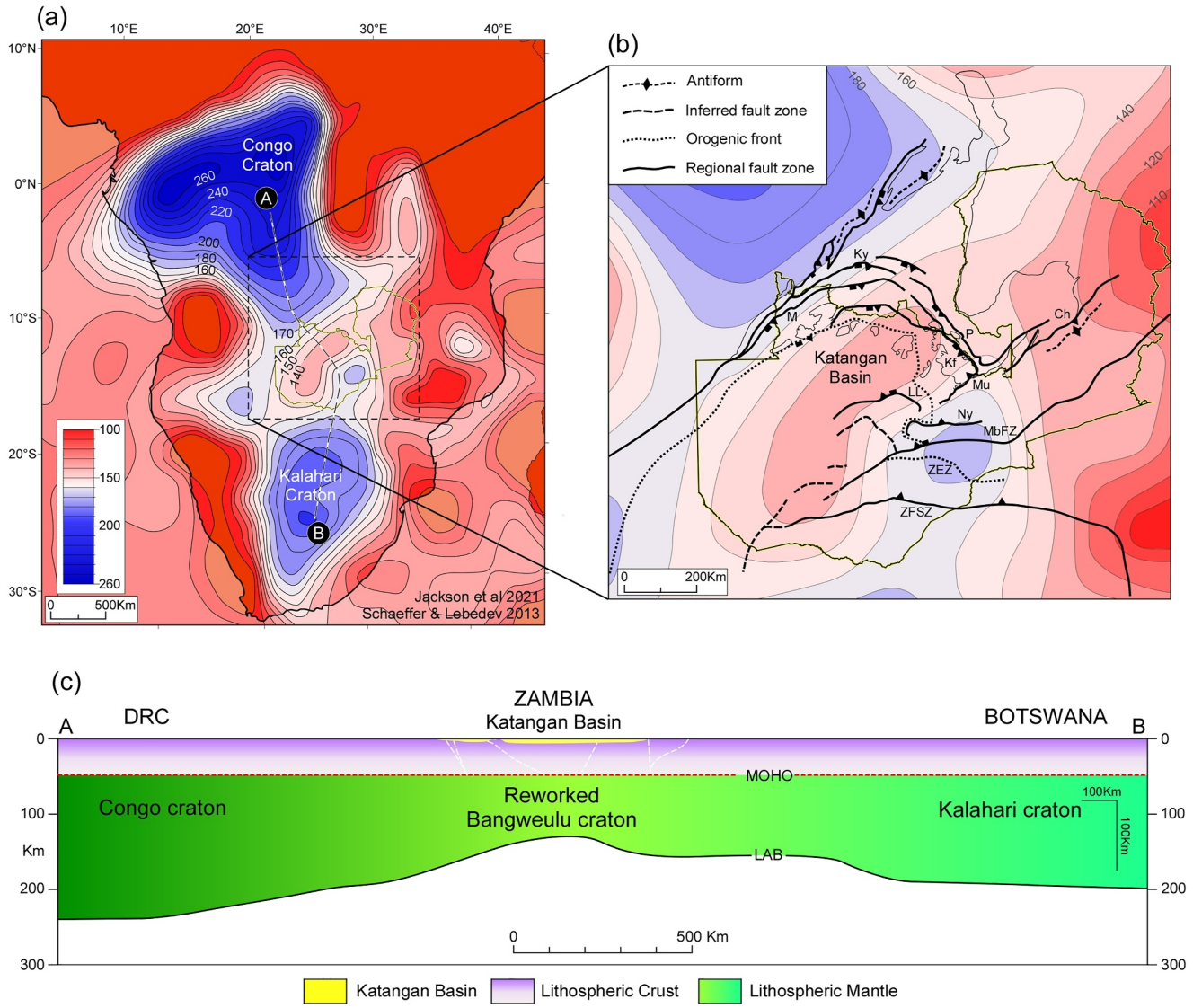

Figure 2. Lithospheric setting of the Katangan Basin. (a) Lithospheric thickness map of Southern Africa based on the Rayleigh wave tomography model of Schaeffer and Lebedev (2013). Note the spatial relationship between the thick lithosphere of the Congo and Kalahari cratons and the elongate NE/SW area of relatively thinner lithosphere beneath Zambia. (b) A close-up of Zambian lithosphere and the major crustal scale faults that define the borders and major fault structures of the Neoproterozoic Katangan basin. The basin occupies a NE/SW trending elongate area of ~140 km thick lithosphere between the thicker >200 km lithosphere of the cratons to the north and south. (c) A north-south cross section of the lithosphere showing the significant topography at the Lithosphere-Asthenosphere Boundary (lithosphere asthenosphere boundary) between the Congo and Kalahari cratons. The Katangan basin occupies the relatively thin zone lithosphere between the two major cratons.

cratonic thickness change is potentially fault controlled. Thirdly, Figure 2b also shows the central basin contour closing due to thickening to the northeast toward the smaller Paleoproterozoic Bangweulu craton. These observations indicate a close relationship between lithospheric thickness change, the northwest basin boundary and the regional location of the Katangan basin.

2.1.2. The Bangweulu Craton Margin

The geophysical definition of the Bangweulu craton as a significant area of thickened, ancient lithosphere is less compelling on the surface wave tomography as that of the Congo and Kalahari cratons. However, its existence as cratonic lithosphere has long been postulated by field mapping of northeastern Zambia (Andersen & Unrug, 1984; Daly & Unrug, 1982; Drysdall et al., 1974). More recently its physical existence has been supported by a magneto-telluric profile that concluded it comprises relatively thick and resistive lithosphere in comparison to the

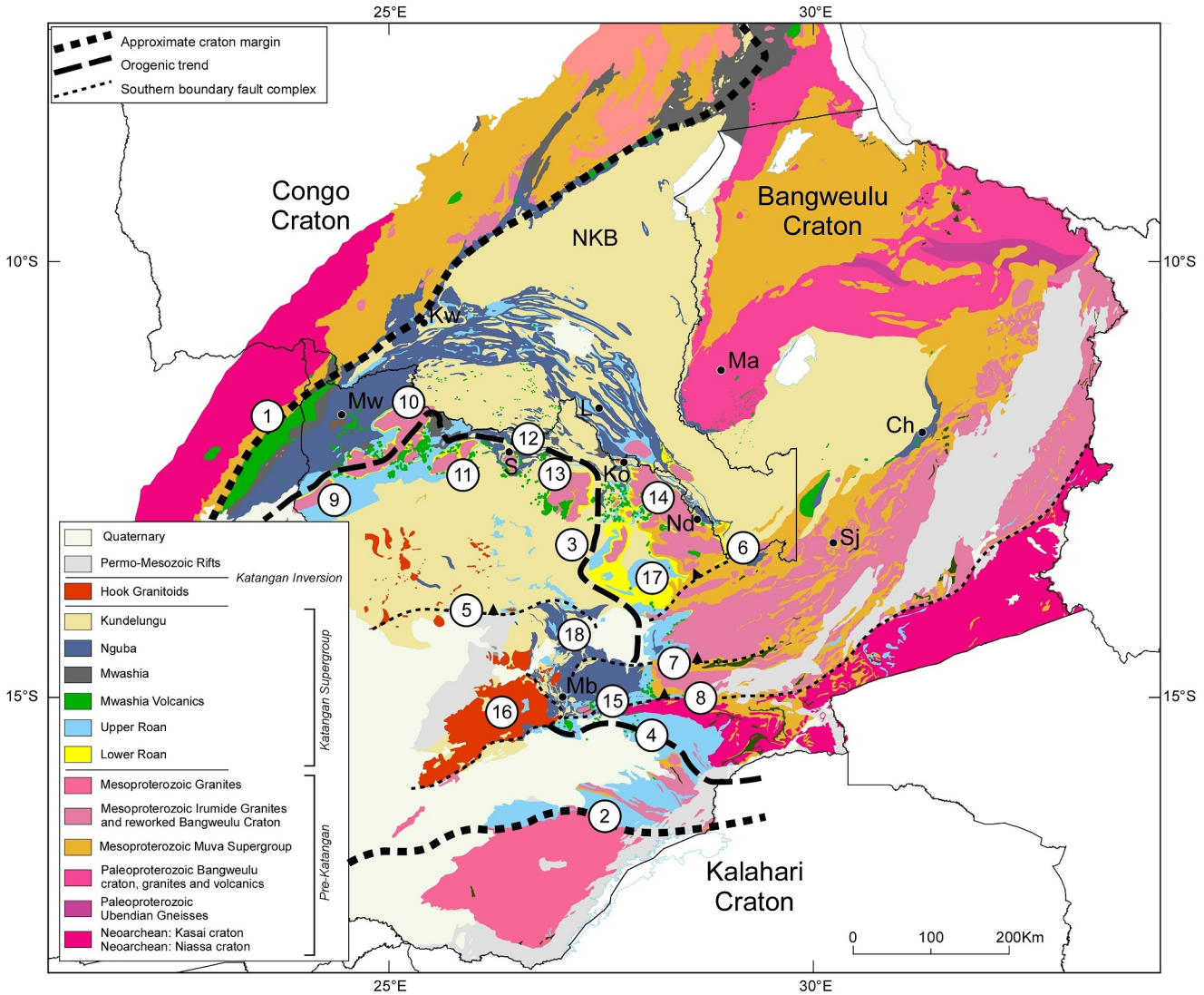

Figure 3. Geological map of the Katangan basin and its regional context. A geological map of the Katangan basin of Zambia and the DRC showing the detail of the basin geology and structure. Modified from the Geological Map of Zambia, 1:1 m (Thieme & Johnson, 1981). Major tectonic features: (1) Approximation of the Congo craton eastern margin; (2) Approximation of the Kalahari craton northern margin – the Zambezi Frontal Shear Zone; (3) Approximate northern boundary of the orogenic HP/HT zone; (4) Zambezi gabbroic-eclogite zone; (5) Lunga-Lumwala fault zone; (6) Mubalashi fault zone; (7) Nyama fault zone; (8) Mwembeshi fault zone; (9) West Lunga dome; (10) Kabompo dome; (11) Mwombezhi dome; (12) Solwezi dome; (13) Luswishi dome; (14) Kafue Anticline; (15) Matala dome; (16) Hook Granite Batholith; (17) Kashiba platform; (18) Kayambe hills fold belt. NKB, Northern Katangan basin; NEKB, Northeastern Katangan basin. Settlements used as reference points: Ch, Chilonga Mission; Ko, Konkola; Kw, Kolwezi; L, Lubumbashi: Ma, Matanda; Mb, Mumbwa; Mw, Mwinilunga; Nd, Ndola; S, Solwezi; Sj, Serenje.

surrounding Proterozoic folded belts (Sarafian et al., 2018). In addition, the granites and volcanics that constitute the surface geology of the Bangweulu craton are well dated as Paleoproterozoic and reveal Archean Sm/Nd model ages indicating an Archean protolith (De Waele et al., 2006). To the SE and SW the Bangweulu craton and its overlying Mesoproterozoic sedimentary basins were deformed in the Irumide orogenic event between 1,050 and 950 Ma (Daly, 1986a, 1986b; De Waele et al., 2006).

The contact between the northern extension of the Katangan basin and the Bangweulu craton has two distinct modes. Along the western margin of the Banweulu craton a flat to gently dipping onlapping relationship (Thieme, 1971) (Figure 3). In contrast, the southeastern margin of the Northeast Katangan basin (NEKB) near Chilonga Mission (Figure 3) is defined by a steeply dipping, northwest facing monocline due to basement involved, northwest directed thrust faulting (Page, 1974a). A comparable northeast facing monocline defines the northeast margin of the Copperbelt (Daly et al., 1984). This linear, basement cored Kafue fault zone defines the

eastern margin of the Kafue anticline (Coward & Daly, 1984) and can be traced several hundred kilometers to the NW into the DRC (Figures 2b and 3).

The Bangweulu cratonic lithosphere thins to the SE and SW from the center of the craton (Sarafian et al., 2018; Schaeffer & Lebedev, 2013). Within the Katangan basin, in addition to the Kafue Dome, several other basement inliers record Paleoproterozoic ages broadly comparable to the Bangweulu craton (De Waele et al., 2006) and indicate that most of the Katangan basin of the Zambian copperbelt is underlain by an extensive Bangweulu craton margin (Figure 2b). The Bangweulu rock types and age connection can be traced to the southern boundary of the basement domal inliers and is marked on Figure 3. South of this line (Figure 3) there is no further basement outcrop or drilled section within the basin.

2.1.3. The Kalahari Craton Margin

As with the Congo craton, the Kalahari craton comprises several geologically distinct Archean and Proterozoic units that amalgamate through the surface wave analysis to define a single, large, unit of lithosphere known as the Kalahari craton (Figure 2a). The definition of the lithospheric shape and thickness of the Kalahari craton is relatively consistent across several studies as summarized by Jackson et al. (2021). The northern margin of the craton lies to the south of the Katangan basin and is here considered as the southern, tectonic boundary of the Zambezi Belt as defined by the Zambezi Frontal Shear Zone (ZFSZ, Figures 2 and 3) and the Mesoproterozoic Choma-Kaloma Batholith of SW Zambia (Hanson, 2003; Loughlin, 1980; Taverner-Smith, 1961).

3. Katangan Basin Evolution

Based on the apparent lack of ocean crust within the Katangan basin, Binda (1994) argued that the Katangan basin was not rift related. However, the majority of publications assume the basin developed as a continental rift basin, argued largely on the basis of associated magmatism (Kampunzu et al., 2000) and facies interpretations of the sedimentology and stratigraphic character of the early Roan sediments (Cailteux & De Putter, 2019; Fleischer et al., 1976; Francois, 1987; Kennedy et al., 2019; Mendelsohn, 1961; Selley et al., 2006). Wendorff (2005, 2011), working primarily in the DRC, added a dynamic element to the lithostratigraphy and proposed discrete basin forming events that resulted in basin expansion over time. Following the regional tectonic model of Porada and Berhorst (2000), Wendorff (2011) argued for two phases of Tonian rifting followed by a foreland basin developed during Ediacaran and Cambrian thrust tectonics. This history and our interpretation of the regional stratigraphy is summarized in the stratigraphic column of Figure 4. To test and develop these interpretations we present quantitative estimates of crustal extension across the basin based on new regional data from deep diamond drill core and reflection seismic data. In addition, we use zircon provenance analysis to identify sediment provenance routing and depositional compartmentalization in the basin and the nature of sediment barriers and sediment entry routes through time.

3.1. Basin Formation

The primary tectonic drivers of extensive basin formation are lithospheric extension and lithospheric loading, the load either applied laterally (foreland basins) or from beneath (cratonic basins). The subsidence profiles of these tectonic settings tend to be markedly different, concave or convex in shape, and are arguably an essential characteristic for a basin to be attributed a tectonic mechanism (Allen & Allen, 2013; Xie & Heller, 2009). Stratigraphic and associated subsidence analysis has been widely used to constrain basin driving mechanisms underpinning basin subsidence (Barton & Wood, 1984; Watts & Ryan, 1976; Xie & Heller, 2009) and is deployed here in the Zambian part of the Katangan basin (Figure 5). The quantitative analysis is only possible in areas of minimal deformation of the basin's sedimentary section. High tectonic strain and metamorphism makes interpretation of the original sedimentary section increasingly unreliable. The analysis presents eight type-sections based around a primary, diamond drill core interpretation together with adjacent outcrop and supplementary data from the literature. The resultant type-sections are a best representation of the immediate area's stratigraphy and sedimentary facies. Such type logs have been created as a profile from the northeastern basin margin at Chilonga Mission (Figure 3), to the Central Rift Zone (CRZ) in the area of Solwezi, an across strike section of approximately 200 km (Figures 3 and 5a).

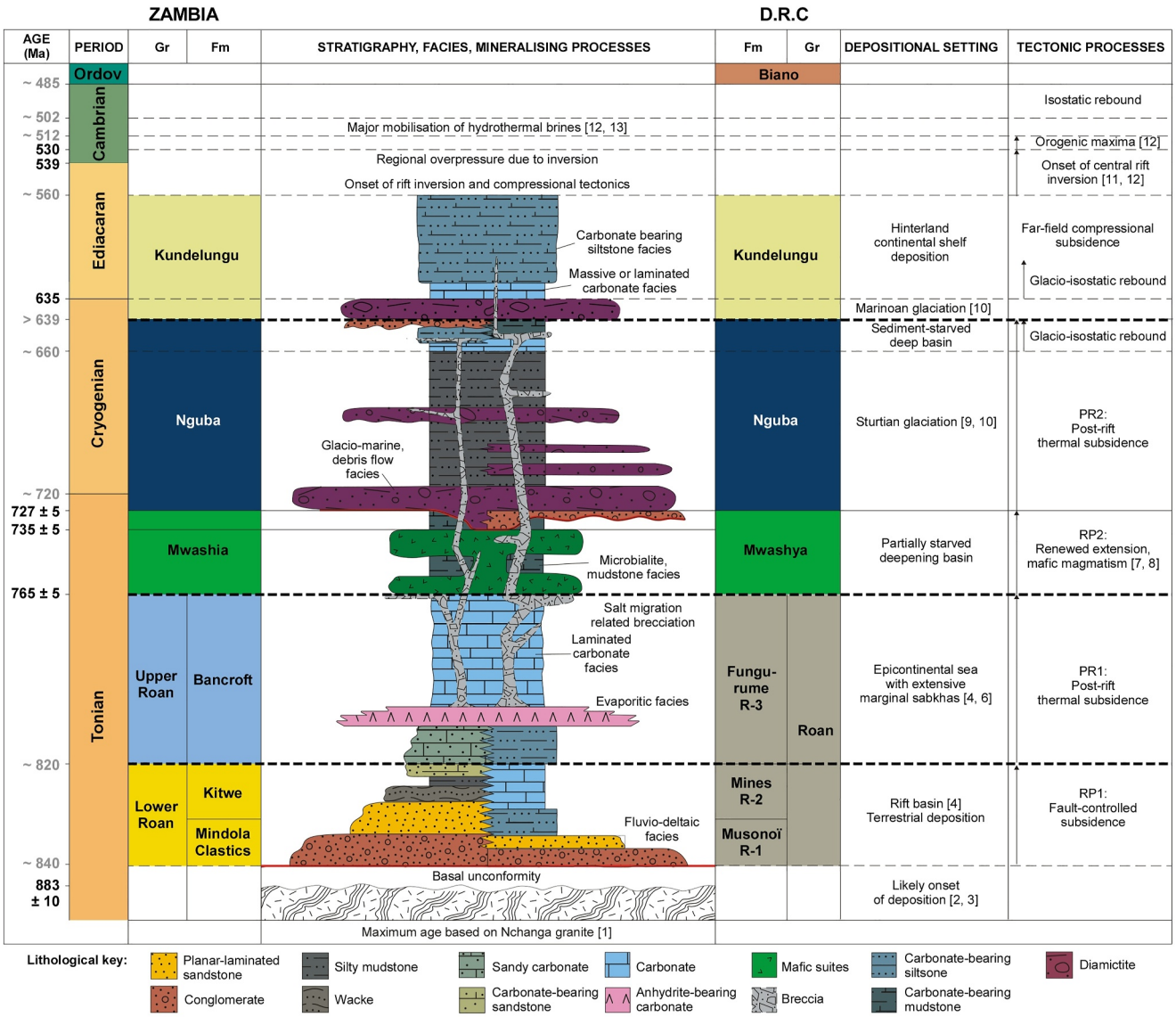

Figure 4. Katangan basin lithostratigraphic summary. Schematic stratigraphic column representing the Katangan basin lithostratigraphic nomenclature and general facies distribution. The southern part of the basin is on the left and the northern on the right. Stratigraphy and facies are represented in the central column with gross depositional environments and tectonic processes outlined on the right. On the left margin are stratigraphic ages from Cohen et al. (2018). Reference numbers referred to: [1] Armstrong et al. (2005), [2] Selley et al. (2018), [3] Cahen et al. (1970), [4] Selley et al. (2006), [5] Muchez et al. (2015), [6] Binda (1994), [7] Key et al. (2001), [8] Kampunzu et al. (2000), [9] Rooney et al. (2015), [10] Halverson et al. (2020), [11] John et al. (2004), [12] Daly et al. (2020), [13] Torrealday et al. (2000).

3.1.1. Subsidence Analysis and Backstripping Methodology

Quantitative subsidence analysis allows the filling of a sedimentary basin to be quantified and basin formation mechanisms to be constrained. Thicknesses of stratigraphic units at the time of deposition are modified by the effects of subsequent sediment-loading and compaction. To see through this complexity, the process of back-stripping (Watts & Ryan, 1976) allows present-day stratigraphy to be corrected for the effects of sediment and water-loading. This allows basin subsidence to be partitioned into subsidence driven by sediment loading, and subsidence driven by tectonic forces (Steckler & Watts, 1978; Watts & Ryan, 1976). By isolating tectonic subsidence, comparisons can be made between different basin subsidence profiles and history. Different basin formation mechanisms create distinct tectonic subsidence profiles, with, for instance, rift basins being characterized by a concave profile of initially rapid tectonic subsidence which reduces exponentially as rifting attenuates and subsidence driven by mantle cooling takes over (McKenzie, 1978; Steckler & Watts, 1978; Xie & Heller, 2009). McKenzie (1978) developed the uniform extension model to quantify several aspects of rift evolution,

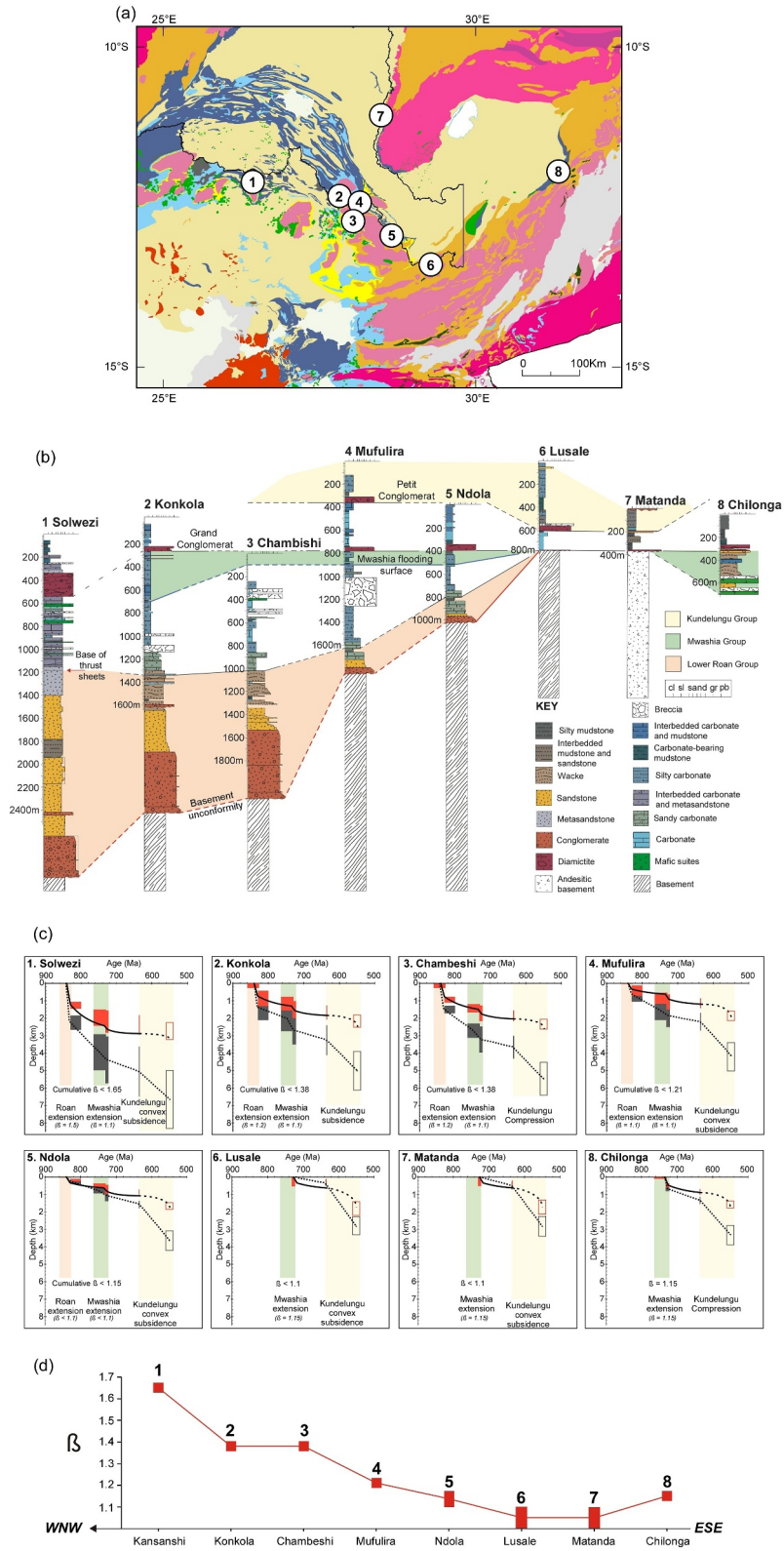
(a)
25°E
30°E
10°S
15°S
0
100Km
1
2
3
4
5
6
7
8
(b)
1 Solwezi
2 Konkola
3 Chambishi
4 Mufulira
5 Ndola
6 Lusale
7 Matanda
8 Chilonga
Grand Conglomerat
Petit Conglomerat
Mwashia flooding surface
Base of thrust sheets
Basement unconformity
Kundelungu Group
Mwashia Group
Lower Roan Group
cl si sand gr pb
KEY
Silty mudstone
Interbedded mudstone and sandstone
Wacke
Sandstone
Metasandstone
Conglomerate
Diamictite
Andesitic basement
Breccia
Interbedded carbonate and mudstone
Carbonate-bearing mudstone
Silty carbonate
Interbedded carbonate and metasandstone
Sandy carbonate
Carbonate
Mafic suites
Basement
(c)
1. Solwezi
2. Konkola
3. Chambeshi
4. Mufulira
5. Ndola
6. Lusale
7. Matanda
8. Chilonga
Age (Ma)
Depth (km)
Roan extension
Mwashia extension
Kundelungu convex subsidence
Kundelungu Compression
(d)
ß
WNW
ESE
Kansanshi
Konkola
Chambeshi
Mufulira
Ndola
Lusale
Matanda
Chilonga

Figure 5.

including associated crustal thinning and subsidence. The uniform extension model invokes two stages of rift basin development: rapid initial fault-controlled subsidence, followed by thermal subsidence as the underlying stretched lithosphere cools. Combined these two stages define the characteristic concave-up tectonic subsidence profile observed in many rift basins (Steckler & Watts, 1978; Xie & Heller, 2009).

Core logging and facies analysis was carried out at eight Katangan basin locations (Figure 5). Type logs were established from detailed facies analysis on a primary core and augmented from adjacent cores and outcrop sections. Decompaction of sedimentary columns and 1-D back-stripping was performed assuming Airy isostasy and analogue petrophysical parameters (Allen & Allen, 2013; Sclater & Christie, 1980; Turer & Maynard, 2003). The calculations involved in decompaction, and back-stripping of sediment columns are well-established (Allen & Allen, 2013; Steckler & Watts, 1978; Watts & Ryan, 1976). The eustatic term in the back-stripping equation was omitted due to there being no reliable and continuous sea level curves for the Neoproterozoic.

The uniform stretching model (McKenzie, 1978) was applied to estimate stretching (β) factors that best fit the tectonic subsidence profiles generated from back-stripping. It was assumed that the fault-controlled subsidence phase lasted 10 Myr (Veevers, 1981) and that the Lower Roan to Upper Roan transition represents the onset of thermal subsidence. Mwashia stretching factors were calculated using the stretched crust at the end of Roan rifting as the starting conditions for Mwashia extension. The type logs and parameters that were used in back-stripping and to compute stretching factors, are provided as supporting data (Supporting Information S1: Stratigraphic logs used in basin subsidence analysis).

3.1.2. Katangan Basin Subsidence Results

Back-stripping of the type logs shows a clear trend of tectonic subsidence increasing across the strike of the basin from east to west, Chilonga to Solwezi (Figure 5a). This trend is particularly clearly developed in the four deepest cores (Figures 5b and 5c). In most of the cores and their associated type logs, evidence of two distinctive rift phases is also present, indicating an initial Lower Roan rifting event and a later Mwashia rifting event.

The eight type cores show a clear increase in total subsidence from low in the northeast (Chilonga and Matanda) to higher in the west (Konkola and Solwezi) (Figures 5c and 5d). Cores with the thickest Lower Roan section in the west have the most pronounced concave-up subsidence signature during Roan extension. Initial subsidence during Roan extension was highest in the furthest west core from Solwezi, with the basin likely developing a syn-rift section greater than 2 km thick during the Lower Roan. Where Lower Roan clastic units are thinnest (<100 m) near Ndola the Roan tectonic subsidence signature is most poorly developed, with minimal Lower Roan extension. The Konkola and Chambishi type logs show an intermediate Roan subsidence profile, (Figures 5c and 5d) with the basin subsiding to a depth of up to 1.5 km during the Lower Roan.

Best-fit β-factors match this trend in the associated tectonic subsidence profiles, with the degree of crustal stretching increasing to the WNW from Ndola to Solwezi (Figure 5d). The Solwezi Region shows the highest degrees of Roan extension, 40% (β-factor of 1.4), whereas in Lubambe this is reduced to 20% (β-factor of 1.2). Around Ndola, the tectonic subsidence during Roan extension is small with a β-factor of a maximum of 1.1.

Mwashia extension is evident in all eight cores, however, due to the deepwater facies, the results are more uncertain that the Lower Roan. The tectonic subsidence recorded is of a lower magnitude than during Roan extension and has a smaller range. In Solwezi and Lubambe, a β-factor of 1.1 fits the tectonic subsidence profile during Mwashia extension. It may have been significantly higher in Solwezi, however, the later nappe emplacement removed the full Mwashia section making the measured outcome a minimum. In Ndola the Mwashia extension is recorded in core, but the magnitude of extension is <10% suggesting crustal stretching during Mwashia times was small to the east of the Kafue anticline. In contrast the basin to the west of Kolwezi (Kennedy et al., 2019) and the northeastern

Figure 5. Analysis of the Katangan basin formation. (a) A map showing the locations of the eight "type logs" that have been used to determine the nature of basin subsidence and its distribution. The locations were chosen by the availability of deep, diamond drill cores, that were then integrated with adjacent data to construct a local "type log." (b) The eight type logs constructed for the basin subsidence analysis. (c) The subsidence profiles of the eight type logs show the total subsidence profile (lower line) and the tectonic subsidence component (upper line). Error bars are included. The yellow and green columns highlight the Roan and Mwashia rifting event respectively. (d). The chart shows the distribution of the calculated extension factor for the eight locations. It demonstrates the increase in cumulate extension from the eastern margin of the basin to the central rift zone where cumulative lithospherical extension is ≥70%. The data also shows that the SE margin of the Bangweulu craton at Chilonga has experienced Mwashia extension.

Chilonga area of Zambia (Figure 3) have thick Mwashia sections preserved implying much greater Mwashia age extension of a minimum of 15% in Chilonga (Figures 5c and 5d) and even greater west of Kolwezi. In both the east and western areas basaltic flows are associated with the Mwashi extension (Figure 3).

3.1.3. Katangan Basin Formation

Despite the limitations of the uniform extension model and 1-D Airy back-stripping, and water depth estimations from facies analysis, the form of tectonic subsidence profiles and best-fit β-factors provide satisfactory first-order results with significant implications. The concave-up tectonic subsidence signatures of the back-stripped cores and their good agreement with McKenzie's (1978) uniform extension model support and quantify a rift origin for the Katangan Basin in Zambia. Lower Roan β-factors of 1.4 and 1.2 for Solwezi and Lubambe, respectively, match those of well constrained rift systems, such as the North Sea, Baikal rift and Oslo Graben (Barton & Wood, 1984; Huismans et al., 2001).

The increasing magnitude of tectonic subsidence and crustal stretching from the eastern margin of the basin toward the CRZ of Solwezi is clear (Figure 5d). The Lusale, Matanda and Chilonga areas are apparently less affected by Roan extension, with a Roan tectonic subsidence signature characteristic of only distal extensional tectonic regimes (Xie & Heller, 2009). The Ndola, Chambeshi, Konkola and Solwezi areas show increasingly high degrees of extension. Solwezi, at the deepest part of the preserved basin and with a thickness of syn-rift Roan stratigraphy of ≥2 km, potentially had a pre-tectonic basin section of the order of 8–10 km.

Mwashia age extension appears to be generally less than in the Lower Roan and the resultant stretching estimates are more uncertain due to the deep-water facies dominating the stratigraphy. Although extensively present, the distribution of Mwashia extension and subsidence distribution also appears to be different from the Lower Roan, with the greatest extension on the northwestern flanks of the basin in the DRC (Kennedy et al., 2019) and the northeastern flanks of the basin in Zambia (Figures 5b–5d). This is evidenced by the fact that the magnitude of tectonic subsidence in IT26 (Figure 5b) during Mwashia extension is comparable to that during Roan extension. An alternative interpretation is that the basin became partially starved during the Mwashia extension and there was no immediate stratigraphic response and therefore record of stretching. What is recorded however, is a strong igneous association with Mwashia age rifting. This is arguably best developed along the northwestern boundary of the basin in the Lwawu area of Zambia, within the Nzilo basin of the DRC and along the eastern margin of the Kibaran Arch (Kampunzu et al., 1991, 2000). An equivalent Mwashia volcanic and gabbroic suite is indicated in the east of the basin where mafic rocks are found in the Chilonga and Serenje areas (Figures 3, 5a, and 5b). In addition, extensive volcanic and basic igneous intrusions occur throughout the CRZ during this period.

The analysis also indicates that the stratigraphic sections of the Upper Roan and the Nguba, developed between the rift phases, represent post-rift periods of continued subsidence due to the thermal relaxation of the previously stretched and thinned continental lithosphere (Figures 5c and 5d). In addition, the significant extension trend implied by the Solwezi result raises the question of whether the Katangan extension resulted in lithospheric break-up and the formation of an ocean basin. Deformation and high grade metamorphism to the southwest of Solwezi precludes further rift analysis via the subsidence analysis and back-stripping technique. The issue of mafic igneous activity and lithospheric break-up will be discussed further in The Discussion Section 5.

3.1.4. Katangan Rift Basin Geometry

Two significant data sets acquired in the Zambian Copperbelt over the last decade support the quantitative extension analysis presented above. Firstly, the drilling of the 2.5 km deep KRX082 diamond cored hole at Kansanshi mine and secondly, the acquisition of a 15 km long seismic reflection line near Konkola. These both demonstrate the basement rifting, its structural geometry, and scale to a degree not previously available. We will briefly discuss each of these data, our interpretation and the implication for rift formation and subsequent deformation.

A schematic cross section of the Solwezi Dome and through the location of the KRX082 collar (Figure 6a) shows a significant rift basin of half graben character. This interpretation is based on the thickening of the Roan syn-rift clastic section from 200 m around the Solwezi dome (Arthurs, 1974) to a minimum of 1,400 m about 10 km to the north (Figures 5b and 6a). The clastic facies at the base of the KRX082 section is not the characteristic conglomeratic section at the base of a typical Lower Roan profile and suggests at least another 100–500 m of clastic

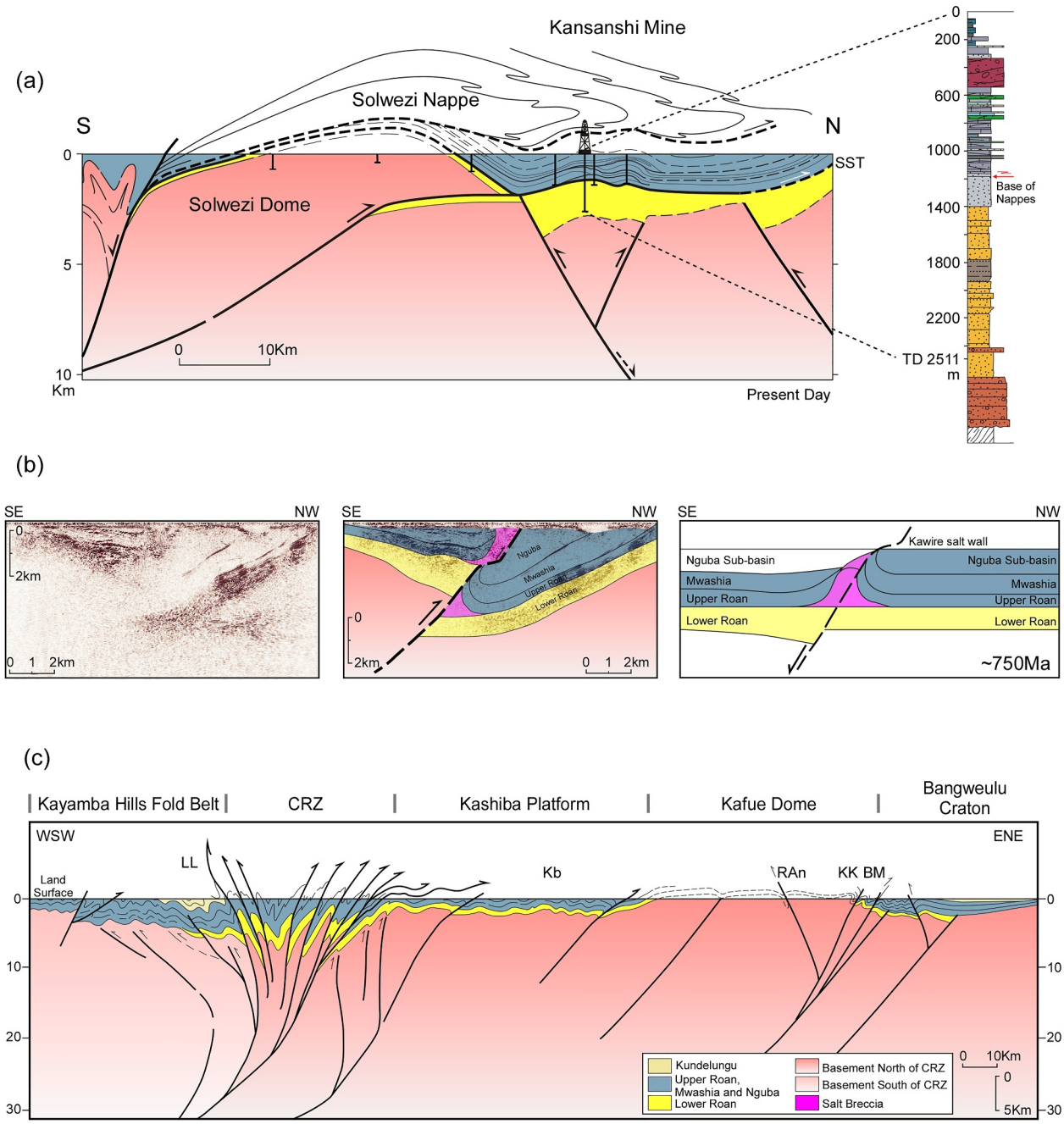

Figure 6. Extensional rift geometries in the Zambian Copperbelt. (a) A core and field constrained section of the Solwezi basement dome (Figure 3). Showing the Solwezi half graben containing a proven minimum of 1,400 m of clastic Lower Roan rock, and an estimated 2,000 m based on regional stratigraphy. This undeformed section is overthrust by the Solwezi nappe of recumbently folded garnet-amphibolite metasediments. The formation of the dome is due to a late reverse fault that elevates the basement. (b) A section across the Kawiri fault of the Konkola area (Figure 3), showing a pre-stack, depth migrated seismic line, an interpretation of the line and a schematic restoration of the interpretation. The basement cored fault that elevates the half graben is interpreted as an original extensional fault due to the Lower Roan thickening toward the fault. The magenta wedge in the hanging wall and foot wall of the Kawiri fault is interpreted as a breccia zone resulting from salt migration from the Upper Roan. Salt weld breccias occur in core and outcrop along the Kawiri fault zone. The seismic image is degraded below the breccia outcrop. (c) A field based schematic cross section from the Bangweulu craton to the Kayambe Hills fold belt (Figure 3 (18)). From the ENE the section crosses a largely undeformed Katangan section of the Bangweulu craton to the upright and ENE verging structures of the margin of the Kafue anticline and the Bwana Mkubwa (BM) and Koloko Kopie area (KK) (Figure 3). In the center of the Kafue anticline is the southerly verging Roan Antelope (RAn) syncline and then the regional westward dip of the Lower Roan clastics and Upper Roan carbonates of the Kashiba platform (Kb) (Figure 3 (17)). Deformation of these rocks increases to isoclinally folded, mylonitic marbles to the west where they dip sharply beneath the intensely deformed Luamala pelitic basin of Mwashia and Nguba age rocks. This deformed zone is bounded on the western side by the Lungu/Luamala thrust (LL) (Figure 3 (5)) where Upper Roan carbonates are thrust westwards over Nguba and Kundulungu age stratigraphy (Vajner, 1998b). The western fold zone of the Kayambe Hills is an upright fold belt of varying intensity (Figure 3 (18)).

section is likely. This implies a potential thickness of the order of ∼1.5–2 km of Lower Roan syn rift sediments. Also shown schematically in the profile is the allochthonous section of high-grade, garnet amphibolite rocks (Arthurs, 1974; Ridgeway & Ramsay, 1986). These high-grade metamorphic rocks are interpreted as being derived from a basin to the south of the Solwezi dome and emplaced over the dome's basement as a large nappe structure. The structure was later elevated by a thick-skinned basement thrust that creates the present Solwezi Dome (Figure 6a). A partial and total restoration of the section shows these rocks coming from a larger basin to the south. A feature coherent with the quantitative subsidence analysis results of highly extended crust and a deep basin to the south of Solwezi.

Similar to the core and outcrop-based rift interpretation of Solwezi, the Konkola post-stack depth migrated seismic data reveals an inverted rift basin of half graben geometry (Figure 6b). The NNW-SSE profile across the Kawiri sub-basin at Konkola (Figure 3) shows a basement rooted thrust fault elevating basement and a Lower Roan age half graben at the northern flank of the Kafue Anticline. The structural setting of the half graben, in the hangingwall of the Kawiri reverse fault, with the Roan section thickening into the fault, indicates that the thrust reactivated an earlier Lower Roan extensional fault dipping to the SE (Figure 6b). The reactivated Kawiri fault continues to join the Kafue fault zone that elevates the basement to form the Kafue Anticline, as interpreted by Coward and Daly (1984). To the NW the Katangan section is shown elevated by a blind basement thrust that also elevates and forms the exposed granitic basement of the Konkola Dome (Figures 3 and 6b). The rift basin interpretations from Solwezi and Konkola, are both data driven examples of rift basin geometry and stratigraphic change in the Katangan Basin. They complement the results of the quantitative crustal extension analysis by showing the structures resulting from the crustal extension. Both examples also exhibit the later impact of basement involved thrust tectonics and rift basin inversion.

These same structural themes are evident to the southeast of Solwezi and Konkola and are shown in the schematic cross section of Figure 6c. The section runs from east to west, from the margin of the Bangweulu craton to the edge of the Hook Granite Batholith and is also discussed in Section 4.1. The section shows the rift margin of the eastern flank of the Kafue Anticline inverted along the east facing Kafue fault zone, the Kafue Anticline and the Kabisha platform of deformed Upper Roan carbonates (Figure 6c). Further west this elevated stratigraphy dips abruptly into the intensely deformed, tightly folded and poorly exposed rift basin of the CRZ. Comprising a thick, highly deformed section of phyllites, the protoliths are interpreted as Upper Roan and Mwashia in age (Vajner, 1998a, 1998b). The western margin of this CRZ is marked by the Luamala Thrust (Vajner, 1998a, 1998b) that emplaces the Katangan sequence westwards toward the Kayamba Hills fold belt (Figure 3 (16)) that includes much younger stratigraphy (Figure 4). This inverted rift interpretation is compatible with the well exposed sections from each margin. The Kabisha carbonate platform displays the regionally present, intense, bedding parallel deformation fabric and localized isoclinal folding of bedding. This early fabric is folded by NW/SE trending open fold structures. Given this evidence of Tonian rift basin formation, and later intense inversion of the CRZ, we now outline our chronostratigraphic interpretation of the basin, how that supports the rift model and reveals the basin development through time.

3.2. Basin Chronostratigraphic Summary

The two Tonian rifting events, and their subsequent periods of thermal subsidence generated and accommodated the Katangan Supergroup. The subsequent, and genetically poorly defined Kundulungu Group does not appear to have a rift origin. Its subsidence profile (Figure 5c) is interpreted here as a result of marginal load driven subsidence. The stratigraphic impact of these subsidence events is shown in the tectono-stratigraphic chart of Figure 7 highlighting the major stratigraphic and structural features that have resulted from the formation of the basin. The section is drawn broadly west to east and is based on data from fieldwork and a series of publicly available well logs. The profile lies largely to the north of the Central Rift Basin (CRZ) where the constraints on stratigraphic age and distribution are widely available.

Traversing from west to east, the pyroxene gneiss of the margin of the Congo craton dated as ∼2,540–2,560 Ma intruded by Paleoproterozoic porphyritic granites dated at ∼2,050 Ma (Key et al., 2001). Across the whole profile similar Paleoproterozoic Bangweulu granites and volcanics are the most commonly exposed Katangan basement. In addition, Mesoproterozoic quartz arenites and schists of the Muva Supergroup (Daly & Unrug, 1982) lay unconformably on the Archean and the associated Paleoproterozoic granite basement. The Muva quartz arenites and siltstones show no metamorphism or penetrative deformation along the western flank of the Katangan basin

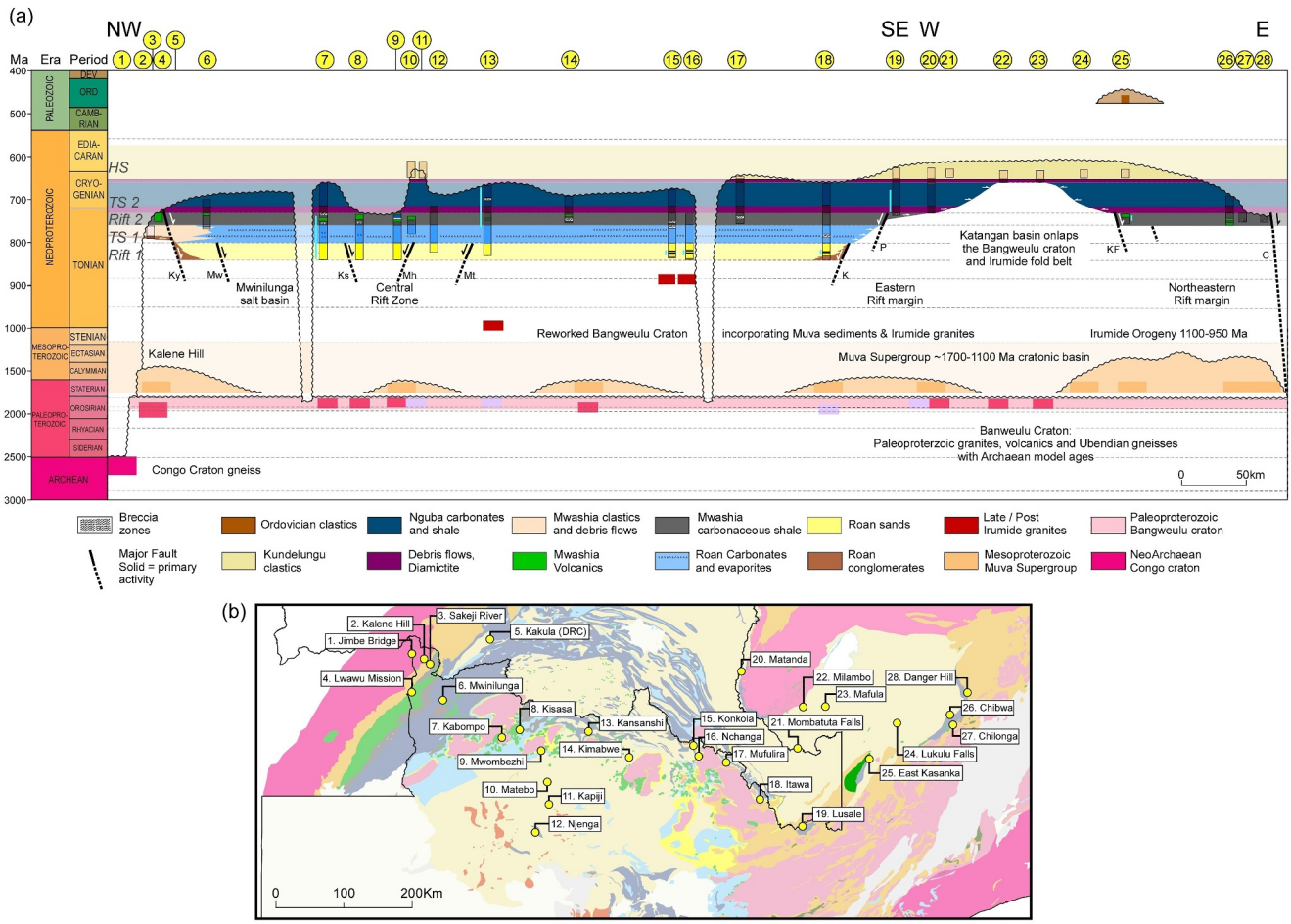

Figure 7. Katangan basin chronostratigraphy. (a) A west to east chronostratigraphic profile showing the stratigraphy and basement of the Katangan basin: the Congo craton gneiss and narrow Mwashia rift in the west; the Northern Rift and Central Rift with its eastern margin crossing the Kafue anticline and onlapping the Bangweulu craton to the point where Kundulungu sits directly on the Paleoproterozoic basement; the Mwashia aged rift on the eastern flank of the Bangweulu craton. (b) A regional map showing the localities of (a). Section localities: (1) Jimbe Bridge; (2) Kalene Hill; (3) Luawu Mission; (4) Sakeji River; (5) Nzilo basin; (6) Mwinilunga; (7) Kabompo Dome; (8) Kisasa; (9) Mwombezhi Dome; (10) Matebo; (11) Kapiji Village; (12) Mahebo; (13) Kansanshi Mine; (14) Kimabwe; (15) Konkola; (16) Nchanga; (17) Mufulira; (18) Mkubwa-Itawa; (19) Lusale; (20) Mutanda; (21) Mombatuta Falls; (22) Milambo; (23) Mafula; (24) Lukulu Falls; (25) East Kasanka; (26) Chibwa; (27) Chilonga; (28) Danger Hill.

and preserve many shallow water sedimentary features such as crossbedding and ripple marks (Key & Banda, 2000). At Kalene Hill (Figure 7b) these rocks are seen dipping gently (5–15′) to the east. They are in turn unconformably overlain by a thin, quartz conglomerate of the Katangan Supergroup, interpreted as an Upper Roan age clastic facies, onlapping the basin margin to the west. The Lwawu and Kanyama faults (Figures 2 and 7b) appear to be active during deposition of the Mwashia sediments and the coeval Lwawu Basalts and associated gabbroic intrusions on the western margin of the basin (Figure 3. Their age is estimated as ~765 Ma by Key et al. (2001). The Kanyama fault zone marks the western boundary fault of the major Lower Roan rift event and its connected structure. The Mwinilunga fault zone (Figures 2b and 7), marks the western margin of the thick section of the Mwinilunga Salt Basin (MSB) as demonstrated in the mapping of Liyunga et al. (2000). Minor indications of salt however, do occur up to ~30 km west of Mwinilunga.

To the east the section touches the Kabompo, Mwombezhi and Solwezi inliers of largely Paleoproterozoic Bangweulu granites with occasional Irumide age granites (Xu et al., 2022), and continues to the Kafue anticline (Figure 3). The eastern margin of the Kafue anticline is defined by the Kafue fault zone which, similar to the Mwinilunga fault zone, marks the edge of the thick Lower Roan basin (Figure 7a). Further eastwards, across the Pedicle fault (Figures 2 and 7), the Katangan stratigraphy progressively onlaps the Bangweulu craton. At the most central part of the Bangweulu craton, the Petit Conglomerat and Kundulungu stratigraphy sit unconformably upon

the Paleoproterozoic granites. The extensive, overlying Kundulungu arenites and shales indicate a third subsidence event of different and more regional impact than the earlier Katangan episodes. There is a broad age coincidence with the onset of distant compressional tectonic regimes to the east and west along the Mozambique and Namibian margins (Goscombe et al., 2020), with Kundulungu deposition. These distal compressional events may have instigated mid-continent, thick skinned thrusting and associated basin flexural subsidence. However, there is little evidence to support or deny this proposition. For now, we can be sure that the Bangweulu craton and most of the Katangan basin experienced subsidence and shallow water clastic and carbonate deposition after the Petit Conglomerat (Figure 4). What drove that subsidence remains to be established.

To the east of the central Bangweulu craton the Katangan basin reappears with what is interpreted as thin Upper Roan sediments and igneous rocks of Mwashia age onlapping from the south and east (Figure 7a). To the east of the NNE trending Kasanka fault (Figure 7a) the Mwashia section reappears with extensive basic volcanics comparable to the Nzilo area of the DRC. This Katanga section terminates abruptly due to uplift along major basement rooted faults of the Chilonga fault zone (Figures 7a and 7b). The occurrence of Mwashia stratigraphy with coeval basalts and volcanics shows a degree of rifting and associated subsidence (Figures 5b–5d). This would indicate the edge of another Katangan age basin to the east that has subsequently been eroded.

Finally, consideration of the basement rocks along the chronostratigraphic profile (Figure 7a), shows the Archean and Paleoproterozoic basement in the west is overlain by Muva and Katangan Supergroup stratigraphy. Moving eastwards, the Katangan basin basement, north of the CRZ and including the basement domal inliers, is dominantly of Paleoproterozoic Crosinian age (De Waele & Fitzsimons, 2007). These observations suggest that all of the major Zambian and DRC Copperbelt is underlain by a Paleoproterozoic magmatic complex contiguous with the Paleoproterozoic granite and volcanics of the Bangweulu craton. This postulation is compatible with Figures 2b and 3 and is further supported in the next section.

3.3. Katangan Sedimentary Provenance and Age

In this section we present the results of 3223 zircon U-Pb analyses from 46 field outcrop samples collected during five field traverses of the Katangan basin and Bangweulu craton Table 1. The U-Pb data is archived with the zenodo open access repository and can be accessed at https://doi.org/10.5281/zenodo.15573786. The specific purpose of this large data set is to identify within the Katangan basin, evidence of sediment routing, major changes in routing over time and to identify stratigraphic compartmentalization within the basin. The work builds on several publications that have used provenance analysis to constrain Katangan basement geochronology and specific aspects of Katangan stratigraphic development. De Waele and Fitzsimons (2007) illuminated the evolution of the regionally relevant Proterozoic igneous and volcanic rocks and Muva sediments of the Bangweulu craton. More recently (Alessio et al., 2019) have used similar analyses to argue for a southeastern extension of the Bangweulu craton and Muva Supergroup. Within the Katangan basin Kampunzu et al. (2005) and Masters et al. (2005) have used the technique to constrain sediment ages and provenance within specific parts of the DRC.

The well-established methodology of preparation, analytical process and isotopic result for each zircon is presented in supporting data (Supporting Information S1): Sediment provenance methodology for zircon U-Pb analysis). The interpretation of the results of the individual outcrop samples is presented and discussed below and supported by Figures 8–10. The location and the maximum age of source provenance for each of the samples is presented in Table 1.

3.3.1. Detrital Zircons: U-Pb Sediment Provenance and Maximum Age Data

Zircon age results and their interpretation are discussed with a focus on sediment maximum age and provenance to examine the sedimentary routing into and within the basin. Table 1 highlights the minimum age of the sample's zircon population and is therefore a constraint on the maximum depositional age of the rock sampled and a test of the stratigraphic grouping. The data sampling roughly followed two profiles across the basin, one NW/SE from Mwinilunga to Mumbwa (Figure 3) and a second along the basement inliers and domes of the Zambian Copperbelt and northeastwards to Mpika (Figures 3 and 8a). The full suite of analytical data is presented in graphic form as Kernel Density Estimate (KDE) charts (Vermeesch, 2012) in two formats, the entire data set in a single chart (Figure 8b) and as each individual samples (Figure 9a). An analytical assessment of the correlation between samples is represented on a multi-dimensional scaling (MDS) chart (Vermeesch et al., 2016) (Figure 9b). The

Tectonics

10.1029/2025TC008955

Table 1
The Provenance Data Set Identifying the 46 Sample Locations, Rock Types and Stratigraphy With the Maximum Depositional Age Noted

Column 1	Column 2	Column 3	Column 4	Column 5	Column 6	Column 7	Column 8	Column 9	Column 10	Column 11	Column 12
Sample_ID	Analysis	Sample_type	Coordinate_system	Longitude	Latitude	Lithology	Sample Weights (kg)	Maximum depositional ages	No. of analyzed zircons	No. of zircons used in KDE	Stratigraphy
Z01	Zircon U-Pb provenance age	Outcrop	LL_WGS84	24.2732	−11.2357	Hematitic arkosic metasandstone	3.1	1988 ± 12 Ma	30	30	Mwashya
Z02	Zircon U-Pb provenance age	Outcrop	LL_WGS84	24.2582	−11.3015	Arkosic metasandstone	5.715	1871.6 ± 0.7 Ma	100	63	Mwashya
Z03	Zircon U-Pb provenance age	Outcrop	LL_WGS84	24.3595	−11.7197	Arkosic metasandstone crosscut by speculraite veinlets	7.725	647.2 ± 2.2 Ma	62	37	Nguba
Z04	Zircon U-Pb provenance age	Outcrop	LL_WGS84	24.4426	−11.7527	Metasandstone with metasiltstone interbeds	2.4	722 ± 14 Ma	30	22	Nguba
Z05	Zircon U-Pb provenance age	Outcrop	LL_WGS84	24.4403	−11.813	Hematitic arkosic metasandstone	4.245	687.3 ± 2 Ma	100	73	Nguba
Z06	Zircon U-Pb provenance age	Outcrop	LL_WGS84	24.8612	−12.0176	Magnitite bearing diamictite	3.5	656 ± 25 Ma	80	74	Nguba
Z07	Zircon U-Pb provenance age	Outcrop	LL_WGS84	24.9093	−12.2923	Hematitic meta-quartz arenite	3.5	1375 ± 7	30	29	Lower Roan
Z08	Zircon U-Pb provenance age	Outcrop	LL_WGS84	25.4024	−11.9532	Quartz sericite talc schist	4	944 ± 8 Ma	101	82	Lower Roan
Z09	Zircon U-Pb provenance age	Outcrop	LL_WGS84	25.2964	−12.2597	Meta-sandstone channel in carbonaceous phyllite	9.29	732 ± 2 Ma	41	23	Mwashya
Z10	Zircon U-Pb provenance age	Outcrop	LL_WGS84	25.68	−12.4059	Hematitic quartz sericite schist with imbricated quartz pebbles	3.7	1099.7 ± 6 Ma	105	101	Lower Roan
Z11	Zircon U-Pb provenance age	Outcrop	LL_WGS84	25.6262	−12.4842	Quartz biotite schist	3.6	679 ± 7 Ma	40	39	Nguba
Z12	Zircon U-Pb provenance age	Outcrop	LL_WGS84	25.5885	−12.55	Calcareous quartz biotite schist	3.9	683 ± 2 Ma	101	60	Nguba
Z13	Zircon U-Pb provenance age	Outcrop	LL_WGS84	25.5576	−12.5832	Porphyroblastic phyllite, biotite porphyroblasts	3.8	765 ± 2 Ma	73	12	Mwashya
Z14	Zircon U-Pb provenance age	Outcrop	LL_WGS84	25.7054	−12.7303	Hematitic calcareous meta-arenite	3.8	601 ± 3 Ma	84	8	Kundelungu
Z15	Zircon U-Pb provenance age	Outcrop	LL_WGS84	25.7542	−12.8276	Meta-quartz arenite	3.8	629 ± 2 Ma	104	89	Kundelungu
Z16	Zircon U-Pb provenance age	Outcrop	LL_WGS84	25.7791	−13.0318	Arkosic metasandstone	4.24	632.5 ± 1.6 Ma	100	43	Kundelungu
Z17	Zircon U-Pb provenance age	Outcrop	LL_WGS84	25.7976	−13.12	Arkosic metasandstone	4.335	689 ± 18 Ma	66	60	Nguba
Z18	Zircon U-Pb provenance age	Outcrop	LL_WGS84	25.7396	−13.4572	Arkosic metasandstone	2.575	623 ± 14 Ma	67	56	Kundelungu
Z19	Zircon U-Pb provenance age	Outcrop	LL_WGS84	25.8876	−13.6179	Arkosic metasandstone	3.225	640 ± 14 Ma	60	45	Nguba
Z20	Zircon U-Pb provenance age	Outcrop	LL_WGS84	26.1703	−13.8877	Meta-sandstone	4.495	502.2 ± 2.9 Ma	51	23	Kundelungu

Tectonics

10.1029/2025TC008955

Table 1
Continued

Column 1	Column 2	Column 3	Column 4	Column 5	Column 6	Column 7	Column 8	Column 9	Column 10	Column 11	Column 12
Sample_ID	Analysis	Sample_type	Coordinate_system	Longitude	Latitude	Lithology	Sample Weights (kg)	Maximum depositional ages	No. of analyzed zircons	No. of zircons used in KDE	Stratigraphy
Z21	Zircon U-Pb provenance age	Outcrop	LL_WGS84	26.3581	−14.0083	Hematitic meta-quartz arenite	2.72	859 ± 13 Ma	100	77	Lower Roan
Z22	Zircon U-Pb provenance age	Outcrop	LL_WGS84	26.5684	−13.8834	Hematitic meta arenite	4.5	789.5 ± 2 Ma	110	108	Lower Roan
Z23	Zircon U-Pb provenance age	Outcrop	LL_WGS84	26.7501	−14.0463	Hematitic meta-quartz arenite	6.5	652.5 ± 0.9 Ma	111	108	Nguba
Z24	Zircon U-Pb provenance age	Outcrop	LL_WGS84	26.5221	−14.2749	Sub-arkosic metasandstone with hematite veinlets	3.51	608.9 ± 1.6 Ma	102	91	Kundelungu
Z25	Zircon U-Pb provenance age	Outcrop	LL_WGS84	26.7145	−14.2512	Hematitic meta-arenite crosscut by hemtite veinlets	2.9	633 ± 2 Ma	110	108	Kundelungu
Z26	Zircon U-Pb provenance age	Outcrop	LL_WGS84	26.5822	−14.3553	Meta-quartz arenite	8	619.1 ± 1.1 Ma	111	111	Kundelungu
Z27	Zircon U-Pb provenance age	Outcrop	LL_WGS84	26.7234	−14.6981	Sub-arkosic metasandstone crosscut by hematite veinlets	2.245	585.4 ± 2.9 Ma	100	91	Kundelungu
Z28	Zircon U-Pb provenance age	Outcrop	LL_WGS84	26.9913	−15.0392	Sericitic metasandstone	3.79	623.8 ± 1.5 Ma	100	83	Kundelungu
Z29	Zircon U-Pb provenance age	Outcrop	LL_WGS84	27.2128	−14.9964	Meta-quartz arenite interbedded with phyllite	4.25	664 ± 2 Ma	101	91	Nguba
Z30	Zircon U-Pb provenance age	Outcrop	LL_WGS84	27.2055	−15.1477	Quartz muscovite schistose conglomerate	4.365	774 ± 17 Ma	100	92	Lower Roan
Z31	Zircon U-Pb provenance age	Outcrop	LL_WGS84	27.628	−15.0167	Hematitic metasandstone interbedded with siltstone	3.31	699.7 ± 1.6 Ma	101	68	Nguba
Z32	Zircon U-Pb provenance age	Outcrop	LL_WGS84	27.7619	−15.202	Quartzite	2.865	754 ± 33 Ma	60	34	Mwashya
Z33	Zircon U-Pb provenance age	Drillhole	LL_WGS84	26.451887	−12.083702	Calcareous metasandstone	1.77	705 ± 23 Ma	60	59	Mwashya
Z34	Zircon U-Pb provenance age	Drillhole	LL_WGS84	26.43214	−12.106977	Metasandstone	3.25	1074 ± 23 Ma	60	58	Lower Roan
Z35	Zircon U-Pb provenance age	Outcrop	LL_WGS84	26.384078	−12.133312	Quart biotite schist	9	609 ± 2 Ma	110	105	Kundelungu
Z36	Zircon U-Pb provenance age	Outcrop	LL_WGS84	26.412798	−12.433678	Meta-quartz arenite	2.945	876 ± 23 Ma	61	55	Lower Roan
Z37	Zircon U-Pb provenance age	Outcrop	LL_WGS84	27.692903	−12.325506	Arkosic metasandstone	5.75	874.1 ± 1.4 Ma	100	72	Lower Roan
Z38	Zircon U-Pb provenance age	Outcrop	LL_WGS84	28.6869	−13.0292	Metasandstone	3.915	984.6 ± 6.1 Ma	101	89	Lower Roan
Z39	Zircon U-Pb provenance age	Outcrop	LL_WGS84	28.9298	−13.4531	Arkosic metasandstone	5.075	789 ± 10 Ma	100	99	Lower Roan
Z40	Zircon U-Pb provenance age	Outcrop	LL_WGS84	29.3021	−13.3767	Cobble meta-conglomerate	5.64	740 ± 12 Ma	100	92	Mwashya

Tectonics

10.1029/2025TC008955

Table 1
Continued

Column 1	Column 2	Column 3	Column 4	Column 5	Column 6	Column 7	Column 8	Column 9	Column 10	Column 11	Column 12
Sample_ID	Analysis	Sample_type	Coordinate_system	Longitude	Latitude	Lithology	Sample Weights (kg)	Maximum depositional ages	No. of analyzed zircons	No. of zircons used in KDE	Stratigraphy
Z41	Zircon U-Pb provenance age	Outcrop	LL_WGS84	30.1103	−12.8265	Sericitic metasiltstone	3.825	629 ± 1 Ma	100	80	Kundelungu
Z42	Zircon U-Pb provenance age	Outcrop	LL_WGS84	30.4611	−12.5245	Meta-quartz arenite	3	692.8 ± 1.2 Ma	111	100	Nguba
Z43	Zircon U-Pb provenance age	Drillhole	LL_WGS84	31.348314	−11.947366	Metasandstone	3.5	717 ± 1.9 Ma	105	98	Mwashya
Z44	Zircon U-Pb provenance age	Outcrop	LL_WGS84	31.5152	−11.631	Conglomerate	2	853 ± 1 Ma	102	74	Mwashya
Z45	Zircon U-Pb provenance age	Outcrop	LL_WGS84	30.6793	−11.4406	Arkosic metasandstone	4.165	624.4 ± 1.3 Ma	101	45	Kundelungu
Z46	Zircon U-Pb provenance age	Outcrop	LL_WGS84	28.674	−10.1416	Metasandstone	4.665	765.7 ± 1.8 Ma	100	75	Mwashya

Note. The number of analyzed zircons, and the number used to define the KDE charts are also specified. Whilst results with a small number of zircon have a large uncertainty associated with them, we consider that releasing the data may be useful for future work on this topic. This detailed data behind this summary can be accessed at the zenodo repository at https://doi.org/10.5281/zenodo.15573786.

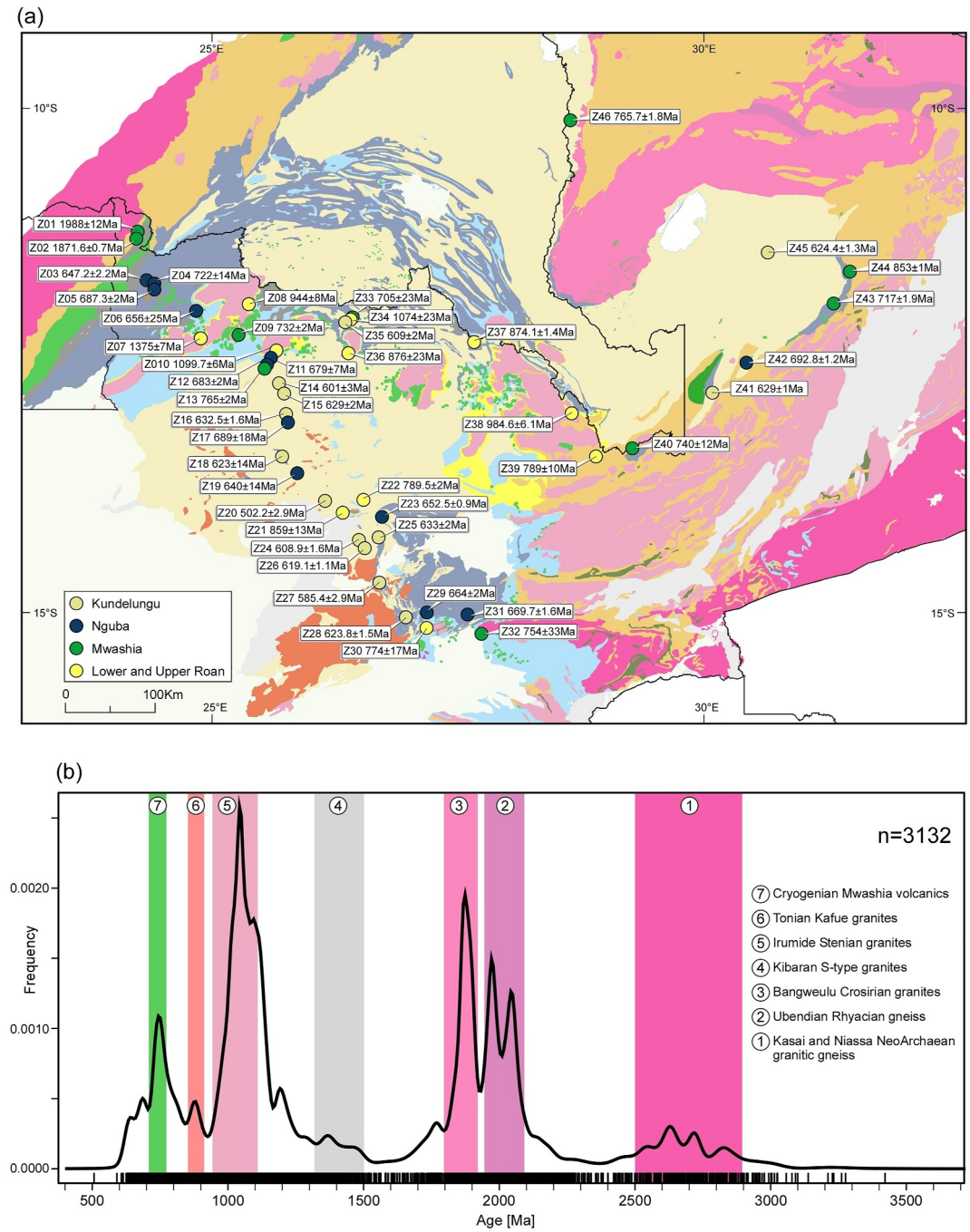

Figure 8. Detrital U-Pb Zircon maximum ages and age frequency chart of Katangan stratigraphy. (a) The geological map of the Katangan basin overlain with the U-Pb minimum provenance ages that define a maximum age for the stratigraphic location. (b) An age - frequency plot from the whole zircon provenance U-Pb age data set. The plot shows seven distinctive age groupings of zircons deposited as a component of the sedimentary fill into the basin. A Neo-archean unit that includes a tail of Meso-archean zircons. These zircons are dominantly found in the west of the basin with one isolated occurrence in the east. A Paleo-proterozoic unit that comprises a broad peak of ages form 1,800–2,100 Ma with an indication of distinctive contributions of 1,800–1,900 Ma ages and 1,950–2,100 Ma ages. These two represent sources from the Ubendian, Rhyacian metamorphic terranes to the north and the 1,800–1,900 Ma Crosirian, Bangweulu cratonic granites. Fourth, a small signal of 1,300–1,500 Ma, Ectasian zircons that appear to be coincident with the Kibaran S-type granites of the DRC to the NW (Tack et al., 2010). The fifth high-frequency peak is of ~950–1,100 Ma derived from the Stenian Irumide, syn and post tectonic granites (Johnson et al., 2005). This highest frequency peak reflects the granites of the extensive Irumide terrane exposed in the Muchinga mountain range. A sixth minor peak follows at 850–900 Ma, just prior to Katangan rifting. The final peak at 700–760 Ma indicates a widespread and voluminous mafic igneous event associated with Mwashia rifting.

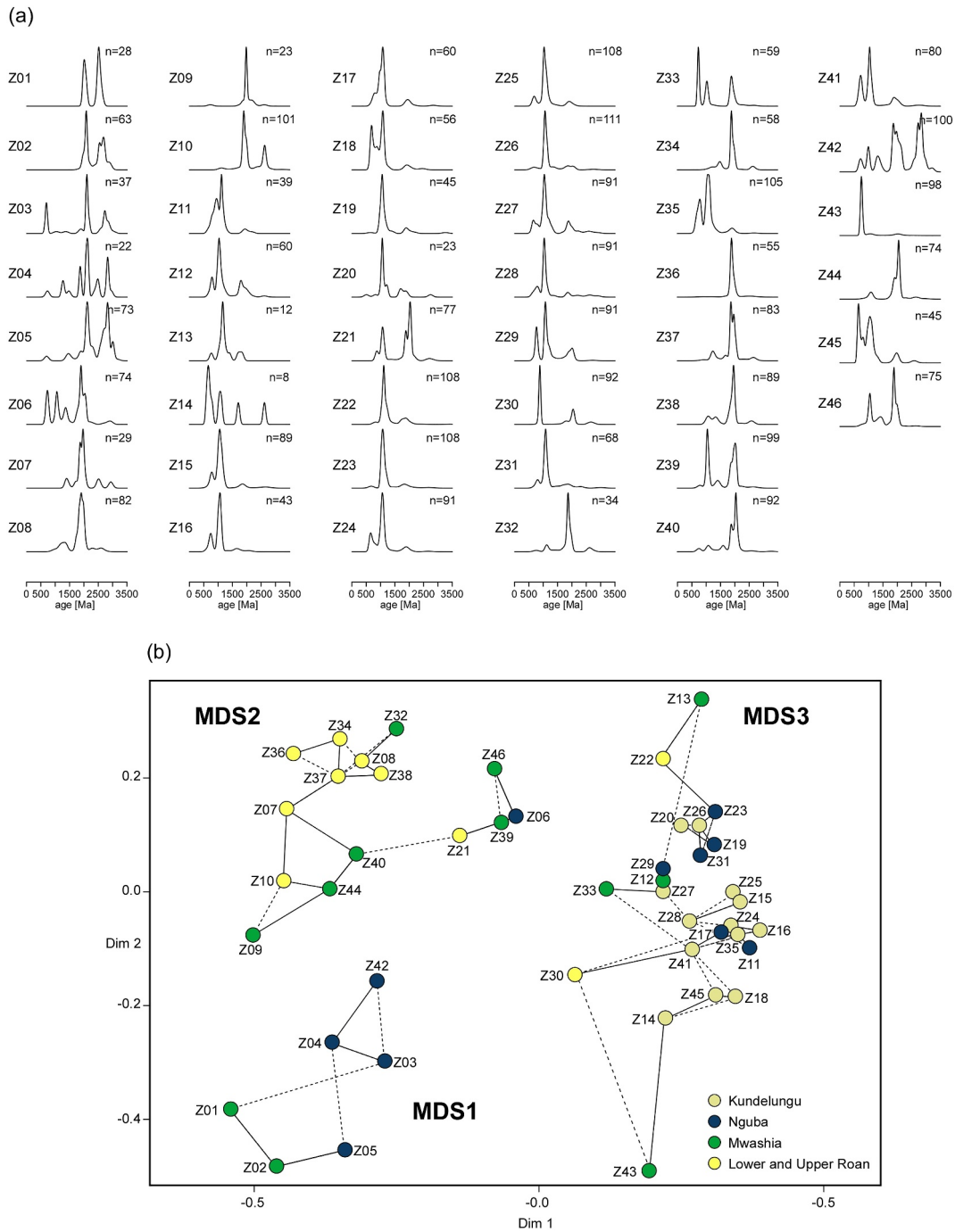

Figure 9. Graphical representation of the provenance data. (a) Shows the kernel density estimates (KDE) of the provenance data, highlighting the frequency distributions of each of the 46 samples. There are visibly different groupings within the charts that potentially indicate different provenance areas and different sediment routing systems. (b) Examines the visible differences by the multi-dimensional scaling (MDS) of the zircon age relationships and divides the samples into three major clusters. Within each grouping, sub-groups are also recognized that may indicate subtly different provenance changes. At the largest scale, three clusters are recognized: MDS1, characterized by frequent Neo-Archean ages that ends abruptly within the CRZ. MDS2, characterized by dominantly Paleoproterozoic ages of the Bangweulu craton: MDS3 characterized by both frequent Paleoproterozoic and Mesoproterozoic age zircons.

MDS chart is then examined for clustering and the geographic and routing interpretation of the cluster distribution (Figures 10a and 10b). The detailed data behind these charts is presented in tabular form in Supplementary file 2 (U-Pb zircon database).

The KDE data of Figure 9a shows three MDS clusters (Figure 9b) implying three provenance relationships at the basin scale. The MDS chart coloring in Figure 9b shows the stratigraphic unit the individual samples originate from. Cluster MSD 1 (Z01-05 & Z042 Figure 10) is characterized by a Neo-Archean and a Siderian zircon population peak and a Paleoproterozoic Orosirian (1,800 Ma–2,050 Ma) signature of the Bangweulu craton. Five of these Mwashia and Nguba samples are clustered in the far NW of the basin. The other (Z42) is from a location some 500 km to the east across the basin (Figures 8a and 9a). Given this large change and Archean gap, we interpret the six samples with Neo-Archean and Paleoproterozoic peaks as sourced from two distinct sources. The five samples in the west we conclude have a provenance in the Congo craton of the Kasai area of the DRC, and the sample in the east from the adjacent Niassa or Tanzanian cratons (De Waele et al., 2006). The northwestern sourced zircons were deposited in the MSB along the western part of the northern rift basin of the Katangan Basin (Figure 10). These data and their provenance interpretation are supported by the data of Rainaud et al. (2003) who recorded a range of Archaen aged zircons in the DRC part of the NRB. However, Rainaud et al. (2003) assumed the zircons represented a hidden, insitu, Mesoarchean basement source. In contrast we trace the ultimate source westwards into the known and proximal Congo craton (Figure 10a.). To the southeast the Archean zircon footprint reduces markedly by the Kabompo dome. (Z06 & 07) and ends in the CRZ area of the Kabompo and Mwombezi domes (Figures 8a and 10).

The MDS2 cluster (Figures 9b and 10) runs from the Kabompo/Mwombezi Dome area eastwards to Chilonga (Figure 7), across the CRZ and NRB of the Zambian Copperbelt to the southeastern edge of the Katangan basin. Samples of Roan, Mwashia and Nguba age are all dominated by KDE compositional spikes in the Paleoproterozoic Crosinian (1,800 Ma–2,050 Ma) with subordinate spikes from Stenian (1,000 Ma −1,200 Ma) Cryogenian and Tonian sources. This distribution indicates the oldest and dominant sediment source is from the Bangweulu craton granite and volcanic rocks. The frequent Stenian spikes reflect the late tectonic granitic magmatism of the Irumide orogeny (Daly, 1986a, 1986b; De Waele et al., 2006) and the Tonian sourced zircons from the pre Katangan granites (Armstrong et al., 2005; Rainaud et al., 2005).

As the majority of MSD2 samples are from Lower Roan stratigraphy, and the dominant underlying Katangan basement is of granites from the Bangweulu Crosinian or Irumide Stenian periods, it may be that these rocks have not traveled far. Rather, they are the erosional products of syn rift highs within the Katangan rift basin and have been locally derived. Alternatively, they may have come from the Bangweulu craton core to the NE where large areas of the Bangweulu craton remained exposed until the beginning of Kundulungu times (Figure 7). Sedimentary facies supportive of both interpretations are recorded in the Lower Roan. Proximal facies due to rift elevated basement drainage areas, and large fluvial drainage and marginal marine facies from the NE are evident. The latter implies a large fluvial fan of Bangweulu detritus passing southwestwards from the present day Bangweulu/Muchinga mountain area to the central rift zone and west to the Kabompo/Mwombezhi area (Figure 10a).

The third MDS3 trend (Figures 9 and 10) lies largely south of the CRZ. Nguba and Kundulungu clastics are the main zircon source rocks. The dominant characteristic between MDS3 samples is the strong Stenian (1,000 Ma −1,200 Ma) link of 1,000–1,050 Ma, Irumide age, granite sourced zircons in samples Z11 to Z35, with two later samples to the NE in sample Z41 from the Kundulungu Group and sample Z44 from the Mwashia Group. Equally striking is how the dominant Bangweulu craton zircons of the Northern Rift have all but disappeared to be replaced by late tectonic Irumide age zircons. By Kundulungu time the center of the Bangweulu craton and the Katangan basin generally (Figure 7) was well buried with little potential for exposed Bangweulu basement within it. Therefore we must look outside of the basin to the northeast and east for the source of these rocks to an exposed area of the Irumide Belt and its late tectonic granites (Daly, 1986a, 1986b; De Waele et al., 2006; Johnson et al., 2005). These granites are most prevalent in the Muchinga Mountain range today and we postulate that this was the source area for MDS3 zircons transported on proximal river and more distal marginal marine systems. This sedimentation and new exposure of the Irumide basement rocks was potentially associated with the onset of the early compressional tectonics discussed in Section 3.1.

In addition to these three distinct regional provenance and drainage system interpretations, two local data discoveries are relevant (Figure 10a). Firstly, zircon sample Z21 comes from a sub-arkosic arenite overlain by a

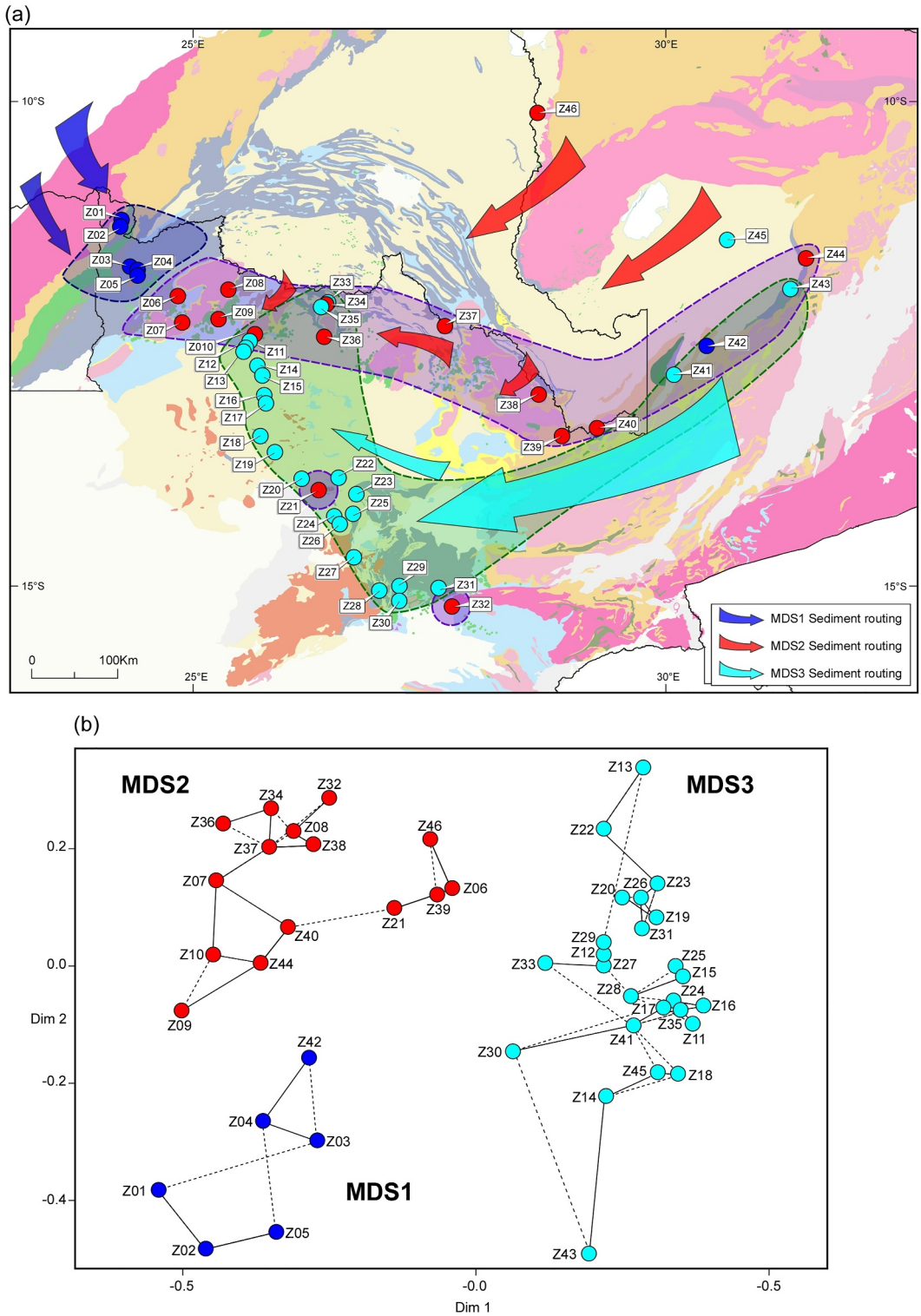

Figure 10. Sediment source areas, routing and potential intra basin boundaries. (a) The Katangan basin geological map shows the distribution of the three MDS clusters marked on the associated MDS chart (b). The distribution defines three distinct sediment pathways, one from the NW and two from the NE, that define the beginnings of a more comprehensive understanding of the formation of the basin and its paleogeography through time. (b) The MDS areas show paleogeographically the provenance data-clustering and regional relationships and one pronounced sediment routing boundary. The MDS1 cluster, characterized by frequent Neo-Archean ages lies west of the Kabompo/Mwombezhi area. This abrupt termination indicates that sediment sourced from the west has not been distributed further east than the CRZ area. The MDS2 cluster is dominated by Paleoproterozoic ages of the Bangweulu craton. Finally, MDS3 is characterized by both strong Paleoproterozoic and Mesoproterozoic frequencies during a mature time in the basin's development.

dolomitic section, exposed in a large upright to south verging anticline (Figure 10a). This sample of 108 zircons cluster with MDS 2 and reveals a maximum age of 859 ± 13 Ma. Although the error bar is large, the data indicates that this sub-arkosic arenite outcrop is a time equivalent of the Lower Roan clastics of the Copperbelt. As such it is the only area in the Southern Rift Basin (SRB) where unequivocal Lower Roan ages have been recorded to date. The overlying dolomite is potentially an Upper Roan equivalent, implying a full Katangan section is possible in the SRB. Such a full section has not been described or unequivocally discovered by drilling. Our result argues that further stratigraphic research is required in the SRB with a view to testing the deep stratigraphy and the presence or otherwise of an extensive Roan section.

Secondly, a quartz arenite sample (Z32) to the south of the Mwembeshi fault zone reveals a maximum age of 754 ± 33 Ma (Figure 10a). The sample clusters with MDS2 (Figure 10b), suggesting the rock has a provenance compatible with the clastic sediments of the Lower Roan facies, but is distinctively younger than the Lower Roan typical of the Katangan basin (Figure 4). The stratigraphic interpretation and its maximum age from zircon provenance analysis, suggests the rock represents an extension of the Katangan basin southwards, comprising a similar facies and provenance, but ~50 Myr younger. This result indicates a southward onlapping basin with time and will be discussed again in Sections 3.4 and 5.

3.4. Katangan Paleographic Development

The integration of the various aspects of the formation of the Katangan basin discussed above, show its footprint widening and deepening with time. This basin growth is evidenced by the two distinctive phases of crustal extension (Section 3.1), the extensive, onlapping, chrono-stratigraphic relationships described (Section 3.2) and the changing provenance and sediment routing pathways identified (Section 3.3). The basin growth is outlined sequentially through a series of graphics in Figure 11.

Figure 11a shows the extensional faults active during the Lower Roan rifting (R1) and the resultant depositional area from the associated subsidence. The early rifting was followed by thermally driven subsidence and drowning of the early rift architecture by an extensive Upper Roan marine carbonate-evaporite system (Figure 11b). This epicontinental environment deepened and widened further with the Mwashia period of extension (Figure 3 (R2)) and the association of an extensive igneous event of extrusive and intrusive mafic rocks of intraplate geochemistry (Kampunzu et al., 1991) (Figure 11c). Deposition during this event and the subsequent thermal cooling resulted in a significant expansion of the basin to the NW, N and NE. The igneous activity was also prevalent in the CRZ (Figures 3, 10c, and 12).

The overlying Kundulungu basin in contrast exhibits little to no unequivocal, intra-basinal, rifting activity. Its poorly constrained subsidence profiles are consistent with a convex upward profile that may indicate a load driven flexural basin forming mechanism (Figure 5). The base of the Kundulungu section, often represented by the Petit Conglomerat, lies unconformably on the Bangweulu basement on the Mporokoso Arch (Figure 7 locations 23 and 24). The time coincidence of the early ~630 Ma age of the initiation of the Kundulungu stratigraphy (Figure 4), and the regionally extensive Pan African collisions along the eastern margin of Africa is compelling (Goscombe et al., 2020). We therefore link the change in subsidence mechanism, from extension and thermal subsidence to crustal loading due to crustal thrust elevation of the marginal areas of the Katangan basin, as a result of distant collisional processes (Goscombe et al., 2020). The consequent subsidence resulted in the fine grained and shallow water clastic and carbonate facies of the Kundulungu Group. This trend culminates ~70 Ma later with the onset of focused north-south closure and deformation of the Katangan basin and the oblique inversion of pre-existing extensional faults (Figure 6) and ultimately the expulsion of the basin fill, localized metamorphism, and emplacement of the allochthonous nappes within the CRZ.

4. Tectonic Model of the Katangan Basin

4.1. Introduction

Post-dating the active rifting and passive, thermal subsidence processes discussed above, two further, significant tectonic processes have played major roles in the formation of the Katangan basin, widespread rift inversion with localized orogenesis, and halokenesis or salt tectonics. Most dominant regionally was the long and incremental process of compressional tectonics, commencing during the Ediacaran and more intensely and localized during the EoCambrian period (~550 Ma to 500 Ma). This event culminating in rift inversion, fold and thrust related

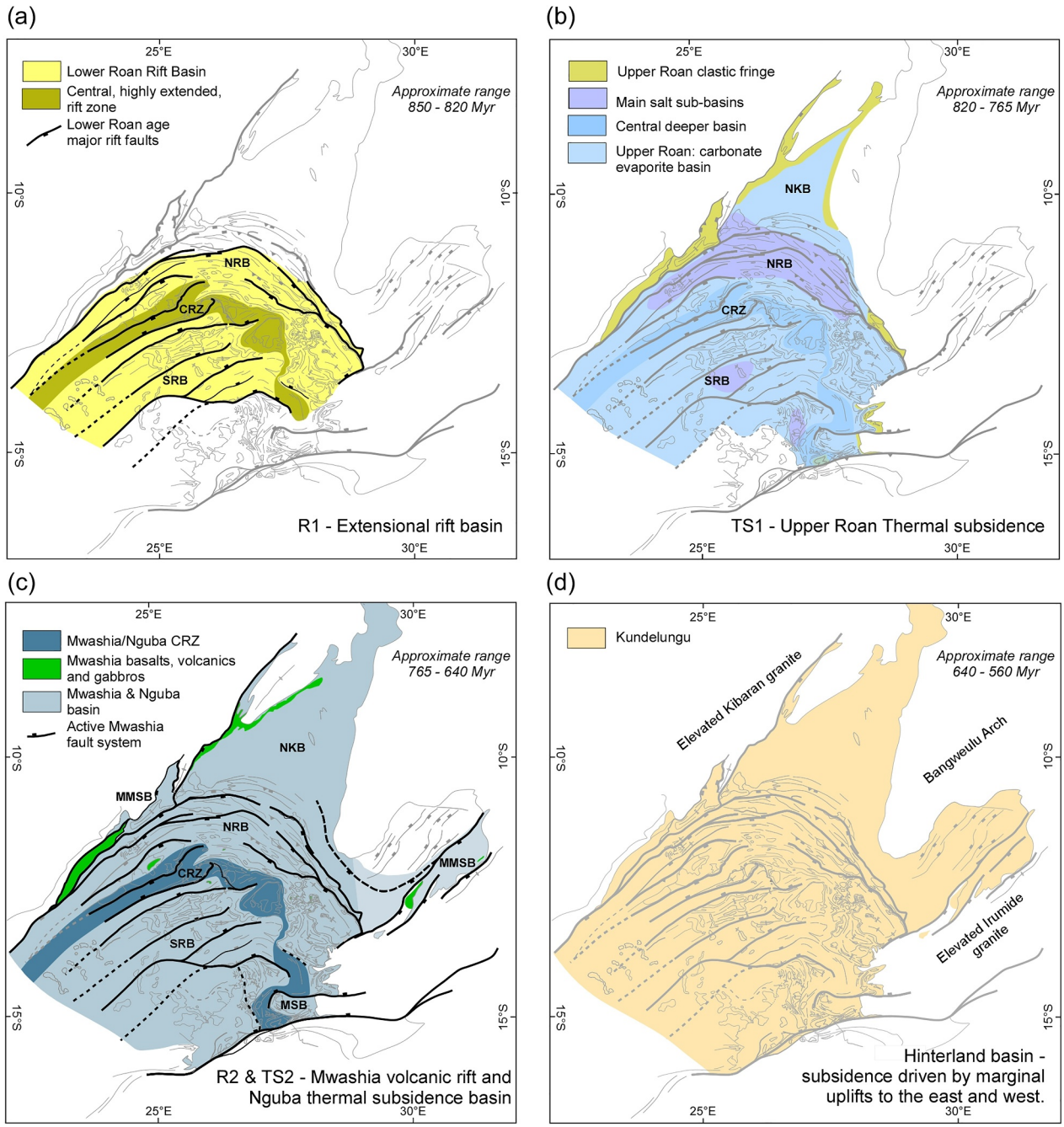

Figure 11. Basin growth through time. Paleo-stratigraphic distribution maps showing the episodes of Katangan basin formation and the expansion of the basin through time. Note Rift basin 2 and Thermal subsidence 2 are included in the 11c map. Abbreviations: NRB Northern rift basin; CRZ Central rift zone, SRB Southern rift basin; R1 and R2 Rift basins; TS1 and TS2 Thermal subsidence phases for the formation of the Upper Roan and Nguba passive subsidence basins. (a) An initial Lower Roan rift basin (R1) developed due to north-south extension during the early Tonian ~850–800 Ma. This resulted in a highly extended central rift zone (CRZ) and two broad, rifted areas; the Northern Rift Basin (NRB) to the north and southern rift basin to the south (SRB). (b) An Upper Roan period of passive thermal subsidence (TS1) covered and widened the rift basin and developed a large epi-continental, carbonate and evaporitic sea covering the Lower Roan rifts. (c) A second rift phase (R2) of Mwashia age (~765–730 Ma) and an Nguba period (~730–640 Ma) of further thermal subsidence (TS2) expanded the area of the Upper Roan sea. The Mwashia period was characterized by basin deepening and widening, with extensive volcanogenic phases at the basin margins and along the earlier formed Central Rift Zone. This Nguba thermal subsidence commenced as a deep water, sediment starved basin. It includes the Sturtian glaciation and the deep water debris flows locally known as the Grand Conglomerate. (d) The final paleogeographic unit is the geographically most extensive Kundulungu Group. It commences with a regional unconformity and deposition of the Petite Conglomerate. The lack of obvious rifting events and the indication of the subsidence profile being convex (Figure 5) suggests that this basin formed due to loading from marginal basement elevations of the Muchinga and Kibaran basement arches. Such "push down" basins are recognized in Central Asia and North America generated by collisional processes that elevate continental mountains on, often reactivated, crustal scale fault systems (Bader, 2019). Kundulungu deposition ceased as the Late Ediacaran orogenesis commenced around 560 Ma.

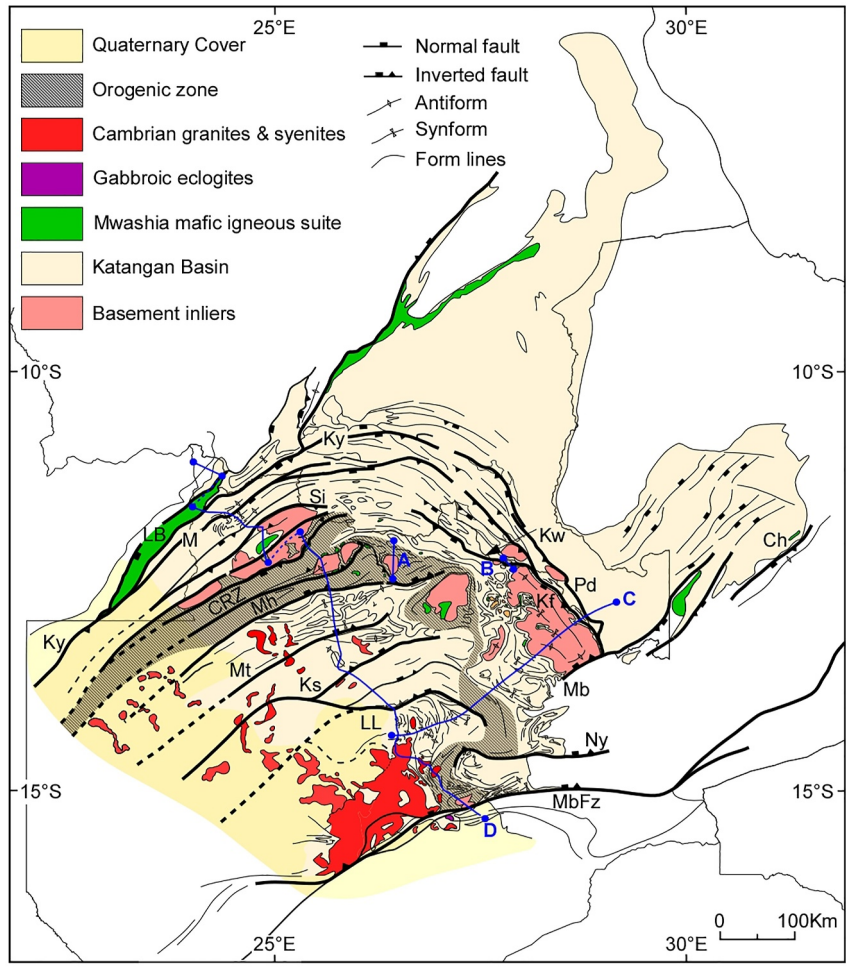

Figure 12. Katangan Basin Structural Map. Structural trend and fault map of the preserved portions of the Katangan basin, built from Geological Survey Department geological map (Thieme & Johnson, 1981) and field work undertaken during five field regional traverses between 2016 and 2021. The map highlights the major structures, basement inliers, representative basaltic, gabbroic, and andesitic volcanic units, and syn and post tectonic granite intrusions. Regionally significant fault zones and bedding trends are marked and define the tectonic domains discussed in the text. The blue lines A, B, C & D indicate the location of the four cross sections shown in Figures 6 and 13. Enboldened are the major fault zones of the basin: Ch, Chilonga; Kf, Kafue; Ks, Kasempa; Kw, Kawire; Ky, Kanyama; LB, Lwawa; LL, Lungu/Lamala; M, Mwinilunga; Mb, Mubulashi; Mh, Maheba; Mt, Matebo; MbFZ, Mwembeshi; Ny, Nyama; Pd, Pedicle; Si, Sialinga. The position of the central rift zone is labeled CRZ.

deformation and local high grade metamorphism. The deformation resulted in basement/cover imbrication and recumbent folding and thrusting of basement lithologies with Katangan metasediments (Coward & Daly, 1984). The arcuate form of the Katangan basin's structure, labeled the Lufilian Arc by Doorninck (1928), is a result of a series of thick-skinned, basement involved reverse faults, inherited from the Tonian rift basin structure. This reactivation is best recorded in Figure 6b, whilst thin skinned, bedding parallel detachments are also evident (Daly et al., 1984; Kampunzu & Cailteux, 1999; Porada & Berhorst, 2000). Garlick (1961) and Unrug (1983) argued that the arcuate shape was the result of marginal clockwise rotation during the Eo-Cambrian deformation. Unrug (1983) associated the rotation with large scale north vergent thrust sheets in the Kolwezi area of the DRC.

Based on detailed mine data from the Nchanga and Chambishi mines, and regional field data, Coward and Daly (1984) and Daly et al. (1984) demonstrated ENE/WSW crustal shortening by basement involved thrusts. These basement rooted thrusts verge dominantly ENE along the eastern flank of the Kafue Anticline and to the WSW along the western margin of the anticline. The anticline is terminated to the south by a SSE verging syncline along the Mubalashi fault zone (Figures 3 and 12). Porada (1989) extended the thrust tectonic model to the whole Katangan basin, describing it as a northerly vergent, asymmetric fold and thrust belt and adopting an Alpine

asymmetric model for the basin. Cosi et al. (1992) increased the thrust tectonic understanding with the recognition of basement cover imbrication in the Kabompo/Mwombezhi area. Kampunzu and Cailteux (1999) further extrapolated the model in detail to the DRC, interpreting thin skinned detachment folds and thrusts. The Porada and Berhorst (2000) deformational model is still used today (Eglinger et al., 2016; Selley et al., 2006).

Taking a metamorphic perspective on the compressional deformation of the Katangan basin, John et al. (2004) concluded that a metamorphic phase of high-pressure amphibolite facies conditions existed in the Domes region of Western Zambia. They attributed it to crustal thickening of the Katangan section resulting in pressure temperature conditions of ∼700°C and ∼10 kbar (John et al., 2003, 2004). This detail supported the earlier more regional observations of Ridgeway and Ramsay (1986) who identified an arcuate, amphibolite facies zone from the Kabompo to the Luswishi dome (Figure 3). The CRZ, identified from quantitative stratigraphy and structure in Section 3, coincides with this zone and indicates the existence of a large rifted basin prior to deformation and closure in the Cambrian.

The other major tectonic process significant in the basin came with the recognition of widespread salt tectonics in the NW by Jackson et al. (2003). Using geometric analogs from modern salt basins, Jackson et al. (2003) interpreted the complex structural geology of the western DRC as a product of northerly vergent thrusts and of large volumes of salt migration. Salt as the driver of much of the rock deformation in the DRC Katangan basin has been supported by the schematic sections of Selley et al. (2018) and the more detailed structural work of Twigg (2020). The latter showing the link between basement routed faults and salt perturbation and migration. We bring two new perspectives to the role of salt: the seismic reflection interpretation of Figure 6b and an interpretation from mapping conducted in the Mwinilungu area (Figure 15).

Considering these two tectonic processes, orogenesis and halokenesis, the context of the earlier rifting framework is critical to an understanding of the basin and its fluid pathways. We take a domain approach, defining areas of comparable rift, rift inversion and salt tectonics and their boundaries. The deformational processes are linked and are discussed as an integrated tectonic model that can be tested as the quantitative geological and geophysical database of the basin grows.

4.2. Katangan Basin Deformation and Its Tectonic Domains

The regional understanding of the Katangan basin's deformation is highly variable, with great detail available in the mined areas and much less data elsewhere over the majority of the basin. The basin wide, structural elements map and schematic cross section in Figures 12 and 13, present a new, holistic view of the basin. The map and section have been built from Geological Survey Department geological maps (Thieme & Johnson, 1981) and field work from five regional traverses between 2016 and 2021. Figure 12 shows the present-day area of the basin underlain by Katangan stratigraphy together with major fault zones, structural form-lines, basement inliers and an indication of the large volumes of Tonian basic rocks and the Ediacran and Cambrian Hook granitic batholith. The structural form lines and associated faults give an impression of the structural style of the basin, it's regional anisotropy and major discontinuities. The majority of the major fault zones were formed in the Katangan rift phase of the basin and influence the structural form that has resulted in the basins arcuate shape.

The western boundary of the basin is defined by the Katangan sedimentary section onlapping onto a basement of Mesoproterozoic Muva stratigraphy (Figure 6) and deeper, Paleoproterozoic and Archean basement (Key et al., 2001). Influencing this onlapping margin are the Lwawu, Kanyama and Mwinilunga fault zones (Figures 2, 12, and 13). The latter two fault zones are broadly traceable across the basin to the eastern margin of the Kafue Anticline (Figure 12). Within the basin a series of rifts are defined, the most deformed and metamorphosed being associated with the western, basement dome inliers.

The primary rift structure and bounding faults are shown in Figure 13 as a NW/SE geological cross section. There is little public data to constrain this section at depth. The figure uses CRUST1.0 (Laske et al., 2013) to estimate the moho depth and on this adds field data and our stratigraphic and structural interpretation. Figures 12 and 13 and their underpinning geology enable the breakdown of the Katangan basin into six structural domains and a granitic batholith (Figure 14) that enable a coherent and comparative discussion of the basin's structural and tectonic history.

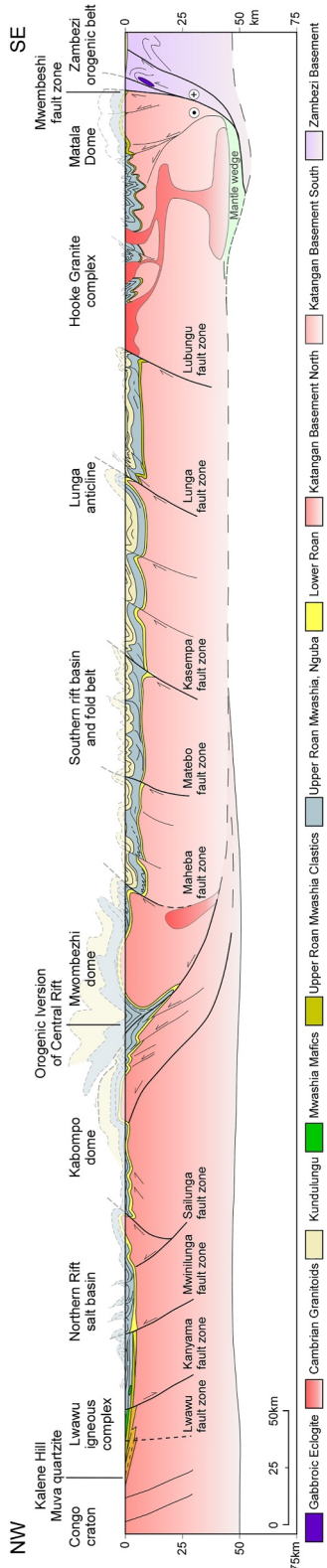

Figure 13. Basin cross section. A geological cross section of the Katanga basin, from Jimbe Bridge in the NW to the Mwembeshi Fault in the SE (Figure 12). The section demonstrates the Katangan sediments onlapping the western basin margin. The Lwawu, Kanyama and Mwinilunga fault zones define the 100–150 km wide, craton to rift basin transition zone. The Lwawa fault appears to be the source of the extensive Mwashia continental flood basalts that occur along the western margin of the basin. The Kanyama fault defines the point of Katangan sediments thickening into the basin and the edge of the thick salt basin that is the continuation into Zambia of the Kolwezi salt basin to the north (NRB). The ~50 km wide, intense deformation zone of the Kabompo and Mwombezi domes is interpreted as an orogenic inversion of the central rift zone (CRZ). The folded southern rift basin (SRB) is interpreted as a regularly spaced series of inverted, NW dipping extensional faults and associated folds, with the Lunga fault elevating the only outcrop of Lower Roan arenites in this central area. The Lunga fault (Figure 3) also marks the start of the deformed Nguba section of the Kayambe Hills (Figure 3), the western side of which is a slate and phyllite belt where the Hook granite cupolas and veins invade the phyllitic Katangan metasediments. The southern basin boundary used in this paper is marked by the northerly dipping fabrics of the Mwembeshi fault zone and the eclogitic gabbroic intrusions of the Zambezi orogen.

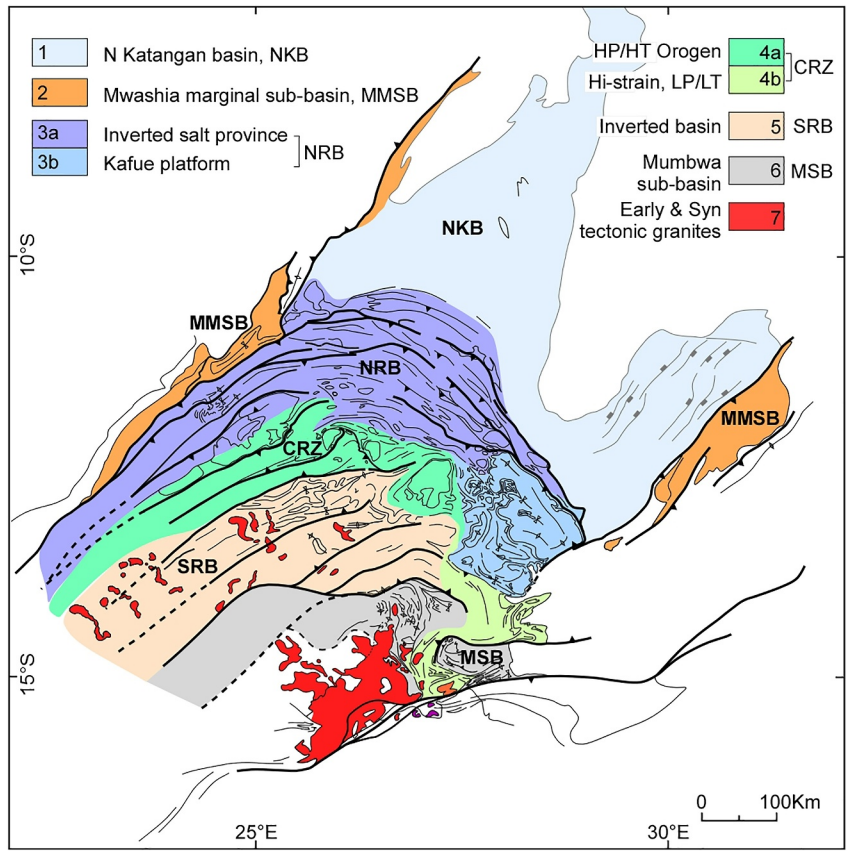

Figure 14. Katangan Basin Tectonic Domains. The tectonic evolution of the Katangan basin portrayed as 6 discrete tectonic domains and a granitic batholith emplaced into the Proterozoic basement and Katangan sediments. The domains describe the outcome of a complex and long-lived period of inter-cratonic, rift basin formation, localized orogenic scale deformation and regional inversion. The domains are colored and labeled in the legend: Northeastern Katangan Basin (NKB); the Mwashia marginal sub-basins (MMS); the Northern rift salt basin & Kabisha Platform (NRB); the Central rift zone and later orogen (CRZ); the Southern rift basin (SRB); the Mumbwa sub-basin (Mwinilunga Salt Basin); and the syn-tectonic granites of the Hook batholith and its outliers.

4.2.1. Domain 1: The Northeastern Katangan Basin (NKB)

The Northeastern Katangan basin (NKB) is the northeasterly extension of the basin into the Kundulungu plateau area of the DRC and the eastern flank of the Bangweulu craton (Figures 11 and 14). In the middle of the domain a NE trending and SW plunging basement arch divides the east and west parts of the basin (Figures 7, 11, and 14). The arch comprises Bangweulu craton granites and volcanics, overlain by Muva Supergroup sediments (Daly & Unrug, 1982) (Figure 7). The only significant deformation of the center of the craton is the NW/SW trending, Luongo fold belt of Irumide age that involves both ganitoid basement and Muva metasediments (Daly, 1984).

Whilst minor folds and thrusts of the Mwashia, Nguba and Kundulungu stratigraphy are developed within this large region, the Katangan sequence generally characterized at surface by sub-horizontal to gently dipping formations and a lack of penetrative deformation, metamorphism or evidence of regional salt movement (Figure 7). A NE/SW basement defined fabric exists beneath the Kundulungu Group on the Bangweulu craton (Figure 14), likely reflecting previous Irumide basement structure. The domain passes southeast and northwestwards into Mwashia aged marginal sub-basins of Domain 2 (Figure 14).

4.2.2. Domain 2: Mwashia, Basin Margin Sub-Basins

The NW and SE margins of the Katangan basin are characterized by a series of fault defined sub-basins of dominantly Upper Roan, Mwashia and younger stratigraphy (Figure 14) and are the sites of extensive basaltic volcanism and gabbroic intrusions (Kampunzu et al., 1991). The SE margin the basin is characterized by a

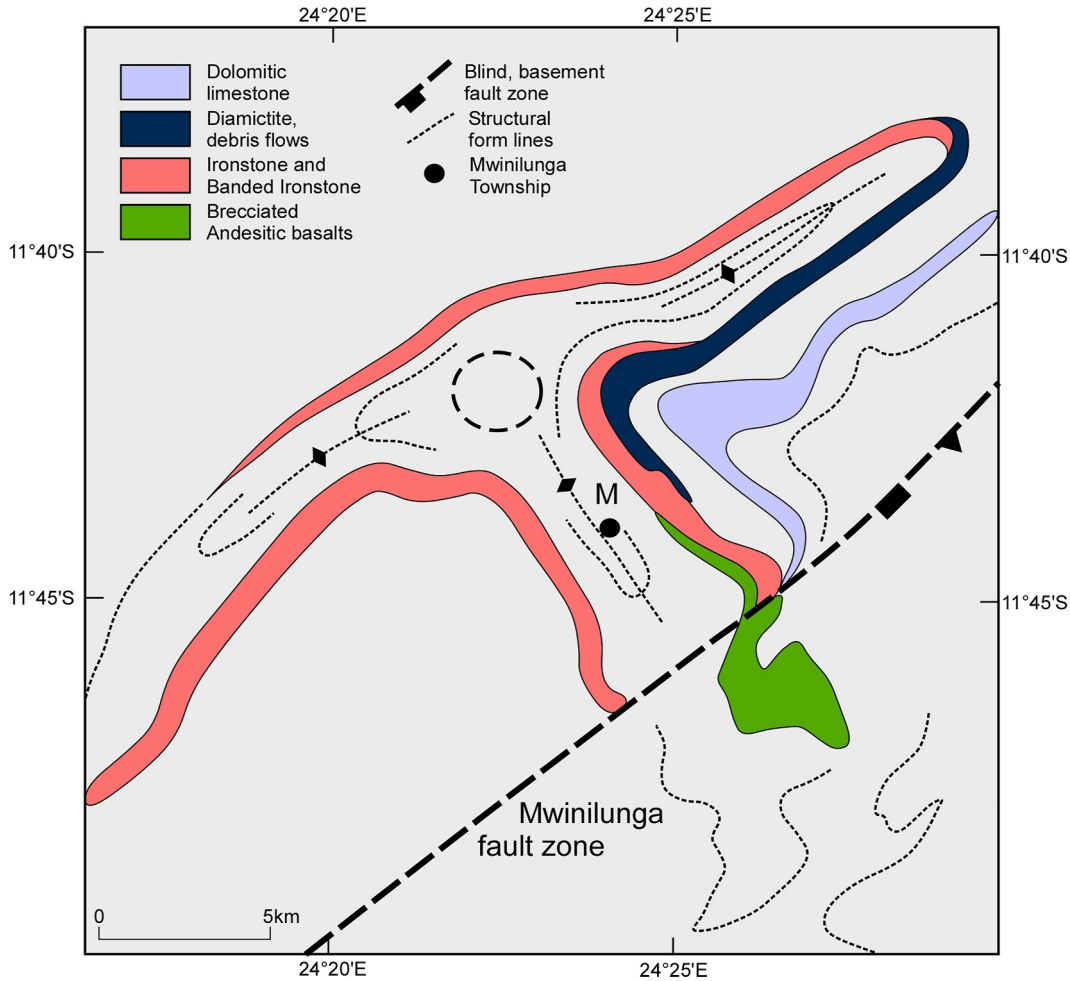

Figure 15. The Mwinilunga salt structure. Structural sketch map of the Mwinilunga radial fold structure The three-way structure is interpreted as radial salt-wall folds, converging on a central salt diapir. The salt structure interpretation is compatible with further complex folded features to the SE (Liyunga et al., 2000). To the NW the salt becomes less significant.

westward onlapping, eastward thickening Katangan section (Figures 7 and 14) with extensive basic igneous rocks recorded in the proximity of Chilonga (Figures 4 and 7 location 28) and Kasanka (Figure 7 location 26). This section terminates eastwards due to a series of NW facing monoclinal, basement cored folds that define the eastern edge of the basin today (Figures 7 and 13). A series of southeast dipping reverse faults along this margin elevate the Mesoproterozoic Irumide basement. These northwest facing monoclines are interpreted to be a result of the compressional reactivation of earlier, down to the east, Mwashia age normal faults formed during Katangan basin formation.

On the NW basin margin several comparable but larger, Mwashia age basins exist, fault and fold defined and with structural and stratigraphic similarities including extensive volumes of Mwashia basaltic volcanics and gabbroic intrusions. The rifts of this Domain occur to the west of the Kanyama fault (Figures 1, 12, and 14). In Zambia, west of the Lwawu fault, Katangan sediments onlap the Proterozoic and Archean basement in the Kalene Mission area. In the DRC the NW margin of the basin onlaps thick Mesoproterozic sediments. Similar to Zambia, Francois (1987) mapped a southeast facing monoclinal relationship with Mwashia correlated rocks overlying basement. The 20–60° dips of bedding to the SE indicates significant basement elevation, by a series of reverse, fault driven monoclinal folds of basement. This complex inverted margin is characterized by the southern Nzilo dome area where Mwashia and Nguba aged debris flows are described juxtaposed against large basement rooted fault zones (Twite et al., 2017).

This basin margin domain of Mwashia age rift basins (Figures 4 and 14) has extensive basaltic volcanism and intrusions (Figure 12) that pass upwards into thick sections of Nguba mudstones and debris flows. No clear evidence of significant volumes of salt have been recorded. The basins are developed upon coarse clastic sections of potentially Upper Roan and Mwashia age. The associated igneous activity suggests deep rooted basement fault systems were active on both the western and eastern faulted margins. A major difference between the western DRC margin and eastern Zambian margin is the latter is largely monoclinally defined. In contrast the western boundary is defined by a gentle, onlapping relationship between Katangan sediments and their basement.

4.2.3. Domain 3: Inverted Northern Rift (NRB) Salt Basins

Domain 3 (Figure 14) encompasses a large area of inverted rift basins (NRB) and extensive salt tectonics lying to the south of the NKB and north of the CRZ. Together with the western margin Mwashia sub-basins it is also the domain that hosts the majority of the large copper deposits of the basin. During the Upper Roan the Katangan basin was a large carbonate/evaporite, epicontinental, marine environment. Today none of the large volumes of mobile salt remain, however, the impacts of it are evident through stratigraphic and structural geometries, structurally displaced rafts of stratigraphy and structural fabrics such as the brecciated welds due to salt diapir, salt wall and salt nappe displacements. Although representing a contiguous tectonic domain, two sub-domains are outlined based on the degree of the basement involved inversion and salt activity (Figure 14). We introduce two new observations of salt activity, one interpreted from seismic reflection data in the Konkola area (Figure 6a) and the other from field observations in Mwinilunga (Figures 14 and 15). Otherwise, this brief description leans heavily on Jackson et al. (2003), Selley et al. (2018), and Twigg (2020). Each of the sub-domains of the NRB is discussed below.

4.2.3.1. Sub-Domain 3a Inverted NRB: Salt Driven Fold Belt With Basement Fault Inversion

Along the SW margin of the Bangweulu craton lie two, long, NW trending, basement rooted fault zones, the Kafue Fault (Kf) and the Pedicle Fault (Pd) (Figure 12). These fault zones typify the major structures of the NRB. They are interpreted as basement rooted, extensional faults (Figures 6b, 7, 12, and 14), reactivated into reverse and oblique-reverse structures during Ediacaran-Cambrian compressional deformation. The Kafue fault elevates the large and complex Kafue Anticline Coward and Daly (1984) and links to the Kawira fault (Figures 2, 6, and 12) and, to the very far west the Mwinilunga fault (Figures 2 and 12). Outboard of this fault lies the basement rooted Pedicle fault (Pd) that creates the Mokambe dome and can be traced through the DRC to link with the Kanyama Fault Zone (Figures 1, 12, and 14). In the hangingwall of these faults a full Katangan section occurs along the eastern margin of the Kafue anticline with the Lower Roan locally pinching out to the west over the center of the Kafue anticline and onlapping basement (Garlick, 1961). The Lower Roan syn-rift sediments onlap to the east and terminate east of the of the Pd (Figure 7).

Coward and Daly (1984) interpreted the Kafue Anticline as the product of the Kafue fault (Figure 12), a SW dipping, NE facing, blind, basement cored thrust fault. A major splay of this fault, the Kawire Fault (Figures 6 and 14), defines the NW termination of the Kafue Anticline. The seismic reflection data of Figure 6b proves this basement rooted, inverted extensional fault as an integral component of the Kafue Anticline extensional fault system. The more easterly Pd Fault zone elevates the Mokambe dome, and to the SE links with the Kf fault that defines the eastern edge of the Kafue anticline (Figure 12). Similar inverted extensional fault geometry interpretations can be applied to the Kafue Anticline as a whole. Frequent SW facing folds being a reflection of original antithetic, down to the NE extensional faults (Coward & Daly, 1984). Sub-Domain 3a continues to the northwest beyond where the Kafue Anticline plunges to the NW and basement inliers no longer appear. These major linear fault systems that define the Zambian and DRC Copperbelt continue to the NW for >250 km (Selley et al., 2006, 2018) and are traceable as contiguous, non-cylindrical, surface fold and thrust structures.

Two features stand out in this fold and thrust belt, the length of the two major fault zones and the abrupt change from deep basement exposure in the SE, to no basement exposure to the NW of Konkola (Figure 3). Defined by contiguous, individual fault structures for over 500 km, from Ndola to the Kolwezi area (Figure 3), the continuity and scale of these curvilinear fault zones suggests basement rooted structures penetrating deep into the crust (Cowie & Scholz, 1992). The degree of compressional deformation on those faults appears to be distinctly less to the NW of Konkola than to the SE, along the margin of the Kafue anticline where basement is significantly elevated. The seismic image of the Kawiri fault, north of the Kafue anticline (Figure 6b), shows a normal fault

reactivated to elevate basement to the surface. This basic structural model applies to the length of the Kafue fault along the eastern margin of the Kafue anticline (Figure 12).

As with the Kawiri interpretation (Figure 6b), we interpret the structures of the DRC as largely salt enhanced features, localized and triggered by movement on the regionally continuous basement faults of the Kafue/Mwinilunga and Pedicle/Kanyama fault zones (Figure 12). This interpretation is consistent with the work of Jackson et al. (2003), Selley et al. (2018), and Twigg (2020). The latter particularly showing the extensional faults associated with the salt driven structural complexity and folds of basement rooted faults.

Also within sub-domain 3a are areas where multiple diapirs and extensive salt walls have coalesced to from distinct sub-basins (Jackson et al., 2003; Selley et al., 2018). The evolution of the sub-basin formations are difficult to date precisely and are likely diachronous, starting to form with or soon after deposition of the evaporite basin of the Upper Roan. Examples of salt wall and diapir geometries, mapped on the basis of seismic data, current sub-basin structure and surface breccias, are clearly defined in the Konkola area of Zambia (Figure 6b) and along and between the major structures of the DRC Copperbelt, notably in the Kakanda region (Twigg, 2020). A similar radial, salt wall convergence is mapped by this work in the Mwinilungu area, in the hanging wall of the Mwinilunga fault zone (Figure 15). The salt wall feature is marked by the three tight, radial anticlines, interpreted as three salt walls, converging on a central salt diapir (Figure 15). In the area to the south of Mwinilunga, mapping by Liyunga et al. (2000) describes far more complex fold features that we also interpret as salt related features. We interpret this wide variation in salt style and complexity as largely a result of thicker areas of original evaporite deposition, and the presence of an irregular Katangan basement surface, such as a faulted graben that triggers salt instability. Such features appear to be exaggerated during the basin inversion as extensional faults reactivated as thrusts (Figure 6b).

Arguably the most complex salt dominated structures in domain 3a lie in the Kolwezi area (Figures 3 and 14). Large, detached blocks of Katangan stratigraphy of kilometric dimensions have been recognized for many years (Francois & Cailteaux, 1981) and are interpreted as having been transported by mobile salt (Jackson et al., 2003; Selley et al., 2018). The interpretation by Jackson et al. (2003) indicates a significant amount of tectonic shortening in the Katangan section directly linked to thin skinned thrust tectonics to the south. In contrast Selley et al. (2018) argues for a much smaller degree of tectonic shortening, attributing the same structures to largely salt migration. Suffice to say, movement of large salt nappes and tectonics dominate the structures of the Kolwezi area of the basin. This is interpreted as an indicator of original thick salt deposition and significant mobility from Upper Roan/Mwashia times onwards. The tectonic detail of the driver being salt or crustal shortening remains to be more precisely defined by subsurface imaging.

4.2.3.2. Sub-Domain 3b Inverted NRB: Major Basement Fault Inversion, Minor Salt Tectonics

Domain 3b covers the area of the Kafue anticline, it's associated basement inliers, and the extensive Katangan Kabisha platform area to the SW (Figures 3, 6c, 12, and 14). Whilst this area has localized indications of salt, most of the surface exposure lies at or below the stratigraphic source of the salt in Upper Roan stratigraphy (Figures 2 and 6). Consequently, little evidence of salt activity remains, except within synclinal remnants like the Chambishi syncline and the flanks of the Kafue anticline where the Mwashia and Nguba sections arguably record evidence of the salt activity. On the SW side of the Kafue Anticline the stratigraphy dips gently off the western flank of the Kafue anticline, defining a flat to west dipping area of Upper Roan carbonates called the Kashiba platform after a large carbonate sink hole (Figures 3 and 6c).

The Kashiba platform (Figure 6c) is intensely deformed to the west with a horizontal to gently dipping, bedding parallel S1 deformation fabric and an extensive area of isoclinally folded marbles (Figure 3). To the west the marbles become interleaved with steep to vertically dipping phyllites of the Mwashia and Nguba Groups that mark the transition to Domain 4b. To the north of the Kashiba Platform, a series of NE facing thrusts and SW facing back-thrusts occur in the Nchanga region defining the irregular outcrop pattern of the Nchanga area (Coward & Daly, 1984). The complex strain and cleavage patterns (Torremans et al., 2018) described in this area reflect the local kinematics driven by reactivating a pre-existing and complex rift fault system geometry. The schematic cross section of Figure 6c summarizes the east to west transition from the flat NKB of the Bangweulu craton, across the Kafue anticline to the Kashiba area and beyond. The section shows the basement cored Kafue Anticline and inverted Northern Basin passing into an increasingly intensely deformed flat lying Kabisha area of

Roan carbonates. This in-turn changing to the steeply dipping phyllite belt of the inverted CRZ and Domain 4 (Figures 6c and 14).

4.2.4. Domain 4: High Strain and Metamorphic Zone (HSZ) and Basement Domes

Domain 4 is an arcuate high strain zone (HSZ) that defines the southern boundary of Domain 3 and the northern boundary of Domain 5. The precise domain boundaries are ill defined due to their transitional nature and sparse outcrop. The Domain includes the four inliers of the Kabompo, Mwombezhi, Solwezi and Luswishi domes and lies to the southwest of the Kafue anticline. It comprises two sub-domains; a northern Sub-Domain (4a) of high strain and high-grade metamorphism of basement and Katangan metasediments; a southeastern Sub-Domain (4b) characterized as a high strain and low metamorphic grade extension of 4a (Figure 14).

4.2.4.1. Domain 4a: High Strain, High Grade Metamorphic Zone With Basement Domes

Sub Domain 4a bears a close resemblance to the metamorphic map of Zambia (Ridgeway & Ramsay, 1986) which shows a ~50 km wide zone of high grade, garnet amphibolite facies rocks, developed around the area of the four basement inliers. The metamorphic facies of Sub-Domain 4a decline along strike to the SE and become an intensely deformed low greenschist facies zone. More detailed and localized metamorphic studies corroborate this regional view (John et al., 2003 & 2004, Barron, 2003). The amphibolite facies rocks experienced deep orogenic burial during the Ediacaran/Cambrian time and were subsequently emplaced to the north over much lower grade rocks of the Solwezi area (Figure 6a).

The field work undertaken as a part of this study supports the generality of allochthonous, high grade metamorphosed Katangan metasediments occurring from the middle of the Kabompo dome to the eastern flank of the Luswishi dome (Figure 14). The lithologies bearing the high-grade mineral assemblages are also intensely deformed with a bedding parallel (S1) fabric developed in pelitic, psammitic and meta-carbonate rocks of the Katangan metasediments. The Solwezi area and core KRX082 demonstrates this thrust and metamorphic inversion relationship most clearly (Figure 6a). The KRX082 core shows high grade, garnet amphibolite facies deformed, folded and emplaced over undeformed, but compacted, clastic rocks of Lower Roan age. These Lower Roan rocks preserve primary sedimentary structures such as cross bedding and ripple marks. Similar sedimentary features occur at outcrop on the margin of the Solwezi dome at the Kifubwe Falls (Arthurs, 1974). The Solwezi thrust sheet is characterized by complex and intense, large, tight to isoclinal, recumbent folds (Arthurs, 1974; Barron, 2003) and best seen today in the main pit of the Kansanshi mine. This thin thrust sheet of high-grade rocks terminates to the north but outcrops around the Solwezi Dome to the south. The dome itself comprises a core of pre-Katangan crystalline basement of Paleo and Mesoproterozoic ages (Xu et al., 2022) and folds the early S1 Katangan tectonic fabric of the thrust sheet. The Dome is interpreted as a late stage, basement cored thrust sheet of relatively minor displacement (10–30 km) compared with the earlier and large displacement of the metamorphic thrust sheet (50–100 km). However, the basement cored nature of the late Solwezi thrust structure generates significant vertical topography of the basement/cover boundary zone. The kinematics of the emplacement of the high metamorphic grade rocks of the Solwezi thrust sheet have yet to be well determined. However, the termination of the Solwezi thrust sheets to the north toward the Chagwama Hills, and the extensive outcrops to the west and south with northward verging structures suggests a southern origin.

The zone of high metamorphic grade and intensely deformed thrust sheets can be traced both west and east from Solwezi. To the west they trend WNW and then swing around the northern tip of the Mwombezi dome to lie between and above the Kabompo and Mwombezi basement domes (Figure 14). From there it trends to the SW plunging below the Kalahari sands and toward Angola. The zone is clearly recognized on the eastern margin of the Kabompo zone where highly deformed Katangan meta-pelites, calc-schists and volcanics are imbricated with the basement (Klink, 1977). This narrow, 10–15 km wide synform comprises steeply dipping metapelites, intensely deformed volcaniclastic and locally, highly strained pillow basalts, above and to the east of the Kabompo Dome (Klink, 1977), together with locally mylonitized carbonates to the north of the Mwombezhi Dome. The basement cover contact zone around the Kabompo and Mwombezhi basement domes is marked by quartz, muscovite, kyanite, talc schists recording deep burial (John et al., 2004). The HSZ's fan-like structure, faces both to NW in the north and to the SE in the south, defining the edge of the Kabompo Dome and apparently surrounding the Mwombezhi Dome. This geometry is portrayed in Figures 12 and 13). To the east of Solwezi, the zone swings around north and south of the Luswishi dome, then trends south alongside the eastern margin of the dome. The

amphibolite facies metamorphic rocks are lost southwards of the Luswishi area where exposures are poor and reappear to the SE as low greenschist facies phyllites (Figure 6c).

4.2.4.2. Domain 4b: High Strain, Low Grade Metamorphic Zone

Sub-domain 4b starts southwest of the Kafue anticline where the zone thins and metamorphism has declined to middle to low greenschist facies. This steeply dipping HSZ continues to the south and southeast (Figures 12 and 14). Here the zone largely comprises vertical to steeply dipping phyllites that define the western margin of the Kabisha platform of flat lying intensely deformed Upper Roan carbonates of Domain 3b (Figures 3, 6c, and 14). To the west these high strain rocks of indeterminate age overthrust the Nguba and Kundulungu section of the Kayamba Hills along the Lumwala thrust zone (Figures 3 and 6c) described by Vajner (1998b). Along this boundary highly attenuated and asymmetric folds, locally of sheath fold geometry, indicate ENE/WSW displacement consistent with the thrust kinematics of the Kafue Anticline (Coward & Daly, 1984). This zone is interpreted as a structural fan, with structures facing both ways away from an upright center but with a clear west facing fold and thrust in the west (Vajner, 1998b) and intense ENE facing isoclinal folds in the dolomites to the east (Figure 6c).

The HSZ then steps to the west and runs north-south from the Lunga fault to the Mwembeshi fault zone, broadly along the eastern boundary of the Hook Granite Batholith (Figures 3 and 14). In this southerly section of the HSZ the Mwashia and Nguba phyllites and schists overthrust the Kundulungu Group to the east, and both are widely intruded by Hook related granite cupolas. The southern termination of the HSZ is a broad zone of east-west fold and faulting toward the proximity of the MFZ where deformed dolomites overlie quartzite tectonites that are exposed around the basement cored Matala dome (Nayendov et al., 2016). Above them the Nguba and Kundulungu sections are folded on a ENE trend parallel to the MFZ. The western boundary of the HSZ is defined by the intrusion of Hook granites.

The coincidence of the high strain and metamorphic zone of Domain 4, deforming and overthrusting the highly extended crust of the CRZ described in Section 3.1, is compelling evidence of a close spatial and mechanical relationship between these two major tectonic events.

We conclude that the Ediacran compressional event exploited the earlier rift fabric and thinned crust, and deformed the CRZ into a narrow orogenic belt, inverting the rift contents in the process. The associated strain and metamorphic grade that occurred with the inversion indicates the orogen was most deformed and thickest in the Kabompo to Luswishi area where major thrust sheets have been mapped, and that the deformation continued southwards to Mumbwa but at lower greenschist grades creating a phyllite and locally, slate belt.

4.2.5. Domain 5: Inverted Southern Rift Basin

To the south and west of the HSZ lies the inverted Southern Rift Basin (SRB) that is characterized by a series of ENE trending fold structures and NW dipping fault zones that segment the basin (Figures 12–14). The SRB lies between the HSZ and the Lunga/Lumala fault zone to the south (Figures 12 and 13). It comprises a wide, poorly exposed region with no significant economic mineral discoveries but many mineral occurrences. The Domain is segmented by four regionally significant, NW dipping fault zones some 50–70 km apart, that separate segments of folded and faulted stratigraphy (Figures 12 and 14). Each segment displays a distinct series of form lines defined by regional mapping of folds and discontinuities (Loughlin, 1980; Page, 1974a, 1974b). From NW to SE the fault lines are known as the Maheba Fault, the Mateba Fault, the Kasempa Fault, and the Lunga fault (Figure 12).

The Maheba fault is a west dipping feature that borders a folded zone of Nguba and Kundulungu rocks dipping gently off the Mwombezhi dome (Figures 12 and 13). The area between the Mwombezhi Dome and the Maheba fault is of low metamorphic grade, but with post-tectonic biotite growth. To the SE of the Maheba fault lies a folded zone of largely Kundulungu stratigraphy between the Maheba and Mateba faults (Loughlin, 1980). The folds are upright to southeasterly vergent and non-cylindrical. East of the Mateba fault lies a large area of easterly and NW trending fold structures that are interpreted as isolated salt related features due to their highly variable orientations and frequent breccias (Figures 12 and 14). East of the Kasempa fault zone there are indications of low angle folding up to the northwest dipping Lunga fault (Figures 12 and 13). The hanging wall of the Lunga fault contains a large, east-west trending and southerly verging anticline exposing steeply dipping, white, quartz and sub-arkosic arenite overlain by a recrystallized dolomitic carbonate (Figure 13). The Lunga fold is arguably one of

the most important structures of the SRB. The two stratigraphic formations outcropping in the Lungu fold compare closely with the Lower and Upper Roan facies of typical Katangan stratigraphy of the NRB (Figures 3 and 4). In addition, the arenite's maximum age, from U-Pb zircon provenance dating, is 859 ± 13 Ma (Figure 8a, Z21). This data supports a Lower Roan age of deposition. Given the structural context and provenance data we conclude that the hangingwall fold of the Lungu fault displays the deepest stratigraphic level exposed in the Southern Basin.

The significance of the SRB and Domain 5 is three-fold. Firstly, from sparse outcrop and relatively shallow drilling to date, we conclude that similar Katangan basin stratigraphy occurs in the SRB as in the NRB, either side of the CRZ. It is therefore unlikely that a major ocean basin existed between them (John et al., 2004). It is far from clear however, how comparable the Katangan sections are in detail and the differences of the two domains appear as great as the commonalities. Secondly, the structure of both basins is separated by the HSZ of Domain 4. The east west trending Lunga fault zone that defines the southern boundary of the Domain, elevates the oldest stratigraphic section, proving the existence of Lower Roan stratigraphy in the SRB (Figure 8a, Z21) and opening the possibility that it is widespread. Thirdly, whilst there is an indication of Upper Roan carbonate/evaporite sequences in both the NRB and SRB, the NRB appears to host far more extensive, and active salt tectonics than the SRB. Throughout much of the NRB salt has been a significant mechanism in driving the basin structuring. In the SRB only the Kasempa area appears to indicate a contribution from salt tectonics, reflected in complex fold geometries.

4.2.6. Domain 6: The Mumbwa Sub-Basin

To the south of the SRB lies Domain 6 and the Mumbwa sub-basin (Figure 14). Domain 6 is defined by the Lunga fault zone in the north and the Membeshi fault zone (MbFZ) to the south, with the Hook Granite Batholith to the west (Figures 12 and 13). The Domain comprises a north-south trending folded belt of fine to medium grained clastics of Nguba age with a Kundulungu section preserved in the Kayambe Hills (Vajner, 1998b) and a synclinal area to the northeast of Mumbwa (Vajner, 1998a) (Figure 3, location 18). A central area of north-south trending upright, penetrative deformation is mapped as the continuation of the HSZ from the NE. To the north of Mumbwa, lies a large, isolated raft of dolomitic carbonate rock that appears to be a salt transported remnant (Figures 12 and 14). The large east-west trending syncline to the NE of Mumbwa is defined by the Nyama Fault Zone on its northern flank (Figure 12). The fault zone occurs as an oblique thrust zone with mylonitic fabrics (Vajner, 1998a) bounding a moderately folded zone of clastic Nguba and Mwashia rocks to the south (Figure 12). These upright folds are underlain by carbonates and a highly deformed quartz arenite and quartz pebble conglomerate that border the contact with the Paleoproterozoic basement of the Matala Dome (Naydenov et al., 2016). To the south of the Mutala dome and across the MbFZ lie the gabbroic eclogites described by Vrana et al. (1975) and the high grade amphibolite facies rocks of the Zambezi belt (Hanson et al., 1993).

The Mwembeshi fault zone is here represented as north dipping, highly oblique thrust structure that defines the southern margin of the sedimentary and regionally low metamorphic grade Katangan Basin. It is argued that much of the adjacent Zambezi metamorphic belt comprises rocks whose protolith is a continuation of the Katangan basin (Drysdall et al., 1974; Johnson et al., 2005). This issue is further examined in the Discussion section below.

4.2.7. Domain 7: The Hook Granite Batholith and Its Associated Outliers

To the west of Domain 6 lies the large area of Domain 7 and the Hook Granite Batholith (Figure 14). The domain occurs between the north northwest dipping Lunga Fault Zone that defines the southern margin of Domain 6 and the MbFZ (Figure 14). To the southwest the batholith intrudes Mesoproterozoic gneisses of the Zambezi belt (Griffiths, 1998) but is largely covered by the Quaternary sand of the Kalahari Desert and earlier Triassic sediments of the Kafue rift basin.

The Hook Batholith and associated, regionally developed, gabbroic intrusions represent a major period of bimodal magmatism (Milani et al., 2015) between 560 and 530 Ma. The batholith is dominated by a largely undeformed core of phenocrystic alkali-feldspar granites, syenite and monzonite granites with occasional rhyolite dykes and associated gabbroic inclusions (Sanz, 2005). To the east of the batholith, several cupolas of similar K-feldspar granites occur in the low-grade metasediments of the Mumbwa sub-basin (Figures 12 and 13). These smaller granites intrude the north/south trending, upright fold structures of Domain 5 and the arenite and pelitic Nguba sediments of the Katangan Supergroup that define the margin of the batholith. These upright, tight to

isoclinal, fold structures are characteristic of the major, low grade, deformational event in the area (Drysdall et al., 1974; Porada, 1989) (Figures 12 and 13). They are also comparable with a highly deformed and inverted, north-south trending margin of the Kashiba platform (Figure 6c).

The coarse phenocrystic to fine grained granitic textures within the batholith are largely undeformed, with local, highly deformed, sheared and mylonitic textures developed in relatively narrow zones. Naydenov et al. (2014) described two such zones, the southern most being a curvilinear splay of the west and north dipping MbFZ, with its trend running smoothly from north-south to east-west over a distance of about 80 km (Figure 12). This structure links with the main Mbz to the east and west. In doing so the shear zone and its faulted, low strain margins define an elliptical, lower strain lens within the granite, indicating that the granites preceded at least part of the MbFZ displacement. Deformation fabrics of the northern shear zone also converge with the batholith's eastern boundary structures of the NNW/SSE trending upright folds of the Nguba sediments. They also curve and smoothly merge with the NNW/SSE folded zone and into the Mbz (Figure 12).

To the SE of the Batholith and the Mbz, is a large area of sporadic gabbroic-eclogite outcrops and float (John et al., 2003; Phillips, 1957). The gabbroic-eclogite rocks are the northern termination of a regional trend of gabbroic-eclogites, eclogite and meta-gabbro (Johns et al., 2003; Prasad & Vrana, 1972; Vrana et al., 1975) that run from the Hook Batholith ∼200 km to the ESE. On the basis of the northerly dipping fabrics and ENE/WSW kinematic indicators, Coward and Daly (1984) postulated that this zone defined an ENE trending tectonic boundary of oblique strike slip kinematics in the Zambezi belt. John et al. (2003) on the basis of PT modeling and minor and trace element patterns similar to recent mid-ocean ridge basalts, concluded that the eclogite assemblages were indicative of a large ocean basin, over 1,000 km wide, between the Congo and Kalahari cratons. John et al. (2003), reported a Sm-Nd isochron, defining an age of 595 ± 10 Ma age for the eclogite facies metamorphism and argued it implies a rapid subduction model to create the Hook Batholith. The earlier argued stratigraphic continuity across the MbFZ and Eclogite Zone between the Katangan basin and Zambezi Belt of (De Swardt et al. (1965) implies a different solution.

Naydenov et al. (2016) describe a range of U-Pb zircon ages for the Hook Batholith granites from 559 ± 18 to 533 ± 3. As observed by Daly (1986a, 1986b), Figure 3, Naydenov et al. (2016) also describe two orthogonal deformational fabric trends, an early north-south oriented fabric followed by an approximately east-west fabric. Invoking an instantaneous clockwise rotation of compression, Naydenove et al. (2016) argue for two discrete and sequential orogenic events related to unspecified and distant regional events outside of their study area. In general terms that may or may not be an appropriate geodynamic model, and it is certainly difficult to test. In our view, the orthogonal and anastomosing, highly heterogeneous, local strain fabrics of the Mumbwa to Lungu fault area represent an evolving, local strain pattern. This continuous strain is interpreted as a result of an irregular, pre-deformational, rift-generated basement and rift architecture, being reactivated during orogenic driven basin inversion. Such large trend variations in strain, due to differential rheology between rift faulted crystalline basement margins, associated sedimentary fill, and large intrusive granite bodies is arguably a more likely explanation for the locally complex strain patterns of the Mumbwa area.

5. Discussion

Interest in the margins of cratons and their relationship to inter-cratonic basins has developed over the last two decades as surface wave tomography has converged on the definition of the thickness and shape of continental lithospheric (Jackson et al., 2021). The notion of mineral systems being associated with the topography of the lithosphere asthenosphere boundary has followed (Griffin et al., 2013; Hoggard et al., 2020). In this paper we have integrated the established lithospheric context of the Katangan inter-cratonic basin with a series of geological studies to build a tectono-stratigraphic model for this prolific copper basin. We have used the model to map the parts of the basin potentially relevant to the formation of major fluid pathways through time. We discuss the evidence for our model and the implications for the basin development and potential fluid pathways aiding mineralization.

Our modified Katangan basin tectono-stratigraphic model is built on four, evidence-based aspects of the basin's formation and deformation:

1. Lithospheric thickness influence on basin location and shape (Section 2);
2. Basin formation process, rift geometry and crustal stretching trends (Sections 3.1 and 3.2);

3. Sedimentary provenance, routing and basin paleogeography with time (Sections 3.3 and 3.4);
4. Basin inversion, orogenesis and rift fault reactivation and compartmentalization (Section 4.1).

The Katangan basin today lies in a lithospheric thickness zone of 170 to 140 km between the Congo, Bangweulu, and Kalahari cratons. The major fault systems of the western basin margin, parallels the tomographic thickness contours of the Congo craton edge (Figure 2b), and the central part of the basin lies approximately in the CRZ trough of 140 km thick lithosphere (Figures 2b and 2c). Whilst we acknowledge that present-day lithospheric thickness is not necessarily a precise indicator of past thickness, we consider it as a possible indicator of past relative thickness and therefore relative strength (Mckenzie et al., 2015). As such the Katangan basin position is consistent with lithospheric thickness distribution and associated relative crustal strength having played a role in both where the CRZ formed, and the general basin shape during the Tonian extensional events. Similarly the same lithospheric thin and CRZ area, was later the focus of compressional deformation, orogenesis and widespread basin inversion. These major tectonic events are interpreted as co-located due to the weaker lithosphere initially focusing regional extension and later compressional strain. If correct this suggest a major weakness in the Central African lithosphere prior to the Tonian that was reactivated repeatedly through the Neoproterozoic.

The measurement of crustal stretching is limited to regions of low grades of metamorphism and deformation of the Katangan stratigraphy, and to the availability of deep cores to estimate basin subsidence shape and scale. What data we have may be uncertain in absolute terms, but as a clear trend it is compelling evidence of an increase of lithospheric stretching from the ENE basin margin to the CRZ (Figure 5). These data both support a rifting process for the basin formation and also identify the potentially weakest part of the underlying lithosphere. It does, however, not imply a major ocean, but nor does it rule out one. Given the minimum of 70% stretching preserved in the CRZ it seems likely that a highly extended rift system existed in Mwashia time, and lithospheric breakup was possible. Together with the field evidence of pillow lavas in the CRZ and the widespread igneous activity (Kampunzu et al., 2000), a highly extended rift system, with a narrow marine basin in the Kabompo/Mwombeshi/Luswishi area is our preferred interpretation. We interpret the CRZ to have been a highly extended rift zone that produced a narrow (50–100 km) and relatively short (200–500 km long) zone of transitional to oceanic crust in the Kabompo to Luswishi area due to NNW/SSE rifting. As the CRZ becomes increasingly oblique to the southeast and southwest the extension may become increasingly strike-slip related which may explain the decline in metamorphic grade to the SE (Figure 14) implying a more narrow opening.

The U-Pb zircon provenance studies further support the idea of a major rift basin associated with the CRZ by defining a significant sediment boundary zone (Figure 10). The boundary prevented the eastward distribution of Archean age zircon detritus from the Congo craton across the CRZ in the Kabompo area. This provenance boundary is further evidence of the CRZ being a major discontinuity in the basin and aligns with it being a major depocenter, across which material from the west could not pass. The size, age and duration of the boundary is unclear, but the evidence implies it was an active boundary from Lower Roan through Nguba times (760–620 Ma) (Figures 8–10). To the east of Kabompo the provenance data indicates both locally and distally sourced Lower Roan and younger sediments were largely routed from the NE (Figures 8–10).

Evidence for fault reactivation and basin compartmentalization is widespread. Most of the long, steep, reverse faults active in the EoCambrian inversion appear to been reactivated, rift forming, extensional faults. The best example of this is seen in the reflection seismic interpretation of the Kawire fault in Figure 6b and the core constrained Solwezi Rift interpretation in Figure 6a. There are however, other reasons that support the existence of large rift forming extensional faults that later became reactivated. The chronostratigraphic section of Figure 7 shows the presence of the major rift forming faults and their associated stratigraphy. Each of these rift boundary faults has experienced significant degrees of contractional, oblique inversion as the deformation front developed from being initially upper crustal and dominantly flat lying and parallel to bedding (S1), to thick skinned and basement rooted across the basin. The early fabric is most intensely developed in proximity to the closure of the CRZ, the thicker-skinned, basement rooted faults came later and elevated the Kafue Anticline and reactivated earlier salt perturbations. Finally, the mapping of the major reverse faults also indicates major stratigraphic changes across them, evidence indicative of syn-sedimentary movement.

This second part of the discussion addresses the compressional tectonic events of the basin, their potential impact with respect to fluid migration, and the role of the Hook Batholith. These three basinal features are captured in the tectonic model, outlined in Figure 16a. Figure 16 compares our model (Figure 16a) with the model originated by

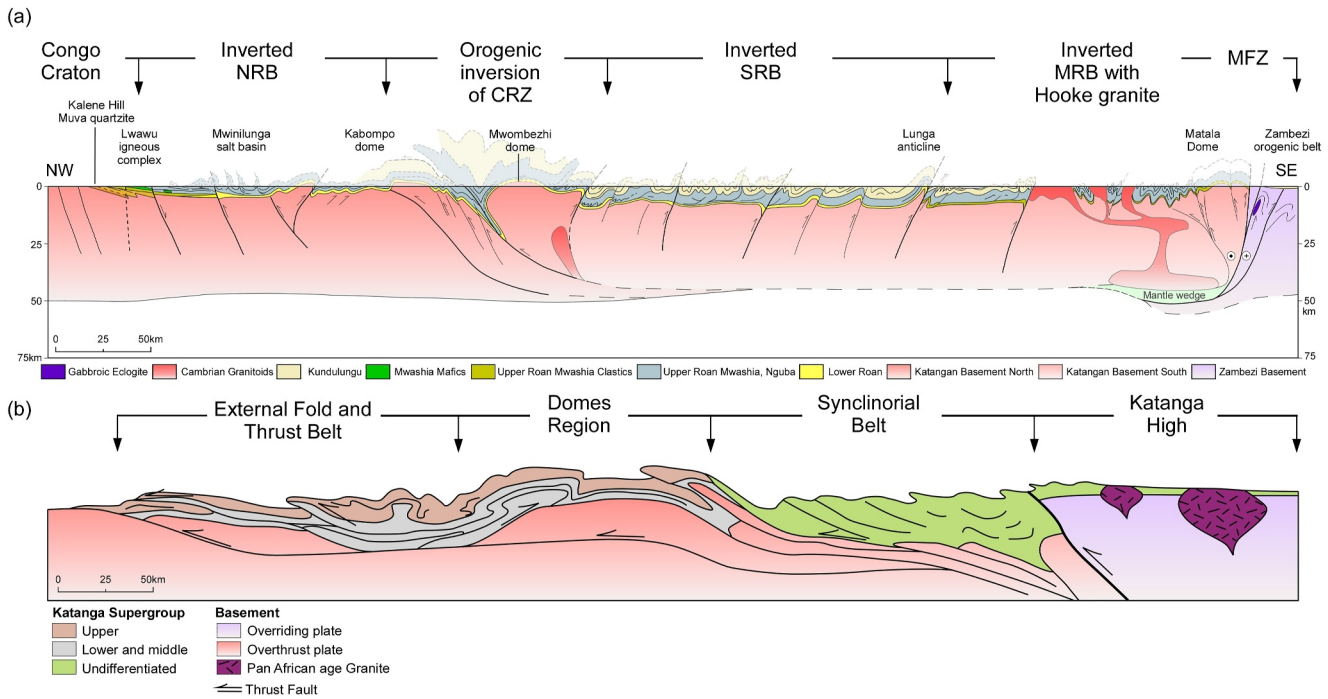

Figure 16. Comparative sections across the Katangan basin, this paper cf. 1989. A comparison of composite basin profiles discussed in this paper, (Figure 12) and the basin model first published by Porada (1989). Section (a) is broadly to scale whilst section (b) has an approximately 2× vertical exaggeration. 16a. The structural profile from Figure 12 outlines the Katangan basin tectono-stratigraphic interpretation developed in this paper. Wide rift basins (NRB and SRB) developed either side of a highly extended central rift zone (CRZ) that experienced intense orogenic inversion. The whole rifted area of the basin is deformed to varying degrees by the EoCambrian orogenic inversion and dominantly faces SE. 16b. The Zientek et al. (2014) schematic section of the Katangan basin, developed by Porada (1989) and Porada and Berhorst (2000). The section is markedly asymmetric with a north verging synclinorium bordered by a basement high to the south and basement domes to the north.

Porada (1989) and developed subsequently by Porada and Berhorst (2000), Selley et al. (2006), Eglinger et al. (2016) (Figure 16b).

Porada and Berhorst (2000) interpreted the DRC fold belt as an extensive thin skinned thrust belt detached above the basement. Wendorff (2005), supported this model on the basis of the extensive breccias being fault related. The lack of outcrop evidence of significant basement involvement in the structures north of the Domes and Kafue anticline implies the detachment would have to lay above basement for over 300 km. An alternative explanation proposed here, is that the curvilinear, and arcuate structural features that dominate the Lufilian Arc structure reflect a pre-existing, basinal, extensional fault system dominated by the Mwinilunga/Kafue fault zone and Kanyama/Pedicle fault zone (Figure 12). The associated anticlinal structures seen at surface are interpreted as a result of inversion on underlying basement fault structures, locally enhanced by salt movement. This distinction is a key issue with regard to regional ore genesis, raising the question whether the mines that exist in the sedimentary section are overlying their original, underlying basement fault systems, as they would be in our model, or not, as implied by the Porada and Berhorst (2000) allocthonous model of large thin skinned horizontal displacements.

Prior to the thick-skinned thrust tectonics and dome formation, an intense bedding parallel deformation fabric (S1) developed along the western flank of the Kafue anticline (McGowan et al., 2003). Coward and Daly (1984) described this deformation as the S1 fabric from an early bedding parallel, ENE directed basement and cover thrusting and detachment event. It is best appreciated in the Kashiba platform area (Figures 3 and 6c) where kinematic indicators suggest a top to the NE to ENE displacement. West of this area, towards the Solwezi and Mwombezhi domes, the displacement direction becomes more northerly and ultimately northwesterly, with comparable S1 mylonitic fabrics associated with the emplacement of the Solwezi thrust sheet of garnet amphibolite metamorphics above what is today the Solwezi Dome and Kansanshi area (Figure 6a).

Fluid migration in the Katangan basin was likely at its most active during the high temperature and pressures associated with the compressional tectonics of the late Ediacran and Early Cambrian (John et al., 2004; Ridgeway

& Ramsay, 1986). The most intense deformation and high temperature and pressure metamorphism occurs along the arcuate CRZ (Figures 12 and 14) and is interpreted as the result of the closure of a highly extended Tonian marine basin. The degree of shortening and closure associated with this event is difficult to estimate. There is little evidence to suggest a major oceanic separation, but equally, pillow lavas and extensive mafic intrusions (Kampunzu et al., 2000) suggest a hyper-extended or transitional crust at a minimum was developed during the Tonian extensional events. In addition, the sediment provenance signature across the CRZ supports a major crustal scale barrier such as a narrow sea of todays Red Sea scale. Given these features, together with a broad similarity of stratigraphy and geological history to the north and south of the CRZ, we conclude that highly extended lithosphere with a transitional or minor oceanic crust component was the likely outcome of the Tonian rifting. Implying that the most extended crust existed between the Kabompo to Luswishi areas. The degree of extension appears to have declined to the SE and SW. This apparent decline may be the result of a more oblique extension than in the Kabompo area.

Finally, given the early to syn-tectonic setting of the Hook Batholith with respect to Katangan deformation, it is likely that the geodynamic processes driving them are connected. The bimodal nature of the batholith is consistent with a model of basaltic magmas being emplaced into the lower continental crust causing rapid and voluminous melting and generation of phenocrystic silicic magma (Brown, 1994; Huppert & Sparks, 1988) (Figure 13). The subsequent question is the source of the alteration of gabbroic rock to eclogite and the mechanism of exhumation. Milani et al. (2015) proposed a model where the batholith formed due to slab role back along a zone of oceanic subduction with subsequent invasion of basaltic magmas into the crust in turn triggering crustal melting at the base or within the crust. The scenario implies the crustal thickening and roll-back occurred before the Lufilian orogenic cycle in order for the batholith to have formed before significant deformation took place. We propose an alternative tectonic process that relies on mantle lithosphere invasion at the base of the crust and similar crustal melting causing extensive granite formation (Huppert & Sparks, 1988), and eclogite formation. We invoke exhumation of the altered mantle derived gabbros by ductile flow (Harris, 2007; Marques et al., 2018) between the upper, Katangan basin plate, and obliquely colliding lower Zambezi plate. Lithospheric scale lateral movement causing oblique, convergent tectonics, crustal fracturing and ingress into the crust of a mantle intrusion would immediately result in extensive crustal melting and granite formation. A similar process along the active San Andreas fault zone has been argued by Hutton and Reavy (1992). In summary, the cause of partial melting and the emplacement of the basic material is uncertain, however, the evidence of a large volume of subducted ocean is unconvincing. Consequently, we interpret that the crustal melting and phenocrystic alkali granites, and associated exhumed gabbroic eclogites have resulted from a highly oblique, convergent orogenic process along a broad zone from the Lunga fault to the MbFZ (Figure 12).

This geological heterogenity across long lived fault zones that defines the compartmentalization of the basin is further complicated by the highly active salt tectonics in the NRB and Mumbwa area. The early salt tectonics would have been driven initially by local, load driven pressure gradients and tilting triggered by rift fault heterogeneities. However, the 200 Myr later regional inversion tectonics, are believed to have exacerbated this complexity and remobilized whatever salt that remained.

Our tectono-stratigraphic model for the Katangan basin attributes the fundamental deformation pattern of the basin to the reactivation of structures defined by Roan age extensional faults (Figure 17). Original structures of lithospheric scale, such as the CRZ dominate the basin along with crustal scale structures such as the major Kanyama-Pedicle and Mwinilunga-Kafue fault zones (Figure 12). Whilst the latter are clearly defined (Figures 12 and 17), the boundaries of the former CRZ is more intensely deformed and less clearly defined. In addition there is a widespread and more ephemeral upper crustal fault population that exists (Figures 12 and 17). The extensional thermal pulse of the rifting events, and much greater temperature and pressure of the orogenic and inversion tectonics and associated amphibolite grade metamorphism, represent the two main, high heat flow events of the basin's history. This focus on the evolution of the early rift basins and their resultant role in the basins deformation history is what makes our interpretation profoundly different to the earlier Porada (1989) model. The anisotropy and heterogeneity indicated in the basin by both the stratigraphic and structural analysis, together with the associated pressure/temperature highs, has likely driven the distribution of large volumes of hydrothermal fluids to be focused and their contents to become concentrated. This perspective is supported by the geochronology of Sillitoe et al. (2017) and offers insight into sediment hosted mineral exploration, both around existing mines and also in the underexplored areas such as the marginal Mwashia sub-basins (Figure 14). It also concludes that the SRB will be better explored by searching for granitic mineral sources rather than rift basins.

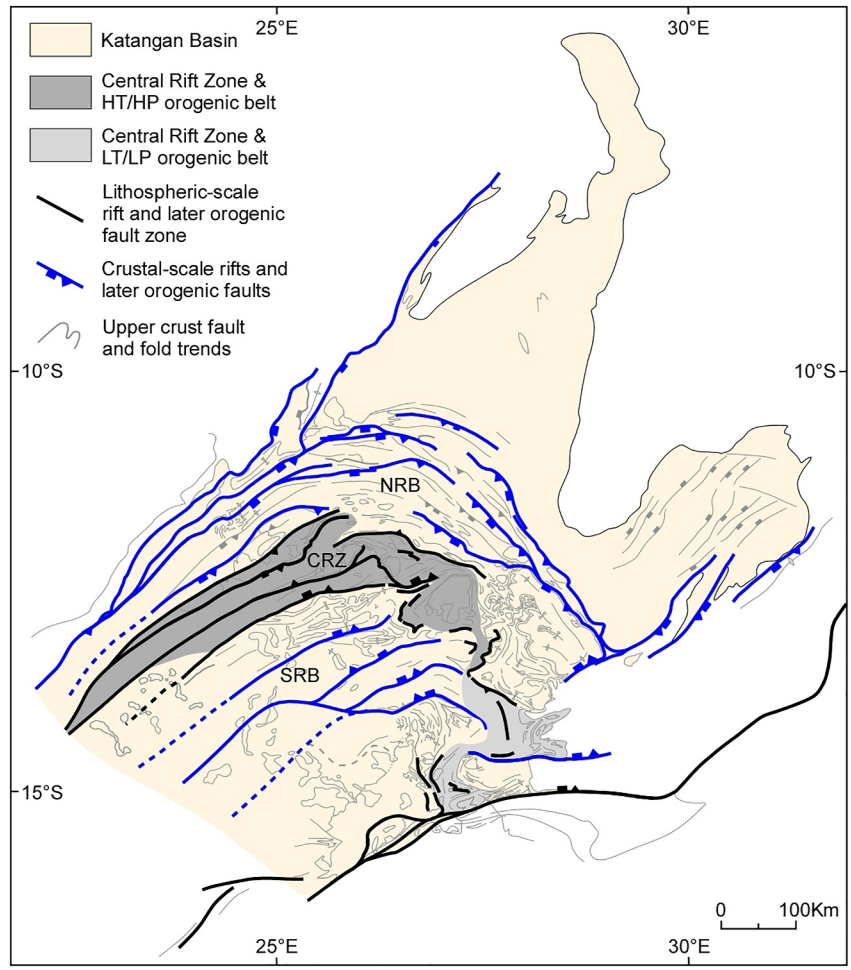

Figure 17. Crustal scale fault systems within the Katangan basin. The schematic map shows three different scales of regional structures that potentially acted as pathways for major hydrothermal fluid movement during the EoCambrian orogenesis, and earlier in the Tonian rifting. The gray area represents the most profound, high strain zone that likely penetrates the whole crust and closed a highly extended CRZ and possibly was the site of lithospheric scale break-up. Associated with it are the highest pressure and temperature conditions experienced by the basin and therefore the source of most fluid movement away from it. The blue faults represent deep crustal structures with major reach laterally. The remaining gray features represent background structural trends showing the extent of upper crustal and surface structure in the terms of fold and faulted Katangan sediments.

6. Conclusions

The paper presents new data and conclusions about the formation and deformation of the Katangan basin. Our interpretations are evidence based from the integration of lithospheric context to detailed crust and surface analyses and observations relevant to crustal structure and potential fluid pathways within the crust. We list our specific conclusions and end by offering a means to test them for further regional scale research and more specific mineral exploration.

1. The Katangan inter-cratonic basin, as preserved, occurs in an area of lithospheric thickness of 170–140 km. This basinal area is generally bounded to the northwest and south by Archean and Early Proterozoic cratonic lithosphere that reaches a thickness of the order of 200–250 km. We conclude that lithospheric thickness differences reflecting lithospheric strength through time, have likely influenced the location of the basin. In turn this has influenced the location of the crustal scale Tonian rift-fault zones that define the basin center, and the reactivation of those faults during orogenesis and basin inversion in the EoCambrian. We also suggest that the onlapping margins of the basin to the northwest in the DRC and north in Zambia are similarly controlled by original lithospheric structure.

2. Stratigraphic profiling of the Katangan sediments has enabled the quantitative estimation of lithospheric extension across the basin. These data show a concave subsidence profile developed in two rift phases (R1 and R2). The degree of subsidence increases progressively from the basin margin to a central rift zone (CRZ). Cumulative extension increases from beta factors of <1.1 at the NE margins of the basin to >1.7 at the Central Rift Zone (CRZ) south of Solwezi. The coincidence of highest extension adjacent to the most intense tectonic deformation suggests the most extended part of the basin experienced the highest deformation and metamorphism of the basin. Associated with R2 is a widespread basic and intermediate, igneous event focussed along the NW and SE basin margins and the along the CRZ.
3. Chronostratigraphic interpretation shows that the basin progressively onlapped it's margins over time, supporting the association of two rifting events followed by periods of thermal subsidence expanding the basin (Figures 7 and 11). The third basin expansion phase is the Kundulungu Group that has no obvious extensional association and is interpreted as a load driven basin due to elevation of the adjacent Muchinga and Kibara terranes.
4. Regional zircon U-Pb provenance data shows the structurally driven, stratigraphic compartmentalization of the basin and major sediment routing changes over time (Figures 8–10). In particular, provenance analysis indicates that the CRZ separates the NRB and the SRB, as sediment provenance changes dramatically across it. The high frequency of Archean zircons from the Congo craton in the NW, cease to exist eastwards and south of the CRZ. In the northern rift basin (NRB), the provenance of Lower Roan clastics is dominated by Paleoproterozoic granites of the age of the immediate Katangan basement. Proximal facies interpretation of Lower Roan sediments indicates these are likely to be local, rift shoulder sources from Bangweulu, Paleoproterozoic basement. In the SRB both Paleoproterozoic (Bangweulu craton) and Mesoproterozoic (Irumide orogen) sources are strongly represented. As the rocks sampled are mostly Kundulungu in age and fine to medium grained clastics, it is unlikely that a mid-basin source was exposed. Hence the sediment routing is more likely distal and from an elevating, northeasterly sediment source area. Also important is the SRB Lungu fault anticline that has a core of sub-arkosic to quartz arenite, overlain by dolomite. The former recorded an 859 ± 15 Ma maximum age indicating that a Lower Roan age section is possible deep in the SRB.
5. Regional structural analysis indicates that the Ediacran/Cambrian (~560–500 Ma) deformation reactivated most existing extensional fault structures causing the widespread inversion of the Tonian rift basins. The degree of deformation ranges from a narrow ~50 km wide, high strain orogenic zone of complete closure of the CRZ and the development of basement involved, thrust tectonics and high grade garnet-amphibolite metamorphism; to distal, isolated fold structures due to local, mild reactivation of individual faults. The southeastward continuation of the inverted CRZ appears to be localized along the western margin of the Kashiba Platform and eastern margin of the Hook batholith (Figure 13). It is defined by a low temperature, high strain upright fold belt of Mwashia and Nguba phyllites, interpreted as an intensely folded continuation of the CRZ (Figures 6c and 14).
6. The arcuate nature of the Katangan basin structure is interpreted to be largely the result of structural inheritance of pre-existing basement structure, crustal rheology and rift fault geometry. The regional structural trends, carved out by extensional faults and later compression and inversion, may have exploited a weak, earlier tectonic boundary or fault zone along the margin of the Bangweulu craton and Irumide orogen. The complex, locally driven fold and strain fabric relationships, particularly during compressional closure of the CRZ as seen in the Mumbwa and Kafue anticline areas, are a result of primary basement structure.
7. South of the MbFZ, deeper exposure with regional metamorphism, gabbroic-eclogite and syenites raises the possibility of a suture zone and discrete terrane, in spite of the stratigraphic similarities to the north of the Mbz. Whatever the protolith to the gneisses and granitic rocks of the Zambezi Belt, the deformation and burial as a whole has been significantly greater than in most of the Katangan basin to the north. Associated with this change is the Hook granite complex, believed to be the result of partial melting of mafic lower crustal rocks associated with gabbroic intrusion/emplacement into the Katangan lower crust. The granite batholith and it's cupolas are interpreted as a result of the lower crustal melt and the oblique compressional history of the MbFZ and the associated E-W trending structures of the Lungu/Luamala, Mubalashi and Nyama fault zones. We conclude the tectonic change implies a highly oblique, top to the south thrust zone forming along the southern margin of the early Katangan basin.
8. We have identified three levels of fault systems and hydrothermal fluid pathways that may have hosted significant mineral brines. Coupled with the stratigraphic variability, the lithospheric, crustal and basin scale fault systems each played a role in basin deformation and orogenesis to potentially transmit fluids within the

basin. The connected anisotropy and heterogeneity of these routes, together with their permeability through time, is an essential insight for deep mineral exploration. Most, and probably all, of the major copper deposits of the Katangan basin are linked with either or both, major fault structures and stratigraphic aquifers. Large scale, diffusive and advective fluid pathways, triggered by early extension or the far greater pressure and temperature conditions of the Ediacaran/Cambrian orogenesis, were the dominant mechanisms to create large, high grade ore bodies.

9. To test and deeply map this proposed connection we need complimentary, crust penetrating, integrated geophysical data to explore the deep crust. In this paper we have expanded the understanding of the surface geology of the Katangan basin. The next steps need to use integrated geophysical tools to verify the existence of the heterogeneity described and its subsurface/surface linkages and origins. Only with both perspectives, will we be able to successfully explore for deeper resources to support electrification and the energy transition.
10. Contrasts and similarities between the SRB south of the CRZ, and the NRB north of it require significant further enquiry. The differences appear to suggest completely different copper systems, magmatic dominated systems in the SRB and hydrothermal, sediment hosted systems in the NRB. In the middle zone of the CRZ, complex, hybrid systems occur. Whilst the evidence of early diagenetic copper is clear, the final configuration of copper concentrations and deposits appears to have been dominated by the orogenic period during the EoCambrian deformation, metamorphism and granite formation.

Conflict of Interest

The authors declare no conflicts of interest relevant to this study.

Data Availability Statement

Data Repository: The zircon U-Pb geochronology data discussed in Section 3.3 *Katangan sedimentary provenance and age*, has been archived with the zenodo open access repository and can be accessed at https://doi.org/10.5281/zenodo.15573786. It can be accessed through https://doi.org/10.5281/zenodo.15573786. *Data*: The data is made available by FQM who supported the analyses undertaken at the facilities of the Centre for Ore Deposits and Earth Sciences (CODES) Analytical Laboratories at the University of Tasmania of Australia between 2016 and 2020. Analyzes were performed with an ASI RESOLution S-155 ablation system coupled to an Agilent 7900qudrupole with a pulse width of 20 ns (Thompson et al., 2018). Results analysis and interpretation was undertaken by authors Zimba M. and Daly, M. C. Data reduction was based on the method of Thompson et al. (2018) and Halpin et al. (2014). The calibration of the U-Pb was checked on the Temora zircon (Black et al., 2003) and the Plesovice zircon (Salama et al., 2008). Uncertainty ranges were normalized in line with Wu et al. (2023). *Software*: All Pb corrections were done using Stacey & Kramer (1975). *Repository of data*: Zenodo open access repository (zenodo.org, https://doi.org/10.5281/zenodo.15573786). *URL/link*: Data – 2025TC008955 @ https://doi.org/10.5281/zenodo.15573786. Software – publicly available. Citations below (Jochum et al., 2011; Stacey & Kramer, 1975). *Access Conditions*: Open access via zenodo repository. *English Translation*: English throughout.

Acknowledgments
The authors acknowledge Mike Christie and First Quantum Minerals (FQM) for supporting the field and analytical work that underpins this paper. We also acknowledge Josh Goldman and Kobold Metals for allowing the inclusion of their seismic reflection data. Country-wide access and field support was provided by the Geological Survey of Zambia, Ministry of Mines, Lusaka. M. C. Daly and M. Purkiss were supported by the UKRI/NERC Copper Basin Exploration Science (CuBES) Project (NERC Grant Reference: NE/T003170/1). The authors acknowledge the late James Mwale as a colleague and early contributor to the work presented here and we thank Richard Hanson, Bert du Waele and a third reviewer for exceptionally helpful reviews.

References

Alessio, B. L., Collins, A. S., Siegfried, P., Glorie, S., De Waele, B., Payne, J., & Archibald, D. B. (2019). Neoproterozoic tectonic geography of the south-east Congo Craton in Zambia as deduced from the age and composition of detrital zircons. *Geoscience Frontiers*, *10*(6), 2045–2061. https://doi.org/10.1016/j.gsf.2018.07.005

Allen, P. A., & Allen, J. R. (2013). *Basin analysis: Principles and application to petroleum play assessment*. John Wiley & Sons.

Andersen, L. S., & Unrug, R. (1984). Geodynamic evolution of the Bangweulu Block, northern Zambia. *Precambrian Research*, *25*(1–3), 187–212. https://doi.org/10.1016/0301-9268(84)90032-9

Armstrong, R. A., Master, S., & Robb, L. J. (2005). Geochronology of the Nchanga Granite, and constraints on the maximum age of the Katanga Supergroup, Zambian Copperbelt. *Journal of African Earth Sciences*, *42*(1–5), 32–40. https://doi.org/10.1016/j.jafrearsci.2005.08.012

Arthurs, J. W. (1974). Geology of the Solwezi area, degree sheets 1226, NW quarter and 1126 SW quarter. Report 36. Geol. Surv. Dept., Ministry of Mines, Zambia. Published by Gov. Printer, Lusaka.

Bader, J. W. (2019). Structural inheritance and the role of basement anisotropies in the Laramide structural and tectonic evolution of the North American Cordilleran foreland. *Wymoing. Lithosphere*, *11*(1), 129–148. https://doi.org/10.1130/L1022.1

Baker, J., Peate, D., Waight, T., & Meyzen, C. (2004). Pb isotopic analysis of standards and samples using a Pb-207-Pb-204 double spike and thallium to correct for mass bias with a double-focusing MC-ICP-MS. *Chemical Geology*, *211*(3–4), 275–303. (Database). https://doi.org/10.1016/j.chemgeo.2004.06.030

Barron, J. W. (2003). *The stratigraphy, metamorphism, and tectonic history of the Solwezi area, Northwest Province, Zambia: Integrating geological field observations and airborne geophysics in the interpretation of regional geology* (Ph.D. thesis) (p. 233). Colorado School of Mines.

Barton, P., & Wood, R. (1984). Tectonic evolution of the North Sea basin: Crustal stretching and subsidence. *Geophysical Journal International*, *79*(3), 987–1022. https://doi.org/10.1111/j.1365-246x.1984.tb02880.x

Batumike, M. J., Cailteux, J. L. H., & Kampunzu, H. (2007). Lithostratigraphy, basin development, base metal deposits, and regional correlations of the Neoproterozoic Nguba and Kundelungu rock successions, central African Copperbelt. *Gondwana Research*, *11*(3), 432–447. https://doi.org/10.1016/j.gr.2006.04.012

Binda, P. L. (1994). Stratigraphy of Zambian orebodies. In A. B. Kampunzu & R. T. Lubala (Eds.), *Neoproterozoic Belts of Zambia, Zaire and Namibia* (Vol. 19). https://doi.org/10.1016/0899-5362(94)90013-2

Black, L. P., Kamos, L., Allen, C. M., Aleinikoff, J. N., Davis, D. W., Korsch, R. J., & Foudoulis, C. (2003). TEMORA 1: A new zircon standard for Phanerozoic U–Pb geochronology [Software]. *Chemical Geology*, *200*(1–2), 155–170. https://doi.org/10.1016/S0009-2541(03)00165-7

Brown, M. (1994). The generation, segregation, ascent and emplacement of granite magma: The migmatite-to-crustally-derived granite connection in thickened orogens. *Earth-Science Reviews*, *36*(Issue 1–2), 83–130. https://doi.org/10.1016/0012-8252(94)90009-4

Bull, S., Selley, D., Broughton, D., Hitzman, M., Cailteux, J., Large, R., & Goldrick, P. (2011). Sequence and carbon stratigraphy of the neoproterozoic Roan group strata of the Zambian Copperbelt. *Precambrian Research*, *190*(2011), 70–89. https://doi.org/10.1016/j.precamres.2011.07.021

Cahen, L., Delhal, J., & Ledent, D. (1970). On the age and petrogenesis of the microcline-bearing pegmatite veins at Roan Antelope and at Musoshi (Copperbelt of Zambia and S-E Katanga). Annales Musée royale de l'Afrique Centrale. *Sciences Geologiques*, *65*, 43–68.

Cailteux, J. (1994). Lithostratigraphy of the neoproterozoic Shaba-type (Zaire) Roan Supergroup and metallogenesis of associated stratiform mineralization. *Journal of African Earth Sciences*, *19*(4), 279–301. https://doi.org/10.1016/0899-5362(94)90015-9

Cailteux, J. L. H., & De Putter, T. (2019). The Neoproterozoic Katanga Supergroup (D. R. Congo): State-of-the-art and revisions of the lithostratigraphy, sedimentary basin and geodynamic evolution. *Journal of African Earth Sciences*, *150*, 522–531. https://doi.org/10.1016/j.jafrearsci.2018.07.020

Cohen, K. M., Finney, S. C., Gibbard, P. L., & Fan, J.-X. (2018). The ICS international chronostratigraphic chart. *Episodes*, *36*(3), 199–204. https://doi.org/10.18814/epiiugs/2013/v36i3/002

Cosi, M., De Bonis, A., Gosso, G., Hunziker, J., Martinotti, G., Moratto, S., et al. (1992). Late Proterozoic thrust tectonics, high-pressure metamorphism and uranium mineralization in the Domes area, Lufilian Arc, northwest Zambia. *Precambrian Research*, *58*(1–4), 215–240. https://doi.org/10.1016/0301-9268(92)90120-D

Coward, M. P., & Daly, M. C. (1984). Crustal lineaments and shear zones in Africa: Their relationship to plate movements. *Precambrian Research*, *24*(1), 27–45. https://doi.org/10.1016/0301-9268(84)90068-8

Cowie, P. A., & Scholz, C. H. (1992). Displacement-length scaling relationship for faults: Data synthesis and discussion. *Journal of Structural Geology*, *14*(10), 1149–1156. https://doi.org/10.1016/0191-8141(92)90066-6

Daly, M. C., Green, P., Watts, A. B., Davies, O., Chibesakunda, F., & Walker, R. (2020). Tectonic and landscape evolution of central Africa and implications for a propagating southwestern rift in Africa. *Geochemistry, Geophysics, Geosystems*, *21*(6). https://doi.org/10.1029/2019GC008746

Daly, M. C. (1984). Preliminary report on the foreland structure of the Irumide belt of Northern Zambia. In J. Klerkx & J. Michot (Eds.), *Géologie africaine: volume en hommage à L. Cahen* (pp. 67–74). Musée royal de l'Afrique centrale.

Daly, M. C. (1986a). Crustal shear zones and thrust belts: Their geometry and continuity in central Africa. *Philosophical Transactions of the Royal Society*. https://doi.org/10.1098/rsta.1986.0028

Daly, M. C. (1986b). The intra-cratonic Irumide belt of Zambia and its bearing on collision orogeny during the proterozoic of Africa. In M. P. C. Coward & A. C. Ries (Eds.), *Collision Tectonics, Spec. Publ. of the Geol. Soc. London* (Vol. 19, pp 321–328). https://doi.org/10.1144/GSL.SP.1986.019.01.18

Daly, M. C., Chakraborty, S. K., Kasolo, P., Musiwa, M., Mumba, P., Naidu, B., et al. (1984). The Lufilian arc and Irumide belt of Zambia: Results of a geotraverse across their intersection. *Journal of African Earth Sciences*, *2*(4), 311–318. https://doi.org/10.1016/0899-5362(84)90003-4

Daly, M. C., & Tosca, N. (2020). A geodynamic model of the Kansanshi Cu-Au system, Zambia. *SEG Conference*. https://www.segweb.org/pdf/events/2020/20rmwale/session-1/Session-1-Talk-9.pdf

Daly, M. C., & Unrug, R. (1982). The Muva Supergroup: A craton to mobile belt sedimentary sequence. *Transactions of the Geological Society of South Africa*, *85*, 155–165.https://hdl.handle.net/10520/AJA10120750_1081

De Swardt, A. M., Garrard, P., & Simpson, J. G. (1965). Major zones of transcurrent dislocation and superposition of orogenic belts in parts of Central Africa. *Bulletin of the Geological Society of America*, *76*(1), 89–102. https://doi.org/10.1130/0016-7606(1965)76[89:mzotda]2.0.co;2

De Waele, B., & Fitzsimons, I. C. W. (2007). The nature and timing of Palaeoproterozoic sedimentation at the southeastern margin of the Congo Craton; zircon U–Pb geochronology of plutonic, volcanic and clastic units in northern Zambia. *Precambrian Research*, *159*(1–2), 95–116. https://doi.org/10.1016/j.precamres.2007.06.004

De Waele, B., Liégeois, J.-P., Nemchin, A. A., & Tembo, F. (2006). Isotopic and geochemical evidence of Proterozoic episodic crustal reworking within the Irumide Belt of southcentralAfrica, the southern metacratonic boundary of an Archaean Bangweulu Craton. *Precambrian Research*, *148*(3–4), 225–256. https://doi.org/10.1016/j.precamres.2006.05.006

Doorninck, V. H. H. (1928). De Lufilische plooiing in den Boven Katanga. G Naeff. 's-Gravenhage.

Drysdall, A. R., Johnson, R. L., Moore, T. A., & Thieme, J. G. (1974). Outline of the geology of Zambia. *Geologie en Mijnbouw*, *51*, 265–276.

Eglinger, A., Vanderhaeghe, O., André-Mayer, A.-S., Goncalves, P., Zeh, A., Durand, C., & Deloule, E. (2016). Tectono-metamorphic evolution of the internal zone of the Pan-African Lufilian orogenic belt (Zambia): Implications for crustal reworking and syn-orogenic uranium mineralizations. *Lithos*, *240–243*, 167–188. https://doi.org/10.1016/j.lithos.2015.10.021

Fleischer, V. D., Garlick, W. G., & Haldane, R. (1976). Geology of the Zambian Copperbelt. In K. H. Wolf (Ed.), *Handbook of strata-bound and stratiform ore deposits* (Vol. 6, pp. 223–352).

Francois, A. P. (1987). Synthese geologique sur l'Arc cuprifere du Shaba (Rep. du Zaire). *Bull. Soc. Belge Geol., Centenaire1987, Hors serie*, 15–65.

François, A. P., & Cailteux, J. (1981). La Couverture Katangienne entre les Socles de Zilo et de la Kambompo, République du Zaire—Région de Kolwezi. Musée Royal de l'Afrique Centrale, Tervuren, Belgique, Annales Serie In 8o. *Sciences Geologiques*, *87*, 50.

Garlick, W. G. (1961). Structural evolution of the Copperbelt. In F. Mendelsohn (Ed.), *The geology of the northern Rhodeisan Copperbelt*. Published by MacDonald.

Goscombe, B., Foster, D. A., Gray, D., & Wade, B. (2020). Assembly of central Gondwana along the Zambezi belt: Metamorphic response and basement reactivation during the Kuunga Orogeny. *Gondwana Research*, *80*, 410–465. https://doi.org/10.1016/j.gr.2019.11.004

Griffin, W., Begg, G., & O'Reilly, S. (2013). Continental-root control on the genesis of magmatic ore deposits. *Nature Geoscience*, *6*(11), 905–910. https://doi.org/10.1038/ngeo1954

Griffiths, C. M. (1998). Geology of the Ngoma area, degree sheet 1525, SE quarter. Report 77. Geol. Surv. Dept., Ministry of Mines, Zambia. Published by Gov. Printer, Lusaka.

Halpin, J., Broughton, D., Emsbo, P., Koziy, L., Hitzman, M. W., Bull, S. W., et al. (2018). Structural configuration of the central African Copperbelt: Roles of evaporites in structural evolution, basin Hydrology, and ore location. *Society of Economic Geologists Special Publication*, *21*, 115–156. https://doi.org/10.5382/sp.21.07

Halpin, J. A., Jensen, T., McGoldrick, P., Meffre, S., Berry, R. F., Everard, J. L., et al. (2014). Authigenic monazite and detrital zircon dating from the proterozoic Rocky Cape group, Tasmania: Links to the belt-Purcell Supergroup [Dataset]. *North America: Precambrian Research*, *250*, 50–67. https://doi.org/10.1016/j.precamres.2014.05.025

Halverson, G., Porter, S., & Shields, G. (2020). The Tonian and Cryogenian periods. In *Geologic time scale 2020* (pp. 495–519). Elsevier.

Hanson, R. E. (2003). Proterozoic geochronology and tectonic evolution of southern Africa. In M. Yoshida, B. F. Windly, & S. Dasgupta (Eds.), *Proterozoic East Gondwana: Supercontinent Assembly and Breakup* (Vol. 206, pp. 427–463). Geological Society, London, Special Publications. https://doi.org/10.1144/GSL.SP.2003.206.01.20

Hanson, R. E., Wardlaw, M. S., Wilson, T., & Mwale, G. (1993). U-Pb ages from the Hook granite massif and Mwembeshi dislocation: Constraints on Pan African deformation, plutonism and transcurrent shearing in central Zambia. *Precambrian Research*, *63*(3–4), 189–209. https://doi.org/10.1016/0301-9268(93)90033-x

Harris, N. (2007). Channel flow and the Himalayan-Tibetan orogen: A critical review. *Journal of the Geological Society*, *164*, 511–523. https://doi.org/10.1144/0016-76492006-133

Hitzman, M. W. (2000). Source basins for sediment-hosted stratiform Cu deposits: Implications for the structure of the Zambian Copperbelt. *Journal of African Earth Sciences*, *30*(4), 855–863. https://doi.org/10.1016/s0899-5362(00)00056-7

Hitzman, M. W., Broughton, D., Selley, D., Woodhead, J., Wood, D., & Bull, S. (2012). *The central African copperbelt: Diverse stratigraphic, structural, and temporal settings in the world's largest sedimentary copper district*. University of Tasmania. Retrieved from https://hdl.handle.net/102.100.100/572953

Hitzman, M. W., & Broughton, D. W. (2017). Discussion: "Age of the Zambian copperbelt". *Mineralium Deposita*, *52*(8), 1273–1275. https://doi.org/10.1007/s00126-017-0767-z

Hitzman, M. W., Kirkham, R., Broughton, D., Thorson, J., & Selley, D. (2005). The sediment-hosted stratiform copper ore system. *Economic Geology 100th Anniversary*, 609–642. https://doi.org/10.5382/AV100

Hoggard, M. J., Czarnota, K., Richards, F. D., Huston, D. L., Jaques, A. L., & Ghelichkhan, S. (2020). Global distribution of sediment-hosted metals by craton edge stability. *Nature Geoscience*, *13*(7), 504–510. https://doi.org/10.1038/s41561-020-0593-2

Huismans, R. S., Podladchikov, Y. Y., & Cloetingh, S. (2001). Transition from passive to active rifting: Relative importance of asthenospheric doming and passive extension of the lithosphere. *Journal of Geophysical Research*, *106*(B6), 11271–11291. https://doi.org/10.1029/2000jb900424

Huppert, H. E., & Sparks, R. S. J. (1988). The generation of granitic magmas by intrusion of basalt into continental crust. *Journal of Petrology*, *29*(Part 3), 599–624. https://doi.org/10.1093/petrology/29.3.599

Hutton, D. H. W., & Reavy, R. J. (1992). Strike-slip tectonics and granite petrogenesis. *Tectonics*, *11*(5), 960–967. https://doi.org/10.1029/92TC00336

Intiomale, M. M., & Oosterbosch, R. (1974). Géologie et géochimie du gisement de Kipushi–Zaire. In P. Bartholome (Ed.), *Gisements stratiformes et provinces cupifères: Centenaire de la Société Géologique Belgique de Liège* (pp. 123–164).

Jackson, J., McKenzie, D., & Priestley, K. (2021). Relations between earthquake distributions, geological history, tectonics and rheology on the continents. *Philosophical Transactions of the Royal Society A*, *379*(2193), 20190412. https://doi.org/10.1098/rsta.2019.0412

Jackson, M. P. A., Warin, O. N., Woad, G. M., & Hudec, M. R. (2003). Neoproterozoic allochthonous salt tectonics during the Lufilian orogeny in the Katangan Copperbelt, central Africa. *Geological Society of America Bulletin*, *115*, 314–330. https://doi.org/10.1130/0016-7606(2003)115<0314:NASTDT>2.0.CO;2

Jochum, K. P., Weis, U., Stoll, B., Kuzmin, D., Yang, Q., Raczek, I., et al. (2011). Determination of reference values for NIST SRM 610–617 glasses following ISO guidelines [Software]. *Geostandards and Geoanalytical Research*, *35*(4), 397–429. https://doi.org/10.1111/j.1751-908X.2011.00120.x

John, T., Schenk, V., Haase, K., Scherer, E., & Tembo, F. (2003). Evidence for a Neoproterozoic ocean in south-central Africa from mid-oceanic-ridge–type geochemical signatures and pressure temperature estimates of Zambian eclogites. *Geology*, *31*(3), 243–246. https://doi.org/10.1130/0091-7613(2003)031<0243:EFANOI>2.0.CO;2

John, T., Schenk, V., Mezger, K., & Tembo, F. (2004). Timing and PT evolution of Whiteschist metamorphism in the Lufilian Arc Zambezi belt orogen (Zambia): Implications for the assembly of Gondwana. *The Journal of Geology*, *112*(1), 71–90. https://doi.org/10.1086/379693

Johnson, S. P., Rivers, T., & De Waele, B. (2005). A review of the Mesoproterozoic to early Palaeozoic magmatic and tectonothermal history of south-central Africa: Implications for Rodinia and Gondwana. *Journal of the Geological Society*, *162*(3), 433–450. https://doi.org/10.1144/0016-764904-028

Jove, C. F., & Coleman, R. G. (1998). Extension and mantle upwelling within the San Andreas fault zone, San Francisco Bay area, California. *Tectonics*, *17*(6), 883–890. https://doi.org/10.1029/1998tc900012

Kampunzu, A. B., & Cailteux, J. (1999). Tectonic evolution of the Lufilian Arc (central Africa Copperbelt) during the neoproterozoic Pan-african orogenesis. *Gondwana Research*, *2*(3), 401–421. https://doi.org/10.1016/s1342-937x(05)70279-3

Kampunzu, A. B., Cailteux, J. L. H., Moine, B., & Loris, H. N. B. T. (2005). Geochemical characterisation, provenance, source and depositional environment of 'Roches Argilo-Talqueuses' (RAT) and mines subgroups sedimentary rocks in the Neoproterozoic Katangan belt (Congo): Lithostratigraphic implications. *Journal of African Earth Sciences*, *42*(1–5), 119–133. https://doi.org/10.1016/j.jafrearsci.2005.08.003

Kampunzu, A. B., Kapenda, D., & Manteka, B. (1991). Basic magmatism and geotectonic evolution of the Pan African belt in central Africa: Evidence from the Katangan and west Congolian segments. *Tectonophysics*, *190*(2–4), 363–371. https://doi.org/10.1016/0040-1951(91)90438-x

Kampunzu, A. B., Tembo, F., Matheis, G., Kapenda, D., & Huntsman-Mapila, P. (2000). Geochemistry and tectonic setting of mafic igneous units in the Neoproterozoic Katangan Basin, central Africa: Implications for Rodina break-up. *Gondwana Research*, *3*(2), 125–153. https://doi.org/10.1016/S1342-937X(05)70093-9

Kennedy, K., Nicholas, E., & Broughton, D. (2019). Basinal setting and origin of thick (1·8 km) mass-flow dominated Grand Conglomérat diamictites, Kamoa, Democratic Republic of Congo: Resolving climate and tectonic controls during Neoproterozoic glaciations. *Sedimentology*, *66*(2), 556–589.

Keppie, J. D. (1977). *The geology of the Mukubwe area, degree sheet 1327, SE quarter*. Report of the Geol. Surv. Dept., Ministry of mines, Zambia (Vol. 48). Published by Gov. Printer, Lusaka.

Key, R., & Banda, J. (2000). *The geology of the Kalene Hills area; explanation of degree sheets 1023 SE, 1024 SW and 1124 NW quarters*. Report of the Geological Survey of Zambia (Vol. 107, p. 34). Published by Gov. Printer, Lusaka.

Key, R. M., Liyungu, A. K., Njamu, F. M., Somwe, V., Banda, J., Mosley, P. N., & Armstrong, R. A. (2001). The western arm of the Lufilian Arc in NW Zambia and its potential for copper mineralisation. *Journal of African Earth Sciences*, *33*(3–4), 503–528. https://doi.org/10.1016/s0899-5362(01)00098-7

Klink, B. A. (1977). *The geology of the Kabompo dome area, degree sheet1224, NE quarter*. Report of the Geol. Surv. Dept., Ministry of mines, Zambia (Vol. 44, pp. 44). Published by Gov. Printer, Lusaka.

Kober, L. (1921). *Der Bau der Erde*. Gebr uder Borntraeger.

Laske, G., Masters, G., Ma, Z., & Pasyanos, M. (2013). Update on CRUST1.0 – A 1-degree global model of Earth's crust, Geophys. *Res. Abstract: EGU General Assembly*, *2013*, 2658.

Liyunga, A. K., Mosley, P. N., Njamu, F. M., & Banda, J. (2000). Geology of the Mwinilunga Area; explanation of Degree Sheet 1124, southwest quarter and that part of 1123, southeast quarter that lies in Zambia. Report of the Geological Survey of Zambia (Vol. *110*, p. 36).

Loughlin, W. P. (1980). *The geology of the Matebo and Luma river areas, degree sheets 1225, SE quarter and 1226, SW quarter*. Report of the Geological Survey of Zambia (Vol. 90, p. 20). Published by Gov. Printer, Lusaka.

Loughlin, W. P. (1998). *Geology of the Idiamala Pool area, degree sheet 1626, NW quarter*. Report of the Geological Survey of Zambia (Vol. 87, p. 36). Published by Gov. Printer, Lusaka.

Mambwe, P., Swennen, R., Cailteux, J., Mumba, C., Dewaele, S., & Muchez, P. (2023). Review of the origin of breccias and their resource potential in the Central Africa Copperbelt. *Ore Geology Reviews*, *156*, 105389. https://doi.org/10.1016/j.oregeorev.2023.105389

Marques, F. O., Ranalli, G., & Mandel, N. (2018). Tectonic overpressure at shallow depth in the lithosphere: The effects of boundary conditions. *Tectonophysics*, *746*, 702–715. https://doi.org/10.1016/j.tecto.2018.03.022

Master, S., Rainaud, C., Armstrong, R. A., Phillips, D., & Robb, L. J. (2005). Provenance ages of the neoproterozoic Katanga Supergroup (central African Copperbelt), with implications for basin evolution. *Journal of African Earth Sciences*, *42*(1–5), 41–60. https://doi.org/10.1016/j.jafrearsci.2005.08.005

McGoldrick, P., Selley, D., Mackay, W., Bull, S., & Broughton, D. W. (2024). AMIRA Project P544: Proterozoic sediment-hosted copper deposits. *Quarterly progress reports and final report for the period July 2000 to October 2003*. Retrieved from https://pid.sarig.sa.gov.au/document/mesac21026

McGowan, R. R., Roberts, S., Foster, R. P., Boyce, A. J., & Coller, D. (2003). Origin of the copper-cobalt deposits of the Zambian Copperbelt: An epigenetic view from Nchanga. *Geology*, *31*(6), 497–500. https://doi.org/10.1130/0091-7613(2003)031<0497:ootcdo>2.0.co;2

McKenzie, D., Daly, M. C., & Priestley, K. (2015). The lithospheric structure of Pangea. *Geology*, *43*(1), 783–786. https://doi.org/10.1130/G36819.1

McKenzie, D. P. (1978). Some remarks on the development of sedimentary basins. *Earth and Planetary Science Letters*, *40*(1), 25–32. https://doi.org/10.1016/0012-821X(78)90071-7

Mendelsohn, F. (Ed.). (1961). *The geology of the northern Rhodesian copperbelt* (Vol. 1, p. 523). Published by MacDonald & Co. Ltd.

Milani, L., Lehmanna, J., Naydenova, K. V., Saalmanna, K., Kinnaird, J. A., Daly, J. S., et al. (2015). A-type magmatism in a syn-collisional setting: The case of the Pan-African Hook Batholith in Central Zambia. *Lithos*, *216–217*, 48–72. https://doi.org/10.1016/j.lithos.2014.11.029

Miller, R. (2013). Comparative stratigraphic and geochronological evolution of the NorthernDamara Supergroup in Namibia and the Katanga Supergroup in the Lufilian Arc of central Africa. *Geoscience Canada*, *40*(2), 118. https://doi.org/10.12789/geocanj.2013.40.007

Muchez, P., André-Mayer, A. S., El Desouky, H. A., & Reisberg, L. (2015). Diagenetic origin of the stratiform Cu–Co deposit at Kamoto in the central African Copperbelt. *Mineralium Deposita*, *50*(4), 437–447. https://doi.org/10.1007/s00126-015-0582-3

Naydenov, K. V., Lehmann, J., Saalmann, K., Milani, L., Kinnaird, J. A., Charlesworth, G., et al. (2014). New constraints on the Pan-African orogeny in Central Zambia: A structural and geochronological study of the Hook batholith and the Mwembeshi zone. *Tectonophysics*, *637*, 80–105. https://doi.org/10.1016/j.tecto.2014.09.010

Naydenov, K. V., Lehmann, J., Saalmann, K., Milani, L., Poterai, J., Kinnaird, J. A., et al. (2016). The geology of the Matala dome: An important piece of the Pan-African puzzle in Central Zambia. *International Journal of Earth Sciences*, *105*(3), 695–712. https://doi.org/10.1007/s00531-015-1222-y

Page, J. (1974a). *The geology of the Chilonga Mission area, degree sheet 1231, NW quarter*. Report of the Geol. Surv. of Zambia (Vol. 56, p. 28). Published by Gov. Printer, Lusaka.

Page, J. (1974b). *Geology of the Lubungu and Lunga areas, degree sheets 1426, NW and SW quarters*. Report of the Geological Survey of Zambia (Vol. 56, p. 23). Published by Gov. Printer, Lusaka.

Phillips, K. A. (1957). *The geology and metalliferous deposits of the Luiri Hill area (Mumbwa district)*. Report of the Geological Survey of Zambia (Vol. 10, p. 82). Published by Gov. Printer, Lusaka.

Porada, H. (1989). Pan-African rifting and orogenesis in southern to Equatorial Africa and eastern Brazil. *Precambrian Research*, *44*(2), 103–136. https://doi.org/10.1016/0301-9268(89)90078-8

Porada, H., & Berhorst, V. (2000). Towards a new understanding of the neoproterozoic- early Paleozoic Lufilian and northern Zambezi belts in Zambia and Congo/Zaire. *Journal of African Earth Sciences*, *30*(3), 727–771. https://doi.org/10.1016/S0899-5362(00)00049-X

Prasad, R., & Vrana, S. (1972). The intrusives of the Chombwa area with special reference to the eclogites. *Geological Survey Zambia Rap.*, *12*, 131–137.

Priestley, K., & McKenzie, D. (2013). The relationship between shear wave velocity, temperature, attenuation and viscosity in the shallow part of the mantle. *Earth and Planetary Science Letters*, *381*, 78–91. https://doi.org/10.1016/j.epsl.2013.08.022

Rainaud, C., Master, S., Armstrong, R. A., & Robb, L. J. (2003). A cryptic Mesoarchaean terrane in the basement to the central African Copperbelt. A cryptic Mesoarchaean terrane in the basement to the central African Copperbelt. *Journal of the Geological Society, London*, *160*(2003), 11–14. https://doi.org/10.1144/0016-764902-087

Rainaud, C., Master, S., Armstrong, R. A., & Robb, L. J. (2005). Geochronology and nature of the Palaeoproterozoic basement in the central African Copperbelt (Zambia and the Democratic Republic of Congo), with regional implications. *Journal of African Earth Sciences*, *42*(2005), 1–31. https://doi.org/10.1016/j.jafrearsci.2005.08.006

Ridgway, J., & Ramsay, C. R. (1986). A provisional metamorphic map of Zambia & explanatory Notes. *Journal of African Earth Sciences*, *5*, 441–446. https://doi.org/10.1016/0899-5362(86)90041-2

Rooney, A. D., Strauss, J. V., Brandon, A. D., & Macdonald, F. A. (2015). A Cryogenian chronology: Two long-lasting synchronous Neoproterozoic glaciations. *Geology*, *43*(5), 459–462. https://doi.org/10.1130/g36511.1

Salama, J., Kosler, J., Condon, D. J., Crowley, J. L., Gerdes, A., Hanchar, J. M., et al. (2008). Plesovice zircon - A new natural reference material for U-Pb and Hf isotopic microanalysis [Dataset]. *Chemical Geology*, *249*, 1–35. https://doi.org/10.1016/j.chemgeo.2007.11.005

Sanz, A. L.-G. (2005). *Pre- and Post-Katangan granitoids of the greater Lufilian Arc – geology, geochemistry, geochronology and metallogenic significance* (Unpublished Doctor of Philosophy Thesis Science Thesis) (p. 734). Faculty of Science, University of Witswatersrand.

Sarafian, E., Evans, R. L., Abdelsalam, M. J. D., Atekwana, E., Elsenbeck, J., Jones, A., & Chikambwe, E. (2018). Imaging Precambrian lithospheric structure in Zambia using electromagnetic methods. *Gondwana Research*, *54*, 38–49. https://doi.org/10.1016/j.gr.2017.09.007

Schaeffer, A. J., & Lebedev, S. (2013). Global shear speed structure of the uppermantle and transition zone. *Geophysical Journal International*, *194*(1), 417–449. https://doi.org/10.1093/gji/ggt095

Scholz, C. H. (2007). The scaling of geological faults. *Earthquakes and Acoustic Emission*, 2–7. https://doi.org/10.1201/9780203936115.ch1

Sclater, J. G., & Christie, P. A. (1980). Continental stretching: An explanation of the post-mid-Cretaceous subsidence of the central North Sea basin. *Journal of Geophysical Research*, *85*(B7), 3711–3739. https://doi.org/10.1029/jb085ib07p03711

Selley, D., Broughton, D., Scott, R., Hitzmann, M., Bull, S., Large, R., et al. (2006). A new look at the geology of the Zambian Copperbelt. *One Hundredth Anniversary Volume*. https://doi.org/10.5382/AV100.29

Selley, D., Scott, R., Emsbo, P., Koziy, L., Hitzman, M., Bull, S. W., et al. (2018). *Structural configuration of the central African Copperbelt: Roles of evaporates in structural evolution, basin hydrology, and ore location, metals, minerals, and society* (Vol. 22, pp. 115–156). Society of Economic Geologists Special Publication.

Sillitoe, R. H., Perelló, J., Creaser, R. A., Wilton, J., Wilson, A., & Dawborn, T. (2017). Age of the Zambian Copperbelt. *Mineralium Deposita*, *52*(8), 1245–1268. https://doi.org/10.1007/s00126-017-0726-8

Singletary, S. J., Hanson, R. E., Martin, M. W., Crowley, J. L., Bowring, S. A., Key, R. M., et al. (2003). Geochronology of basement rocks in the Kalahari Desert, Botswana, and implications for regional Proterozoic tectonics. *Precambrian Research*, *121*(1–2), 47–71. https://doi.org/10.1016/S0301-9268(02)00201-2

Stacey, J. S., & Kramer, J. D. (1975). Approximation of terrestrial lead isotope evolution by a two-stage model [Software]. *Earth and Planetary Science Letters*, *26*(2), 207–221. https://doi.org/10.1016/0012-821X(75)90088-6

Steckler, M. S., & Watts, A. B. (1978). Subsidence of the Atlantic-type continental margin off New York. *Earth and Planetary Science Letters*, *41*, 1–13. https://doi.org/10.1016/0012-821X(78)90036-5

Sweeney, M., Turner, P., & Vaughan, D. J. (1986). Stable isotope and geochemical studies in the role of early diagenesis in ore formation, Konkola Basin, Zambian copper belt. *Economic Geology*, *81*(8), 1838–1852. https://doi.org/10.2113/gsecongeo.81.8.1838

Tack, L., Wingate, M., De Waele, B., Meert, J., Belousova, E., Griffin, B., et al. (2010). The 1375Ma "Kibaran event" in Central Africa: Prominent emplacement of bimodal magmatism under extensional regime. *Precambrian Research*, *180*(1–2), 63–84. https://doi.org/10.1016/j.precamres.2010.02.022

Taverner-Smith, R. (1961). *The geology of the Mpanza Mission area, degree sheet 1626, NE quarter*. Report 10. Geol. Surv. Dept., Ministry of Mines, Zambia. Published by Gov. Printer, Lusaka.

Thieme, J. G. (1969). The geology of the Mansa area, degree sheet 1128, NE & SW quarters. Report 26. Geol. Surv. Dept., Ministry of Mines, Zambia. Published by Gov. Printer, Lusaka.

Thieme, J. G. (1971). *The geology of the Musonda Falls area, degree sheet 1028, SE quarter*. Report 32. Geol. Surv. Dept., Ministry of Mines, Zambia. Published by Gov. Printer, Lusaka.

Thieme, J. G., & Johnson, R. L. (1981). *The geological map of the Republic of Zambia, 1:1,000,000*. Geol. Surv. Dept., Ministry of Mines, Zambia. Published by Gov. Printer, Lusaka.

Thompson, J. M., Meffre, S., & Danyushevsky, L. (2018). Impact of air, laser pulse width and fluence on U–Pb dating of zircons by LA-ICPMS [Dataset]. *Journal of Analytical Atomic Spectrometry*, *33*(2), 221–230. https://doi.org/10.1039/C7JA00357A

Torrealday, H. I., Hitzman, M. W., Stein, H. J., Markley, R. J., Armstrong, R., & Broughton, D. (2000). Re-Os and U-Pb dating of the vein-hosted mineralization at the Kansanshi copper deposit, northern Zambia. *Economic Geology*, *95*(5), 1165–1170. https://doi.org/10.2113/95.5.1165

Torremans, K., Gauquie, J., Boyce, A., Barrie, C., Dewaele, S., Sikazwe, O., & Muchez, P. (2013). Remobilisation features and structural control on ore grade distribution at the Konkola stratiform Cu–Co ore deposit, Zambia. *J.Af.E.S.*, *79*, 10–23. https://doi.org/10.1016/j.jafrearsci.2012.10.005

Torremans, K., Muchez, P., & Sintubin, M. (2018). Non-cylindrical parasitic folding and strain partitioning during the Pan-African Lufilian orogeny in the Chambishi–Nkana basin, central African Copperbelt. *Solid Earth*, *9*(4), 1011–1033. https://doi.org/10.5194/se-9-1011-2018

Turer, D., & Maynard, J. B. (2003). Combining subsidence analysis and detrital modes of sandstones to constrain basin history: An example from the eastern pontides of Turkey. *International Geology Review*, *45*(4), 329–345. https://doi.org/10.2747/0020-6814.45.12.329

Twigg, H. (2020). *The geology of Kakanda, DRC – implications for lithological and structural controls of Cu-Co mineralisation of the Roan Group*. Unpublished Master of Science Thesis (p. 154). Colorado School of Science.

Twite, F., Broughton, D., Nex, P., Kinnaird, J., Gilchrist, J., & Edward, D. (2017). Lithostratigraphic and structural controls on sulphide mineralisation at the Kamoa copper deposit, Democratic Republic of Congo. *Journal of African Earth Sciences*, *151*, 212–224. https://doi.org/10.1016/j.jafrearsci.2018.12.016

Unrug, R. (1983). The Lufilian Arc: A microplate in the Pan African collision zone of the Congo and the Kalahari cratons. *Precambrian Research*, *V21*(3–4), 181–196. https://doi.org/10.1016/0301-9268(83)90040-2

Vajner, V. (1998a). *Geology of the country north-east of Mumbwa, degree sheet 1427 SW quarter*. Report 29. Geol. Surv. Dept., Ministry of Mines, Zambia. Published by Gov. Printer, Lusaka.

Vajner, V. (1998b). *Geology of the Luamala and Lukunga areas, degree sheet 1427, NE and NW quarters*. Report 52. Geol. Surv. Dept., Ministry of Mines, Zambia. Published by Gov. Printer, Lusaka.

Van Doorninck, N. H. (1928). De Lufilische plooiing in den Boven Katanga (Belgischen Congo) naar eigen waarnemingen en naar critisch overzicht van de er over verschenen publicaties. PhD Thesis Technische Universiteit Delf., G. Naeff. Den Hague, Netherlands.

Van Wilderode, J., Heijlen, W., De Muynck, D., Schneider, J., Vanhaecke, F., & Muchez, P. (2013). The Kipushi Cu–Zn deposit (DR Congo) and its host rocks: A petrographical, stable isotope (O, C) and radiogenic isotope (Sr, Nd) study. *J.Af.E.S.*, *79*, 143–156. https://doi.org/10.1016/j.jafrearsci.2012.11.011

Veevers, J. J. (1981). Morphotectonics of rifted continental margins in embryo (East Africa), youth (Africa-Arabia), and maturity (Australia). *The Journal of Geology*, *89*(1), 57–82. https://doi.org/10.1086/628564

Vermeesch, P. (2012). On the visualisation of detrital age distributions [Software]. *Chemical Geology*, *312–313*, 190–194. https://doi.org/10.1016/j.chemgeo.2012.04.021

Vermeesch, P., Resentini, A., & Garzanti, E. (2016). Na R package for statistical provenance analysis [Software]. *Sedimentary Geology*, *336*, 14–25. https://doi.org/10.1016/j.sedgeo.2016.01.009

Vrana, S., Prasad, R., & Fediukova, E. (1975). Metamorphic Kyanite eclogites in the Lufilian Arc of Zambia. *Contributions to Mineralogy and Petrology*, *51*(2), 139–160. https://doi.org/10.1007/bf00403755

Watts, A. B., & Ryan, W. B. F. (1976). Flexure of the lithosphere and continental margin basins. In *Developments in geotectonics* (Vol. 12, pp. 25–44). Elsevier. https://doi.org/10.1016/0040-1951(76)90004-4

Wendorff, M. (2003). Stratigraphy of the Fungurume group – Evolving foreland basin succession in the Lufilian fold-thrust belt, Neoproterozoic-Lower Palaeozoic, Democratic Republic of Congo. *South African Journal of Geology*, *106*(1), 17–34. https://doi.org/10.2113/1060017

Wendorff, M. (2005). Evolution of neoproterozoic-lower Paleozoic Lufilian Arc, central Africa: A new model based on syn-tectonic conglomerates. *Journal of the Geological Society*, *162*(1), 5–8. https://doi.org/10.1144/0016-764904-085

Wendorff, M. (2011). Tectonosedimentary expressions of the evolution of the Fungurume foreland basin in the Lufillian arc, neoproterozoic-lower Palaeozoic, central Africa. In D. J. J. Van Hinsbergen, S. J. H. Buiter, T. H. Torsvik, C. Gaina, & S. J. Webb (Eds.), *The Formation and Evolution of Africa: A Synopsis of 3.8 Ga of Earth History* (Vol. 357, pp. 69–83). Geological Society, London, Special Publications. https://doi.org/10.1144/SP357.5

Wingate, M. T. D., Pisarevsky, S. A., & De Waele, B. (2010). *Paleomagnetism of the 765 Ma Luakela volcanics in Northwest Zambia and implications for Neoproterozoic positions of the Congo Craton*. https://doi.org/10.2475/10.2010.05

Wu, Y., Fang, X., & Ji, J. (2023). A global zircon U–Th–Pb geochronological database [Dataset]. *Earth System Science Data*, *15*(11), 5171–5181. https://doi.org/10.5194/essd-15-5171-2023

Xie, X., & Heller, P. L. (2009). Plate tectonics and basin subsidence history. *Geological Society of America Bulletin*, *121*(1–2), 55–64. https://doi.org/10.1130/B26398.1

Xu, K. K., Xie, W., Sun, K., Ren, J. P., Gong, P. H., He, S. F., et al. (2022). Geochronology, geochemistry, and petrogenesis of I- and A-type granites in the Solwezi Dome of the Lufilian Arc: Implicationsfor the late-Mesoproterozoic magmatic and geodynamic evolution in northern Zambia. *Arabian Journal of Geosciences*, *15*(23), 1729. https://doi.org/10.1007/s12517-022-10971-0

Zientek, M. L., Bliss, J. D., Broughton, D. W., Christie, M., Denning, P. D., et al. (2014). Sediment-hosted stratabound copper assessment of the neoproterozoic roan group, central African Copperbelt, Katanga basin, Democratic Republic of the Congo and Zambia: U.S. Geological Survey scientific investigations report 2010–5090–T, 162. https://doi.org/10.3133/sir20105090T

References From the Supporting Information

Wiedenbeck, M., Alle, P., Corfu, F., Griffin, W. L., Meier, M., Oberli, F., et al. (1995). 3 natural zircon standards for U-Th-Pb, Lu-Hf, trace-element and REE analyses [Dataset]. *Geostandards Newsletter*, *19*, 1–23. https://doi.org/10.1111/j.1751-908X.1995.tb00147.x